1984

Application of modulated hydrodynamic voltammetry to the study of anodic electrocatalysis

Deborah S. Austin
Iowa State University

Austin, Deborah S.

APPLICATION OF MODULATED HYDRODYNAMIC VOLTAMMETRY TO THE STUDY OF ANODIC ELECTROCATALYSIS

Iowa State University PH.D. 1984

Application of modulated hydrodynamic voltammetry to the study of anodic electrocatalysis

by

Deborah S. Austin

A Dissertation Submitted to the
Graduate Faculty in Partial Fulfillment of the
Requirements for the Degree of
DOCTOR OF PHILOSOPHY

Department: Chemistry
Major: Analytical Chemistry

Approved:

Signature was redacted for privacy.

In Charge of Major Work

Signature was redacted for privacy.

For the Major Department

Signature was redacted for privacy.

For the Graduate College

Iowa State University
Ames, Iowa

1984

TABLE OF CONTENTS

		Page
	DEDICATION	viii
I.	INTRODUCTION	1
II.	LITERATURE REVIEW	3
	A. Anodic Electrocatalysis and the Role of Surface Oxides in Oxygen-transfer Reactions	3
	B. Hydrodynamically Modulated Voltammetry	12
III.	EXPERIMENTAL	15
	A. Chemicals	15
	B. Instrumentation	15
	1. Voltammetric studies	15
	a. Electrodes	15
	b. Rotators	16
	c. Potentiostats	16
	d. Computer system	16
	e. Miscellaneous	17
	2. Flow injection system	17
IV.	SQUARE-WAVE HYDRODYNAMICALLY MODULATED VOLTAMMETRY	21
	A. Theory	22
	B. Experimental Procedure	22
	1. Staircase potential waveform	22
	2. Triple-step potential waveform	25
	C. Optimization of Parameters	25
V.	SURVEY OF ANODIC REACTIONS USING CYCLIC VOLTAMMETRY AND SQUARE-WAVE HYDRODYNAMICALLY MODULATED VOLTAMMETRY	31
	A. Introduction	31
	B. Residual Curves	32
	C. Anodic Reactions	43

1. Arsenic(III) 43

2. Nitrite 52

3. Iodide 59

4. Chloride 73

5. Bromide 83

6. Hydroquinone 95

D. Summary 105

VI. THE ANODIC OXIDATION OF IODIDE IN ACIDIC MEDIA AT A Pt ELECTRODE 109

A. Literature Review 109

B. Voltammetric Studies 115

1. Cyclic Voltammetry 115

2. Square-wave hydrodynamically modulated voltammetry 121
a. Staircase potential waveform 124
b. Triple-step potential waveform 127

3. Summary 131

C. Flow Injection Detection 134

VII. THE REDUCTION OF IODATE 148

A. Introduction 148

B. Cyclic Voltammetry 150

C. Square-wave Hydrodynamically Modulated Voltammetry 167

VIII. CONCLUSIONS 173

IX. FUTURE RESEARCH 175

X. BIBLIOGRAPHY 176

XI. ACKNOWLEDGEMENTS 186

XII. APPENDIX 187

LIST OF FIGURES

		Page
Figure III-1.	Flow-through cell utilized for constant potential and multi-step potential amperometric detection	18
Figure IV-1.	Staircase potential waveform	24
Figure IV-2.	Triple-step potential waveform	26
Figure V-1.	I-E and ΔI-E curves of Pt in 0.5 M H_2SO_4	33
Figure V-2.	I-E and ΔI-E curves of Pd in 0.5 M H_2SO_4	35
Figure V-3.	I-E and ΔI-E curves of Au in 0.5 M H_2SO_4	37
Figure V-4.	I-E and ΔI-E curves of Ir in 5.0 M H_2SO_4	39
Figure V-5.	I-E and ΔI-E curves of 0.5 mM As(III) in 0.5 M H_2SO_4 at a Pt RDE	45
Figure V-6.	I-E and ΔI-E curves of 0.5 mM As(III) in 0.5 M H_2SO_4 at a Au RDE	49
Figure V-7.	I-E and ΔI-E curves of 0.5 mM NO_2^- in 0.5 M H_2SO_4 at a Pt RDE	53
Figure V-8.	I-E and ΔI-E curves of 0.5 mM NO_2^- in 0.5 M H_2SO_4 at a Au RDE	55
Figure V-9.	I-E and ΔI-E curves of 0.5 mM I^- in 0.5 M H_2SO_4 at a Au RDE	62
Figure V-10.	I-E and ΔI-E curves of 0.5 mM I^- in 5.0 M H_2SO_4 at an Ir RDE	66
Figure V-11.	I-E and ΔI-E curves of 0.5 mM I^- in 0.5 M H_2SO_4 at a Pd RDE	70
Figure V-12.	I-E and ΔI-E curves of 0.5 mM Cl^- in 0.5 M H_2SO_4 at a Pt RDE	76
Figure V-13.	I-E and ΔI-E curves of 0.5 mM Cl^- in 0.5 M H_2SO_4 at a Au RDE	81
Figure V-14.	I-E and ΔI-E curves of 0.5 mM Br^- in 0.5 M H_2SO_4 at a Pt RDE	85

Figure V-15. I-E and ΔI-E curves of 0.5 mM Br^- in 0.5 M H_2SO_4 at a Au RDE 87

Figure V-16. I-E and ΔI-E curves of 0.5 mM hydroquinone in 0.5 M H_2SO_4 at a Pt RDE 98

Figure V-17. I-E and ΔI-E curves of 0.5 mM hydroquinone in 0.5 M H_2SO_4 at a Au RDE 102

Figure VI-1. I-E curves of I^- in 0.5 M H_2SO_4 at a Pt RDE as a function of I^- concentration 112

Figure VI-2. I-E curve of 0.5 mM I^- in 0.5 M H_2SO_4 at a Pt RDE 116

Figure VI-3. I-E curves of 0.5 mM I^- in 0.5 M H_2SO_4 at a Pt RDE as a function of E_a 119

Figure VI-4. I-E curves of 0.5 mM I^- in 0.5 M H_2SO_4 at a Pt RDE as a function of E_a 122

Figure VI-5. ΔI-E curve of 0.5 mM I^- in 0.5 M H_2SO_4 at a Pt RDE 125

Figure VI-6. ΔI-E_3 curve of 0.5 mM I^- in 0.5 M H_2SO_4 at a Pt RDE utilizing the triple-step potential waveform illustrated in Figure IV-2 129

Figure VI-7. Plots of ΔI vs. t_2 as a function of E_2 for 0.5 mM I^- in 0.5 M H_2SO_4 at a Pt RDE 132

Figure VI-8. Expected anodic response following a positive potential step into a region where a transport-limited reaction is occurring 136

Figure VI-9. Expected anodic response following a positive potential step into a region where oxide formation occurs. 137

Figure VI-10. Expected anodic response following a positive potential step into a region where oxide formation occurs 138

Figure VI-11. Expected anodic response following a positive potential step into a region where oxide formation occurs 139

Figure VI-12. Flow injection peaks for 100 μM I^- in 0.5 M H_2SO_4 at a Pt wire electrode 141

Figure VI-13. Peak height vs. t_{ads} for triple-step amperometric detection of 100 μM I^- in 0.5 M H_2SO_4 at a Pt wire electrode 145

Figure VII-1. I-E curves of Pt in 0.5 M H_2SO_4 as a function of E_a 151

Figure VII-2. I-E curve of 4 X 10^{-5} M IO_3^- in 0.5 M H_2SO_4 at a Pt RDE 153

Figure VII-3. I-E curves of 4 X 10^{-5} M IO_3^- in 0.5 M H_2SO_4 at a Pt RDE as a function of E_a 157

Figure VII-4. Theoretical I_d-E_d and I_r-E_d behavior 160

Figure VII-5. Theoretical I_d-E_d and I_r-E_d behavior 163

Figure VII-6. I_r-E_d curve of 4 X 10^{-5} M IO_3^- in 0.5 M H_2SO_4 at a Pt/Pt RRDE 165

Figure VII-7. ΔI-E curve of 4 X 10^{-5} M IO_3^- in 0.5 M H_2SO_4 at a Pt RDE 169

Figure VII-8. ΔI-E curves of 4 X 10^{-5} M IO_3^- in 0.5 M H_2SO_4 at a Pt RDE as a function of E_a 171

LIST OF TABLES

		Page
Table II-1.	Evidence of electrocatalysis by surface oxide	5
Table III-1.	Pine Instrument's electrode utilized for the study of anodic electrocatalysis	15
Table IV-1.	Time response of the MSR to a voltage step	28
Table V-1.	Practical anodic potential limits for CV and QHMV	41
Table V-2.	Mass-transport dependent reactions observed by QHMV simultaneously with O_2 evolution	106
Table V-3.	General trends of electrocatalysis observed for mass-transport coupled reactions	107
Table V-4.	Mass-transport dependent reactions observed by QHMV occurring simultaneously with O_2 evolution at a Pt electrode	108
Table VI-1.	Multi-step potential waveforms utilized for the amperometric detection of I^- at a Pt electrode	140

DEDICATION

In memory of my grandfather-R. H. Engle

who inspired me to explore the wonders of science.

I. INTRODUCTION

The development of new electroanalytical techniques evolves from the limitations of existing techniques. The progression of polarographic techniques from conventional dc polarography to normal pulse polarography to differential pulse polarography is a prime example. With each advance, the interference from charging current, which flows as the electrode area increases, was minimized further. Although Hg has an excellent cathodic potential range, the anodic potential range is limited by dissolution of Hg. Solid electrodes, e.g., Pt and Au, have wide anodic potential ranges. Therefore, voltammetric techniques utilizing solid electrodes were introduced, but their use is not without inherent limitations. Double-layer charging and oxidation/reduction of the surface atoms result from changes in the applied electrode potential. Surface reactions, such as the anodic formation and cathodic dissolution of oxide, cause substantial current to flow which often obscures the analytical signal of interest. Hydrodynamically modulated voltammetry was developed to overcome these limitations by effectively isolating the signal of interest, i.e., the mass-transport coupled component of the total signal, from the background current components.

Although background currents produced by the oxidation of the metal surface are viewed as an interference when attempting to measure the mass-transport coupled current by conventional cyclic voltammetry, surface oxides in the early stage of formation have been found to catalyze many anodic reactions. However, as growth of the oxide film proceeds, loss of catalytic activity is observed. A catalytically active surface can

be continually regenerated by modulating the applied electrode potential. Simultaneous modulation of the electrode potential and the rotational velocity allows one to investigate the effect that the potential-dependent surface state has on anodic reactions which are coupled to the mass-transport of the analyte from the bulk solution.

The objectives of this research project included the development of the software necessary for modulated hydrodynamic voltammetric techniques and their application to the study of surface-catalyzed reactions. Based on preliminary results, the oxidation of I^- in acidic media at a Pt electrode was chosen to be studied in further detail.

II. LITERATURE REVIEW

A. Anodic Electrocatalysis and the Role of Surface Oxides in Oxygen-transfer Reactions

Electrochemical reactions are influenced markedly by the applied electrode potential. The potential-dependent rate constant (k) for electrochemical reactions is given by the equation (1)

$$k = k^0 \exp\{-\alpha nFE/RT\}$$

where k^0 is the standard rate constant, α is the transfer coefficient, n is the number of electrons, F is the Faraday constant, E is potential, R is the gas constant, and T is temperature. Also significant in electrochemical reactions are the choice of electrode material and the properties of the electrode surface, i.e., surface morphology and the presence of oxides. Electrochemical reactions can be catalyzed, thus, the term electrocatalysis was coined. Appleby (2) defined electrocatalysis as "the study of heterogeneous catalytic reactions that involve reactant and product species transferring electrons through an electrolyte-catalyst interface". Electrocatalytic effects were reported first in the literature in 1928 by Bowden and Rideal (3). They observed, for reactions such as the deposition of H, differences in the exchange current density for different electrodes at the same potential. Presently, interest in electrocatalysis is in the area of energy conversion devices. Electrocatalyzed reactions directly convert combustion energy into electricity. The major objective is to develop a system

which produces the maximum reaction rates at potentials close to the reversible potential, thereby minimizing cost.

The catalytic participation of surface oxygen at a Pt electrode in electro-oxidative processes was implicated by Russian scientists in the early 1950's (4-6). In the early to mid-1960s, surface oxides on noble metal electrodes were demonstrated to affect the mechanism of a reaction in addition to the kinetics of the reaction (7-10). Numerous examples of anodic oxidation of inorganic compounds are cited in Table II-1 in which the involvement of surface oxides at metal electrodes has been suggested. Note that the oxidation products of the species listed in Table II-1 have a greater oxygen content than the reactant species, e.g., $H_3AsO_3 \longrightarrow H_3AsO_4$, $I^- \longrightarrow IO_3^-$, and $SO_3^{2-} \longrightarrow SO_4^{2-}$, thereby inferring that the electrode serves as an O-transfer catalyst. Since the involvement of surface oxides is apparently an integral part of the electrocatalytic process, the formation of oxides on noble metal electrodes, in particular Pt, merits discussion.

An excellent survey of literature pertaining to the formation of oxides on noble metal electrodes prior to 1965 was presented by Gilman (46). Recent reviews of literature were reported by Belanger and Vijh (47) and Cabelka (48). The evolution of O_2 at noble metal electrodes was reviewed by Hoare (49). The intention of this discussion is to summarize those conclusions most widely accepted among present-day researchers.

Angerstein-Kozlowska et al. (50), Conway and Gottesfeld (51), and Tilak et al. (52) have studied extensively the formation of surface

Table II-1. Evidence of electrocatalysis by surface oxide

Electrode	Reactant	Reference
Pt	I^-	11-19
	Br^-	20
	Mn(II)	21, 22
	As(III)	23-25
	SO_2	4, 5, 26-29
	NO_2^-	4, 5, 30
	CO	31-37
	$S^{2-}(HS^-)$	38
	SO_3^{2-}	4, 30
	U(IV)	6
Au	$S^{2-}(HS^-)$	39, 40
	As(III)	41
	NO_2^-	42, 43
Pd	SO_2	44
Rh	CO	45

oxides on Pt in acidic solutions. They concluded that the initial step involves the production of adsorbed OH radicals by the reaction

$$H_2O \longrightarrow \cdot OH + H^+ + e^-.$$

They also demonstrated that the formation of the equivalent of a monolayer of lower surface oxide occurs in a stepwise manner: the anodic wave can be deconvoluted into three peaks corresponding to oxides with surface stoichiometry of Pt_4OH (ca. 0.89 V vs. NHE), Pt_2OH (ca. 0.95 V vs. NHE), and PtOH (ca. 1.05 V vs. NHE). The "lower oxide" will be designated as "PtOH". The initial PtOH produced with low surface coverage can be reduced by a nearly reversible cathodic process. The reversible PtOH has only transient existence; however, with time, as well as a result of local potential fields, the adsorbed OH radicals and Pt atoms undergo place-exchange to produce "OHPt" which is more stable than PtOH. The reduction of this oxide species occurs at a more negative reduction potential. For E > 1.0 V in acidic media, a monolayer of adsorbed OH is formed rapidly with subsequent conversion by oxidation to the "higher oxide" designated as "PtO". Place-exchange also occurs with the PtO species to form "OPt".

Angerstein-Kozlowska et al. (53) also investigated the effect of adsorbed ions on the initial stage of oxide formation. As a result of competition between the ions and the OH radicals for adsorption sites on the electrode surface, the potential at which oxide formation commences is shifted to more positive values. Adsorbed ions also facilitate place-exchange between Pt atoms and adsorbed OH, thereby

decreasing the number of OH species available on the surface for reaction with the analyte. As mentioned previously, place-exchange is promoted at higher potential values. Therefore, the combination of adsorbed ions and higher potential values contribute to the shortening of the potential range over which PtOH exists for a significant period of time.

The electrochemical evolution of O_2 at Pt anodes has been investigated by several researchers (54-57). Damjanovic and Jovanovic (54) proposed that the process involves the direct participation of O-atoms in the oxide film. The participation of the surface oxygen is supported by the work of Rozental and Veselovskii (55) and Churchill and Hibbert (56) using a tracer technique. The Pt surface oxide was formed by anodic polarization in an ^{18}O-enriched aqueous solution followed by the evolution of O_2 from the enriched oxide surface in an unlabeled aqueous solution. The initial gas evolved was rich in the dimer ^{18}O-^{16}O resulting in the progressive depletion of ^{18}O from the surface oxide. Damjanovic and Jovanovic (54) postulated that the evolution of O_2 proceeds according to the scheme:

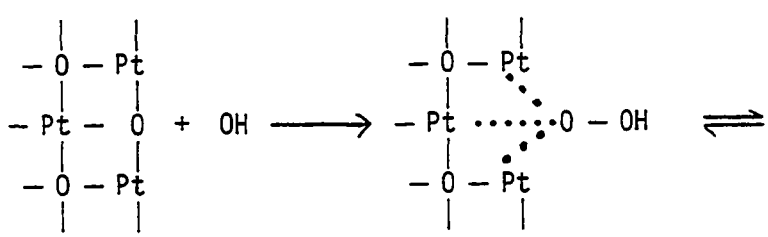

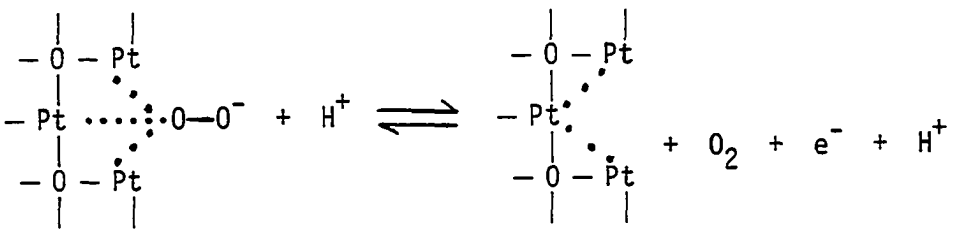

The first step in the mechanism involves the generation of OH radicals on the PtO surface. When O_2 molecules leave the surface of the electrode, the oxide must be reformed which involves OH radicals as an intermediate product:

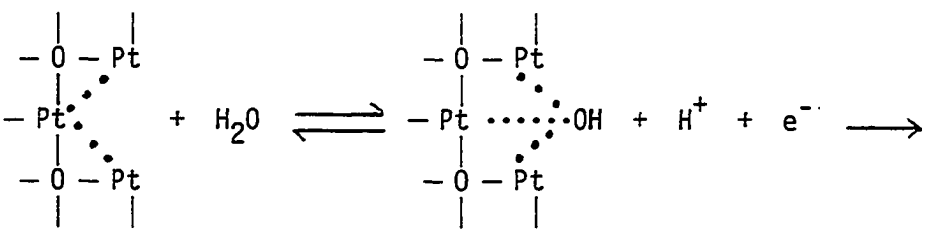

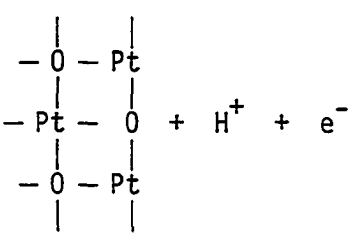

The apparent abundance of OH radicals present on the electrode surface during O_2 evolution and the fact that catalysis is observed in the presence of the lower oxide (i.e., PtOH) causes one to suspect that O_2 evolution may also exhibit an electrocatalytic effect on many anodic

reactions.

The potential for onset of surface oxidation at a Au electrode has been widely disputed. Hoare (58), using double-layer capacitance measurements, first observed the possible existence of adsorbed oxygen at E < 1.06 V vs. SCE which greatly influences the electrochemical properties of the electrode. For example, the electro-oxidation of organic molecules presumably requires a surface oxygen loosely bound to the metal substrate. Maximum oxidation rates for olefins at Au electrodes are observed in the region 0.95 V < E < 1.1 V (59). Other researchers (60-63) maintain that no Au oxidation occurs until E > 1.06 V, and they attribute the change in capacitance at E < 1.06 V to impurities in the electrode material or in the electrolyte solution. Results of recent studies utilizing ellipsometry (59, 64), reflectance spectroscopy (59, 64, 65), and a photochemical method (66, 67) support the existence of adsorbed oxygen, presumably as AuOH, at E < 1.06 V as proposed by Hoare (58). The onset of AuO formation occurs at E > 1.06 V with monolayer coverage attained at ca. 1.2 V. For E > 1.2 V, further oxidation of the surface occurs producing Au_2O_3 up to ca. 1 nm in thickness. Application of E > 1.8 V leads to the formation of a highly-hydrated, highly-colored (reddish brown), surface layer with the dominant species being $Au(OH)_3$ (68). The latter two oxides differ in electronic and ionic conductivity; Au_2O_3 is a semiconductor whereas $Au(OH)_3$ is a conductor.

Gold(III) oxide, loosely held on the electrode surface, flakes off exposing Au sites (69-71). Oxygen evolution and continued formation of

Au_2O_3 can occur at the exposed Au sites, both reactions involving intermediate production of an OH species (70-72).

Literature pertaining to the anodic oxidation of Pd is limited (47, 69, 73-76). The stability and reactivity of surface oxides on Pd are highly dependent upon the electrode history. Palladium dissolution occurs at a freshly polished electrode during the initial scans of potential which results in roughening of the electrode surface hence, an increase in the real area of the electrode. However, after repetitive potential cycling, surface roughening ceases, the electrode stabilizes, and activity toward oxygen adsorption increases. Palladium oxide formation occurs in a stepwise fashion during the positive scan of potential by a mechanism similar to oxide formation on Pt. Initially, a PdOH species is formed at E > 0.48 V, reaching monolayer coverage at ca. 0.7 V, followed by the formation of the more stable oxide PdO. With time, place-exchange of Pd and O occurs. Formation of PdO_2 begins at a potential corresponding to the evolution of O_2 on Pd (ca. 1.2 V). Since PdO_2 is known to be unstable in acid, Hoare (77) proposed that O_2 evolution at a Pd electrode occurs by decomposition of PdO_2 in the reaction $PdO_2 \longrightarrow PdO + \frac{1}{2}O_2$. Hence, the anodic current observed is the result of regeneration of PdO_2 by the reaction $PdO + H_2O \longrightarrow PdO_2 + 2H^+ + 2e^-$.

The anodic behavior of an Ir electrode displays unique characteristics in comparison with that of other noble metal electrodes (46, 76, 78). Voltammograms recorded in an electrolyte of 1 M H_2SO_4 are fairly symmetrical about the potential axis in the region of oxygen adsorption

and oxygen desorption indicating reversibility of the electrode reaction. A continual increase in the anodic oxide formation current and the cathodic oxide dissolution current is observed upon repetitive potential cycling owing to the buildup of oxide on the electrode surface. The extent of continuous oxide buildup decreases as the concentration of the acidic electrolyte solution increases. In 5 M H_2SO_4, current does not change significantly with continuous potential cycling; however, reversible behavior is not observed. Irreversibility of oxygen adsorption and oxygen desorption increases as the potential scan is reversed at more positive potential values. The surface oxidation of Ir occurs with initial formation of IrOH at E > 0.16 V, and further oxidation to IrO at E > 0.95 V. At E > 1.15 V, IrO is converted to IrO_2. Initially, O_2 evolution takes place at a potential where a mixture of IrO and IrO_2 sites exist. A decrease in the anodic current for O_2 evolution occurs at ca. 1.4 V as a result of a change in the properties of the metal ions in the anodic film. The existence of an IrO_3 species has been observed at high potentials by Frazier and Woods (79), and Kim et al. (68). The former authors speculated also that IrO_3 participates directly in the O_2 evolution reaction as represented by the equations:

$$IrO_3 \longrightarrow IrO_2 + O$$
$$2O \longrightarrow O_2$$

The electrocatalytic activity of the oxide toward O_2 evolution depends upon the number of sites within the oxide that can react according to the above equations. Hence, the activity is proportional to the

quantity of IrO_3. Gottesfeld and Srinivasen (80) reported that the rate of O_2 evolution is 5-10 times faster on a well-developed oxide layer than on a freshly polished electrode at which the oxide layer is not yet well-developed.

B. Hydrodynamically Modulated Voltammetry

Miller, Bellavance, and Bruckenstein (81) examined the feasibility of hydrodynamically modulated voltammetry at rotating disk electrodes based on the application of sine-wave and square-wave modulations about a nonzero, average rotational velocity. An important experimental advantage which resulted from the use of superimposed modulations on a steady speed was the ability to separate the convective-diffusion controlled component of the total current from background components, which result from surface processes and decomposition of the supporting electrolyte and are not influenced by variation in the rotational velocity. Subsequent investigations (82-87) have focused on the sinusoidal version of hydrodynamically modulated voltammetry (SHMV). The theoretical basis of the technique has been developed extensively. Although SHMV has been applied for the determination of heterogeneous kinetic parameters for quasi-reversible and irreversible systems and the determination of diffusion coefficients, major emphasis has been placed on application of SHMV for trace analysis. Recent advances in SHMV include amplitude enhancement (88) and operation in the derivative mode (89). Both modifications were developed to increase the sensitivity of the extracted signal, thus extending the analytical applicability for

submicromolar electroanalysis. Miller and Bruckenstein (84) concluded that SHMV "... can frequently overcome severe complications arising from interfering discharge of supporting electrolyte and thereby extract serviceable voltammetric waves ..."; however, no specific examples have been reported which exploit this advantage. Blaedel and coworkers (90-92) investigated the square-wave version of hydrodynamically modulated voltammetry, which they referred to as "pulsed rotation voltammetry". The determination of reaction rate constants and transfer coefficients, and application to trace analysis have been emphasized. In addition, Engstrom and Blaedel (93) recognized the advantages of automating the square-wave technique through use of small computers. The theory and application of hydrodynamically modulated voltammetric techniques have been reviewed by Wang (94).

Both the sine-wave and square-wave versions of hydrodynamically modulated voltammetry are capable of extracting the convective-controlled faradaic signal from a total current dominated by surface-controlled processes, however, the interest in this research project focused on square-wave hydrodynamically modulated voltammetry (QHMV) under computer control. The choice to apply QHMV for the study of electrocatalysis was based on the following factors: 1) Instrumentation is simplified since no filtering device or lock-in amplifier is required. 2) The technique is automated easily with control of the experiment and data acquisition provided by a small computer. 3) Under computer control and the use of a staircase potential waveform, the time necessary to complete an experiment is relatively short. 4) All instrumentation is commercially

available, allowing researchers to assemble the instrumentation quickly and focus their attention on the data produced. Furthermore, emphasis on application of QHMV in this project was shifted from a quantitative interest in trace analysis to a qualitative interest in the characterization of reactions under mixed surface and transport control. Application of hydrodynamically modulated voltammetry for micro- and submicromolar analysis has been given considerable attention, however, the technique will never compete successfully with other electroanalytical techniques available for trace analysis. The complexity of real-life samples mandates the use of chromatography for separation of components thus eliminating the practicality of analysis in a batch cell which is required for rotational velocity modulations. Even though a pulsed-flow technique has been investigated (95), this detection system is not feasible in conjunction with chromatography.

The ability to observe mass-transport controlled current occurring simultaneously with O_2 evolution is by far the most salient feature of QHMV. There is a wealth of information available in a potential region previously inaccessible by conventional voltammetry. Anodic reactions once avoided due to the complexity of the anodic signal now can be studied. Future research with hydrodynamically modulated voltammetric techniques may provide further extension of the available potential range which is limited by dissolution of the electrode material, not the production of O_2.

III. EXPERIMENTAL

A. Chemicals

All solutions were prepared from reagent grade chemicals and triply distilled water. The water was passed through an ion-exchange column following the first distillation, distilled from an alkaline permanganate solution (0.1 M $KMnO_4$/0.1 M KOH), and finally distilled from a 1 M H_2SO_4 solution. Dissolved O_2 was removed from all solutions by saturation with N_2. A blanket of N_2 was maintained above the solution throughout experimentation.

B. Instrumentation

1. Voltammetric studies

a. Electrodes The rotating disk and ring-disk electrodes (RDE and RRDE) (Pine Instrument Co., Grove City, PA) are listed in Table III-1.

Table III-1. Pine Instrument's electrodes utilized for the study of anodic electrocatalysis

Model	Type	Electrode Material	Area (cm^2)
AFMD28	RDE	Pt	0.166
AFMD28	RDE	Au	0.162
AFMD19	RDE	Pd	0.197
AFDT06	RRDE	Pt,Pt	0.459, 0.059
AFMDI1980	RDE	RuO_2/TiO_2[a]	0.201

[a] Anode material supplied by Dow Chemical Co. (Freeport, TX).

An Ir electrode (0.496 cm^2) was fabricated in the machine shop in the Department of Chemistry, Iowa State University. Prior to each use, the electrodes (except for RuO_2/TiO_2) were polished with 0.05 μm Buehler Alumina on microcloth then thoroughly rinsed with triply distilled water.

b. Rotators The model PIR rotator (Pine Instrument Co.) was used with the AFDT06 electrode for ring-disk studies. This rotator had nine fixed speeds between 400 and 10,000 rpm. The rotator model MSR (Pine Instrument Co.) was used with the model AFMD electrodes and the Ir electrode. This rotator was a solid-state, servo-controlled system capable of rapid acceleration and deceleration. The speed could be set from 100 to 10,000 rpm within 1% accuracy. Acceleration from 1000 rpm to 4000 rpm occurred in 22 ms. An external analog signal applied to the input jack on the speed control box made possible the application of modulated waveforms.

c. Potentiostats Potentiostatic control for application of triangular and staircase potential waveforms was achieved by the model RDE-3 potentiostat (Pine Instrument Co.). The faster potentiostatic response necessary for application of the triple-step potential waveform was achieved with a PAR-174A potentiostat (EG&G Princeton Applied Research Corp., Princeton, NJ). A miniature, saturated calomel electrode (SCE) served as the reference electrode and all potentials are reported as volts vs. SCE.

d. Computer system External signals for control of rotational velocity and electrode potential were generated, and data were acquired, under computer control. The computer (model 6800, Southwest Technical

Products Corp., San Antonio, TX) was equipped with 32-K bytes of memory, four 12-bit digital/analog (D/A) converters, and eight multiplexed 12-bit analog/digital (A/D) converters. Peripheral devices included a Beehive International B-150 computer terminal (Salt Lake City, UT), a Centronics microprinter P-1 (Hudson, NH), and floppy disk storage. Programming was done in BASIC. Program listings are given in the Appendix.

e. Miscellaneous Current-potential (I-E and ΔI-E) and current-time (I-t) curves were recorded on a X-Y recorder (model 7035B, Hewlett Packard, San Diego, CA; or model Omnigraphic 100 Recorder, Houston Instruments, Bellaire, TX). An oscilloscope (model 122A, Hewlett Packard) was used in preliminary experiments to optimize conditions for QHMV by observing the time required for the rotation speed to be established following a step change in the external analog input. Also, the response of the electrode current following a step change in the rotation speed was monitored.

2. Flow injection system

The flow injection apparatus was assembled as described by Hsi (96). The flow-through cell was constructed by the machine shop of the Department of Chemistry, Iowa State University, and is illustrated in Figure III-1. A 25-gauge Pt wire (3 mm long) served as the working electrode. The cell was submerged in a beaker filled with supporting electrolyte. A Pt-wire counter electrode and the reference electrode were also placed in the beaker. The dispersion constant for this flow injection system was 0.45. A microprocessor-controlled potentiostat (model UEM detector, Dionex, Inc., Sunnyvale, CA) was utilized for the

Figure III-1: Flow-through cell utilized for constant potential and multi-step potential amperometric detection

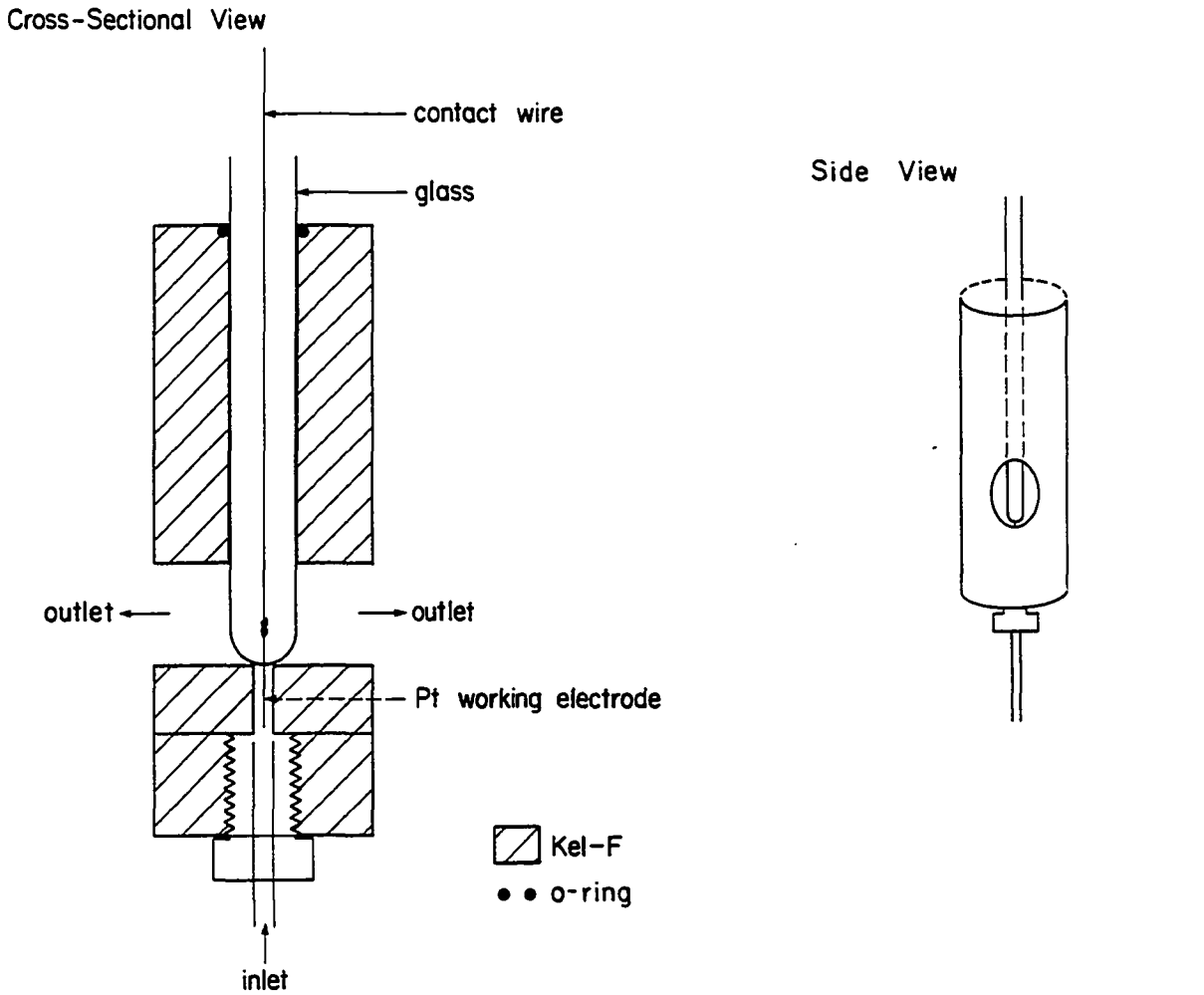
Cross-Sectional View
contact wire
glass
outlet
outlet
Pt working electrode
Kel-F
o-ring
inlet
Side View

application of double-step and triple-step potential waveforms. Data were recorded using a stripchart recorder (model 250-1, Curken, Inc., Lincoln, NE).

IV. SQUARE-WAVE HYDRODYNAMICALLY MODULATED VOLTAMMETRY

A. Theory

The theoretical basis of QHMV is relatively straightforward. Total current (I_{tot}) observed at a solid electrode is expressed as follows:

$$I_{tot} = I_{conv} + I_{solv} + I_{surf} + I_{ch} \qquad (1)$$

where I_{conv} is the convective-coupled component of current, I_{solv} is the current produced by electrolysis of the solvent, I_{surf} is the faradaic current from surface-controlled processes such as the formation or reduction of oxide and reactions involving adsorbed species, and I_{ch} is the double-layer charging current. The transient currents, I_{surf} and I_{ch} are independent of mass transport. Since the concentration of H_2O at the electrode surface is not a function of the rotational velocity, I_{solv} is not dependent upon mass transport. Therefore, isolation of I_{conv} from I_{tot} can be achieved by modulating the rate of convective transport of electroactive species to the electrode surface, i.e., by variation of the rotational velocity of the electrode. The value of I_{tot} is measured at two rotational velocities (i.e., the upper (u) and lower (l) velocity) and the difference is computed. The resultant signal (ΔI) is a function solely of the mass-transport component of total current at the two velocities (equation 2).

$$\Delta I = I_{tot,u} - I_{tot,l}$$

$$\Delta I = (I_{conv,u} + I_{solv} + I_{surf} + I_{ch}) - (I_{conv,l} + I_{solv} + I_{surf} + I_{ch})$$

$$\Delta I = I_{conv,u} - I_{conv,l} \quad (2)$$

If the mass-transport coupled reaction behaves according to the Levich equation, the theoretical limiting signal, ΔI_{lim} (coul/s) can be calculated by equation 3,

$$\Delta I_{lim} = 0.62\ nFAD^{2/3}\nu^{-1/6}(\omega_u^{1/2} - \omega_l^{1/2})C^b \quad (3)$$

where n is the number of electrons (eq/mol), F is the Faraday constant (96,484 coul/eq), A is the area of the electrode (cm^2), D is the diffusion coefficient (cm^2/s), ν is the kinematic viscosity (cm^2/s), ω is the angular velocity (rad/s), and C^b is the bulk concentration of analyte (mol/cm^3).

B. Experimental Procedure

1. Staircase potential waveform

QHMV, utilizing a staircase potential waveform (Figure IV-1), was performed according to the following sequence: 1) Experimental parameters were specified, including the cathodic (E_c) and anodic (E_a) limits for the potential scan, the potential step increment (ΔE), the lower (W_l) and upper (W_u) rotation speeds, the time delay (t_d) required after application of a change in rotation speed (ΔW) to allow current stabilization prior to the measurement of current, and the number of data points (N) to be collected at each rotation speed. 2) The average

Figure IV-1: Staircase potential waveform

Arrow indicates point at which measurement of current commences.

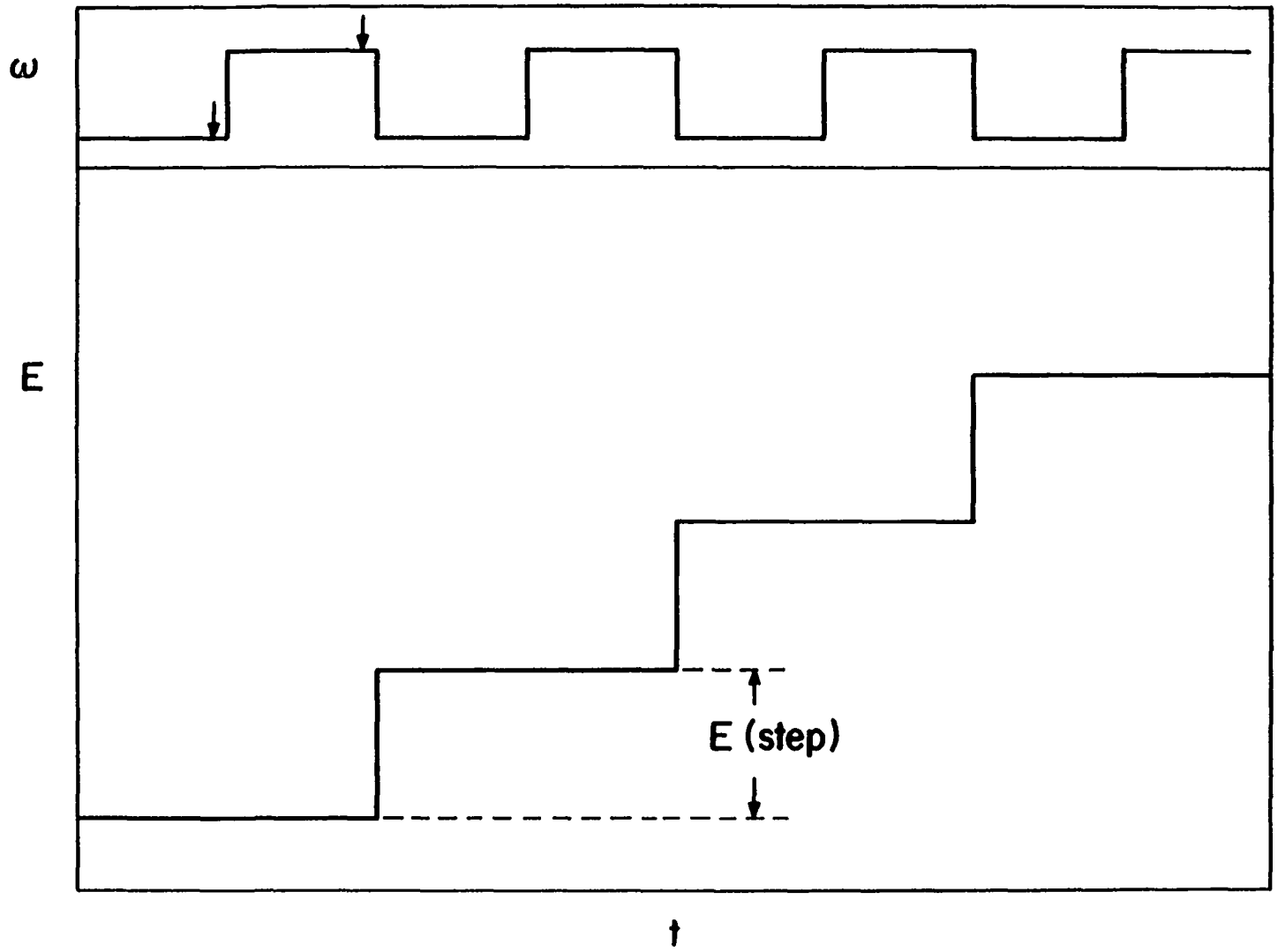
ω
E
E (step)
t

of the N values of current measured at W_l and W_u was calculated for each value of potential, and the difference between the two average current values (ΔI) was computed. 3) Finally, the data were plotted as ΔI vs. E.

2. Triple-step potential waveform

QHMV was applied also utilizing the triple-step potential waveform illustrated in Figure IV-2. The waveform consisted of an initial potential value (E_1) which resulted in reduction of PtOH and PtO, an oxidizing potential (E_2) for which surface oxidation was initiated, and a sampling potential ($E_3 < E_2$) at which the faradaic signal was measured. The triple-step waveform was applied at both W_l and W_u during each modulation cycle of rotation speed, and ΔI was calculated corresponding to ΔW. Potential E_3 was incremented by ΔE after completion of each modulation cycle. The time spent at each potential is designated by t_1, t_2, and t_3, respectively.

A plot of ΔI vs. t_2 was generated for a series of E_2 values by holding E_2 constant and incrementing t_2 following each modulation cycle of rotation speed. Similarly, plots of ΔI vs. t_3 were constructed for several values of E_2 by holding E_3 constant and incrementing t_3 at the completion of each modulation cycle of rotation speed.

C. Optimization of Parameters

The time required for relaxation of the hydrodynamic boundary layer to a steady-state value following a step-wise change in the disk speed has been discussed in detail by Albery, Hillman, and Bruckenstein (97). The relaxation time is dependent upon the final rotation speed and the

Figure IV-2: Triple-step potential waveform

Arrow indicates point at which measurement of current commences.

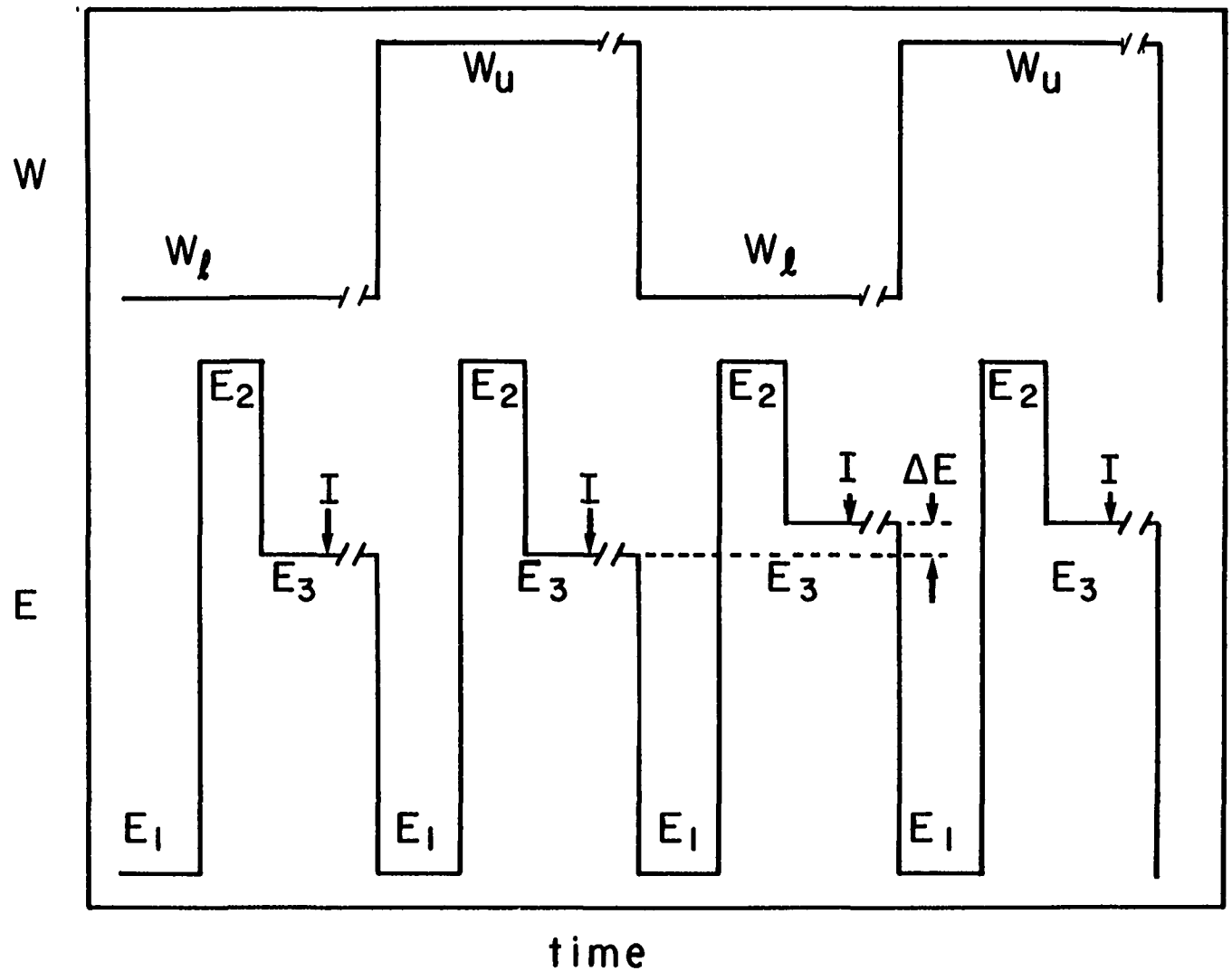
W
E
W_u
W_l
W_u
W_l
E_2
E_2
E_2
E_2
I
I
I
ΔE
I
E_3
E_3
E_3
E_3
E_1
E_1
E_1
E_1
time

Schmidt number (the dimensionless ratio ν/D), and has been shown to occur within 4% of the time required for a single rotation.

The time required for the rotation speed to be established following a step change in the voltage applied to the speed controller is given in Table IV-1. Note that the time required to achieve the final speed upon deceleration is longer than the time required to establish the final speed upon acceleration for equal values of $|\Delta W|$.

Table IV-1. Time response of the MSR to a voltage step

Initial Speed (rpm)	Final Speed (rpm)	Time to achieve 95% of final speed (ms)
1000	2000	20
1000	3000	30
1000	4000	30
2000	1000	30
3000	1000	40
4000	1000	60

When stepping from W_l to W_u, the thickness of the diffusion layer (δ) decreases and any excess reactant in the hydrodynamic layer is depleted quickly as it diffuses to the electrode. The time required for this process is determined by the distance through which the reactant must diffuse. The thickness of the diffusion layer is given approximately by $\delta = 1.61\ D^{1/3}\omega^{-1/2}\nu^{1/6}$. Because of the reciprocal dependence of δ on ω, δ at 4000 rpm is less than δ at 1000 rpm. Therefore, one would expect the current to stabilize faster when stepping

from 1000 rpm to 4000 rpm than when stepping from 4000 rpm to 1000 rpm. This expected behavior was verified experimentally. In addition, the time required for the total current to stabilize following deceleration to the same rotation speed was found to be independent of the value of the upper rotation speed.

To produce a well-defined ΔI-E curve for a staircase potential waveform, especially in the regions of rapidly changing current, the potential increment should be small. The resolution of a 12-bit D/A converter is 5 mV. Therefore, an analog scaling device was constructed to increase the resolution of the D/A converter so that the potential could be set accurately even at small values of ΔE. The potential range of the D/A converter was -10 V to 9.995 V, whereas for most electrode materials, a potential range of -2.0 V to 2.0 V is sufficient. The full range of the D/A converter was utilized with the analog scaling device, thus increasing resolution. For example, if a potential of 1.0 V was to be applied at the electrode, the computer was programmed to output a signal of 1.0 V/DV (DV is the deamplification factor). If DV = 0.2, the potential output by the computer was 5.0 V. The signal output by the computer was passed through a variable deamplifier (E_{out} = DV E_{in}) then applied to the potentiostat. The actual potential applied was measured by passing the potential signal from the potentiostat through a variable amplifier ($E_{out} = E_{in}/DV$) to the A/D converter. The computer was programmed to account for the scaling factor when storing the measured potential values. For the case where DV = 0.2, the resolution of the D/A converter was 1 mV. By making the deamplification factor variable,

one could choose the factor which provided maximum resolution for each system being investigated.

Following a time delay (t_d), the current, measured at each rotation speed, was sampled N times and the values were averaged to minimize the effect of current fluctuations (i.e., noise). Each current measurement required 10 ms. Typical values of t_d and N were 150 ms and 10. Upon completion of each modulation cycle, the ΔI value was calculated and stored.

Each of the parameters discussed (i.e., ΔE, t_d, N) and data manipulation affects the total time required to complete an experiment, which in turn affects the value of ΔW and the frequency of modulation which can be applied. A thermal circuit breaker protected the motor of the rotator from overheating; therefore, if the ΔW was too large, and/or the frequency was too high, the experiment could not be completed without triggering the circuit breaker. Consequently, a compromise between ΔW and frequency was made. For example. the rotator could not be modulated between 1000 rpm and 5000 rpm at 1 Hz for a 20-min period without tripping the circuit breaker. However, modulation between 1000 rpm and 4000 rpm at 1 Hz could be applied for successive 20-min periods over 6-8 hr with minimal shutdown. Modulation between 1000 rpm and 4000 rpm was applied typically.

V. SURVEY OF ANODIC REACTIONS USING CYCLIC VOLTAMMETRY AND SQUARE-WAVE HYDRODYNAMICALLY MODULATED VOLTAMMETRY

A. Introduction

Numerous anodic reactions were examined by the application of cyclic voltammetry (CV) and square-wave hydrodynamically modulated voltammetry (QHMV). Current-potential (I-E) curves were recorded as a function of rotational velocity (ω) or potential scan rate (ϕ). The current produced by a mass-transport limited reaction increases as ω is increased according to the Levich equation

$$I = 0.62\ nFAD^{2/3}\nu^{-1/6}\omega^{1/2}C^{b}$$

Mass-transport limited current is independent of ϕ. On the other hand, the current produced by surface-controlled reactions, i.e., current limited by the area of the electrode, is dependent on ϕ and independent of ω. The dependence on ϕ is observed since the amount of charge (q) is constant for the scan of potential between two potential values. Hence, when ϕ is increased, the time necessary to pass through the potential region decreases and the instantaneous current ($I = dq/dt$) must increase. The study of electrochemical reactions is complicated when mass-transport and surface reactivity contribute simultaneously to the control of the reaction rate. The development of QHMV has made possible the extraction of the convective-coupled component from the total current. Hence, current-potential curves (ΔI-E) are simplified and the study of electrochemical reactions is facilitated. A significant advantage of QHMV is

the ability to observe mass-transport coupled reactions occurring simultaneously with O_2 evolution as well as oxide formation.

The investigation of anodic reactions electrocatalyzed by an intermediate stage of noble metal oxides was of major interest in this research project. Anodic reactions involving O-transfer mechanisms derived the most benefit from the oxide layer. Six anodic reactions will be discussed in some detail. The results obtained for the remainder of the analytes investigated are summarized briefly at the end of this section.

B. Residual Curves

The characteristic I-E and ΔI-E curves obtained for Pt, Au, Pd, and Ir electrodes in the absence of electroactive species will be described briefly. The so-called "residual curves" in acidic media are shown in Figures V-1, V-2, V-3, and V-4. The curves for Pt and Au in basic media are similar in appearance to those in acidic media, except that the potential at which reactions such as oxide formation and reduction, O_2 evolution, and H_2 evolution are observed to shift 59 mV negative per unit of pH. The practical anodic limit (E_a) of the potential scan in CV is usually considered to be that value for which the current from O_2 evolution has risen to become a significant fraction (ca. 0.2-0.5) of the analytical signal for faradaic reactions under study. The practical limit for QHMV is that value for which the error in computing ΔI is a significant fraction of the transport coupled signal of interest. The practical anodic limits observed in this research for CV and QHMV for

Figure V-1: I-E and ΔI-E curves of Pt in 0.5 M H_2SO_4

----- I-E curve

Electrode rotation speed (W): 1000 rpm

Potential scan rate (ϕ): 6 V/min

----- ΔI-E curve

Lower rotation speed (W_l): 1000 rpm

Upper rotation speed (W_u): 4000 rpm

Potential step increment (ΔE): 5 mV

Time delay (t_d): 150 ms

Number of data points (N): 10

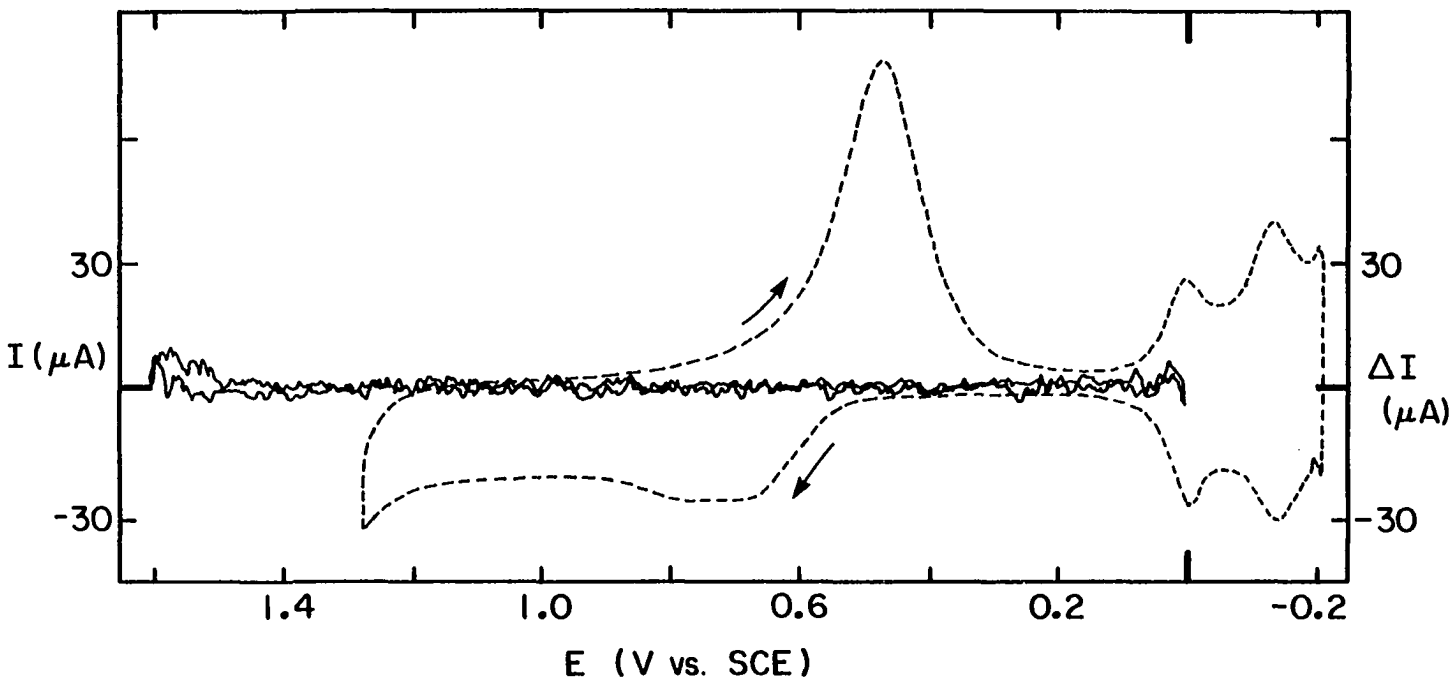
30
I (μA)
-30
30
ΔI
(μA)
-30
1.4
1.0
0.6
0.2
-0.2
E (V vs. SCE)

Figure V-2: I-E and ΔI-E curves of Pd in 0.5 M H_2SO_4

----- I-E curve

Electrode rotation speed (W): 1000 rpm

Potential scan rate (ϕ): 6 V/min

——— ΔI-E curve

Lower rotation speed (W_l): 1000 rpm

Upper rotation speed (W_u): 4000 rpm

Potential step increment (ΔE): 5 mV

Time delay (t_d): 150 ms

Number of data points (N): 10

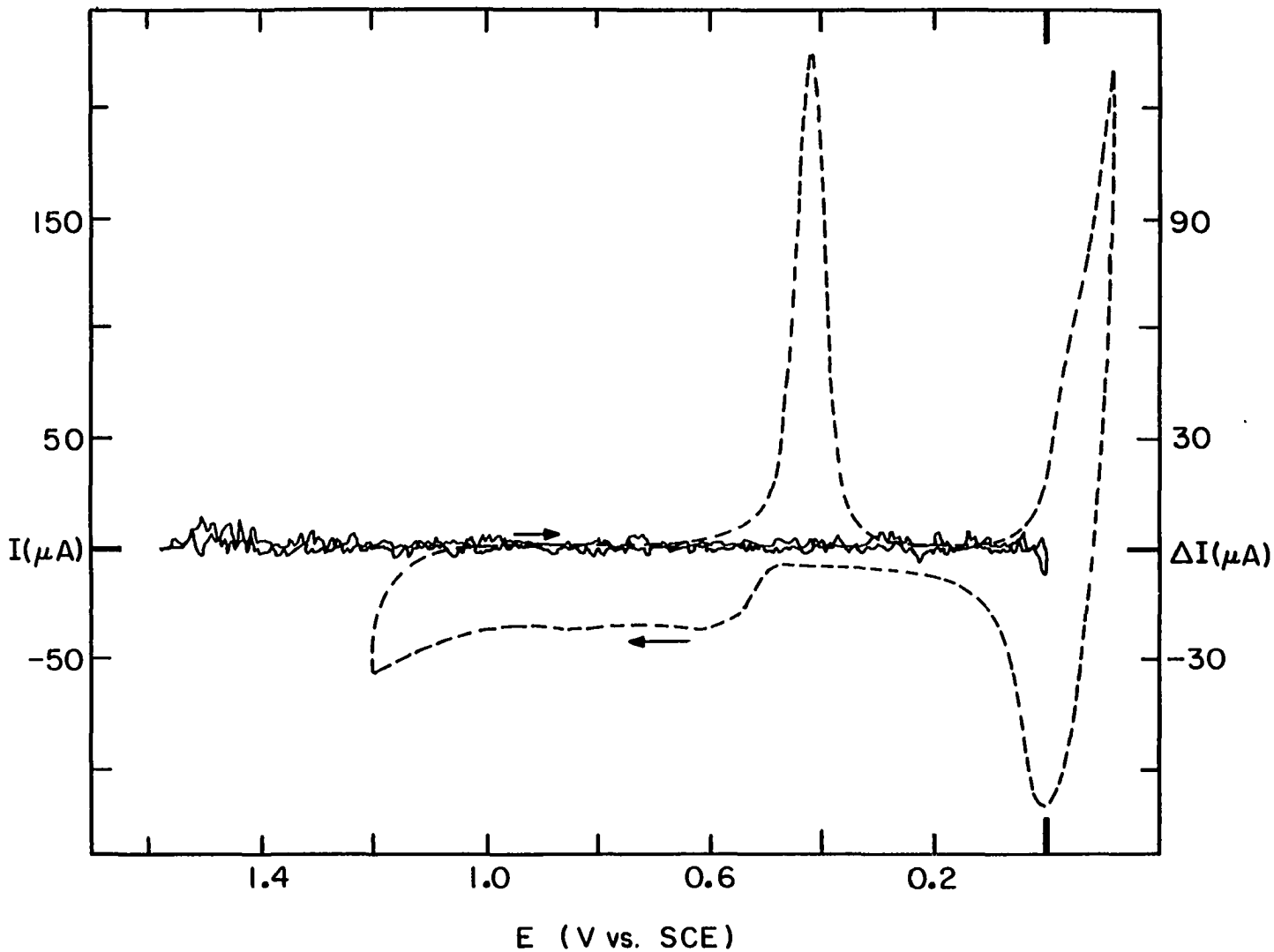
150
50
I(μA)
-50
90
30
ΔI(μA)
-30
1.4
1.0
0.6
0.2
E (V vs. SCE)

Figure V-3: I-E and ΔI-E curves of Au in 0.5 M H_2SO_4

----- I-E curve

Electrode rotation speed (W): 1000 rpm

Potential scan rate (ϕ): 6 V/min

——— ΔI-E curve

Lower rotation speed (W_l): 1000 rpm

Upper rotation speed (W_u): 4000 rpm

Potential step increment (ΔE): 5 mV

Time delay (t_d): 150 ms

Number of data points (N): 10

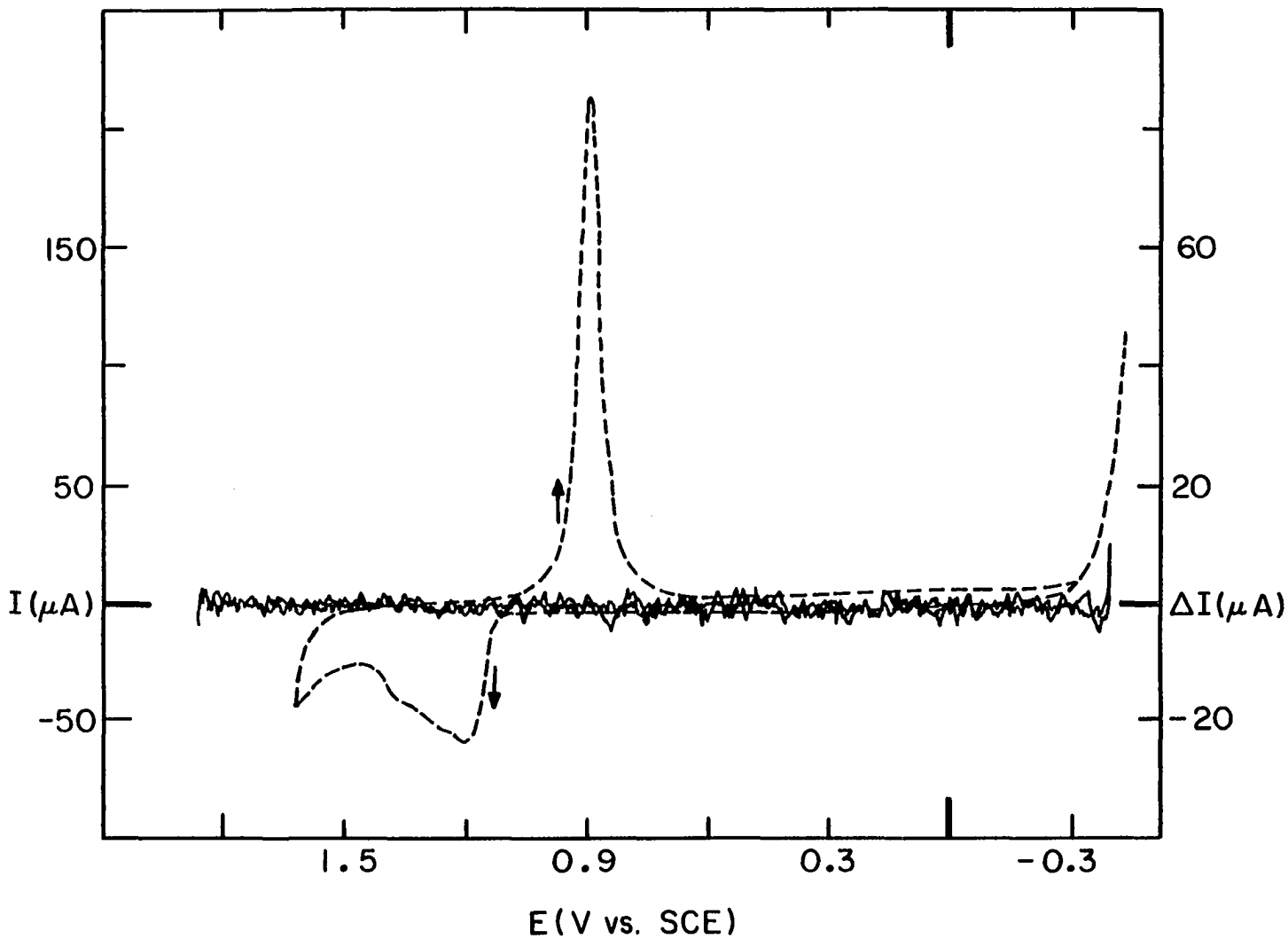
150
50
-50
I(μA)
60
20
-20
ΔI(μA)
1.5
0.9
0.3
-0.3
E(V vs. SCE)

Figure V-4: I-E and ΔI-E curves of Ir in 5.0 M H_2SO_4

----- I-E curve

Electrode rotation speed (W): 1000 rpm

Potential scan rate (ϕ): 6 V/min

——— ΔI-E curve

Lower rotation speed (W_l): 1000 rpm

Upper rotation speed (W_u): 4000 rpm

Potential step increment (ΔE): 5 mV

Time delay (t_d): 200 ms

Number of data points (N): 25

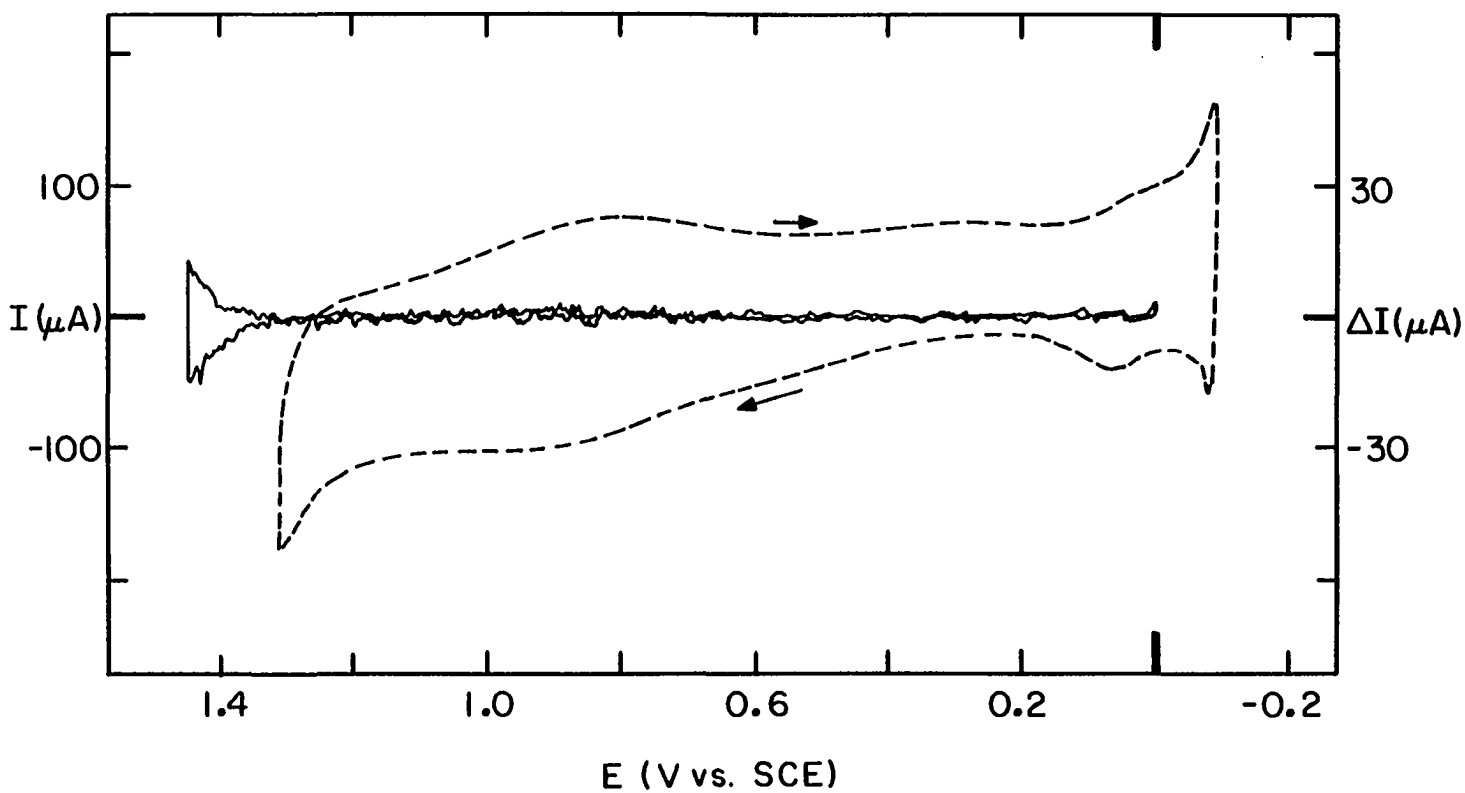
100
I (μA)
-100
30
ΔI(μA)
-30
1.4
1.0
0.6
0.2
-0.2
E (V vs. SCE)

each electrode are listed in Table V-1. Note that for QHMV, the anodic potential limit is extended approximately 150-400 mV beyond the limit for CV depending upon the electrode material.

Table V-1. Practical anodic potential limits for CV and QHMV.

Electrode Material	Electrolyte	Anodic Potential Limit (V vs. SCE)		Extension of E_a by QHMV (mV)
		CV[a]	QHMV[b]	
Pt	0.5 M H_2SO_4	1.3	1.65	350
	0.1 M NaOH	0.6	1.0	400
Au	0.5 M H_2SO_4	1.6	1.85	250
	0.1 M NaOH	0.6	0.9	300
Pd	0.5 M H_2SO_4	1.2	1.6	400
Ir	5 M H_2SO_4	1.3	1.45	150

[a] The potential at which the current from O_2 evolution is a significant fraction (ca. 0.2-0.5) of the analytical signal for faradaic reactions under study.

[b] The potential for which the error in computing ΔI is a significant fraction of the transport coupled signal of interest.

The residual I-E curve for a Pt electrode in 0.5 M H_2SO_4 is shown in Figure V-1. The small anodic current observed in the region 0.1 V < E < 0.55 V during the positive scan of potential is due to charging of the double-layer. At E > 0.55 V, surface oxide is formed: PtOH in the region 0.55 V < E < 0.81 V and PtO at E > 0.81 V. Appreciable O_2 evolution occurs at E > 1.25 V. During the negative scan of potential,

reduction of the surface oxide occurs yielding the large cathodic peak at E_p = 0.48 V. The formation and dissolution of adsorbed atomic H occurs on the cathodic and anodic scans, respectively, for 0.1 V > E > -0.2 V. Molecular H_2 is evolved at E < -0.2 V.

The processes occurring at a Pd electrode parallel those on Pt; however, the shape of the I-E curve is unique to Pd (Figure V-2). Double-layer charging current occurs in the region 0.2 V < E < 0.5 V followed by formation of Pd oxide at E > 0.5 V. The evolution of O_2 commences at E > ca. 1.15 V. Reduction of Pd oxide occurs at E_p = 0.41 V producing a sharper peak than observed for Pt. No characteristic peaks are observed for the adsorption of H on Pd owing to the complicating factor that H atoms not only adsorb on Pd but also absorb into the metal.

The useful potential range for CV at Au is broader than for either Pt or Pd (Figure V-3). The double-layer region extends from -0.4 V < E < 0.8 V during the positive scan of potential. Oxidation of the Au surface occurs at E > ca. 0.8 V. The anodic wave produced by oxidation of Au to AuOH in the potential region 0.80 V < E < 1.06 V is observed only at high current sensitivities. The conclusion that AuOH is produced is supported by results obtained utilizing nonelectrochemical methods (64, 65, 68). The anodic wave observed at E > 1.06 V is produced by the formation of AuO. Oxygen evolution begins at ca. 1.5 V. The Au oxide is reduced rapidly with E_p = 0.88 V. Continuing the negative potential scan, only double-layer charging current is observed in the region 0.7 V > E > -0.4V and reduction of H^+ occurs at E < -0.4 V. Adsorption of H atoms on Au is minimal; therefore, cathodic and anodic waves for

generation and dissolution of adsorbed H are not observed.

An electrolyte solution of 5 M H_2SO_4 was utilized for voltammetric studies at an Ir electrode. The highly acidic electrolyte minimizes the continuous buildup of oxide which occurs in less-concentrated acidic electrolytes with each subsequent cycle of potential. The residual I-E curve for Ir is shown in Figure V-4. The anodic dissolution of adsorbed H from the surface produces the current peaks at -0.08 V and 0.06 V on the anodic scan of potential. At E > 0.16 V, oxidation of the Ir surface occurs. Evolution of O_2 begins at ca. 1.25 V. During the negative scan of potential, no sharp peak is observed for cathodic dissolution of oxide. Instead, reduction of the oxide occurs over a broad range of potential overlapping with the region of the H adsorption wave.

C. Anodic Reactions

1. Arsenic(III)

The electro-oxidation of As(III) at a Pt electrode has been studied in detail by several researchers (23-25, 48, 98, 99). Arsenic ions adsorb on Pt and exhibit an inhibitory effect on the anodic formation of surface oxide (25, 48). Arsenic(III) is oxidatively desorbed as As(V). Zakharov and Songina (23), Lown and Johnson (24), and Cabelka et al. (25) reported that the mechanism of As(III) oxidation involves the transfer of an O-atom from the oxide to the As(III) species as indicated schematically by

$$PtO[O] + As(OH)_3 \longrightarrow PtO + OAs(OH)_3$$

The I-E curve recorded for As(III) is shown in Figure V-5a. Although the oxidation of As(III) is thermodynamically allowed at $E > 0.32$ V, no current was observed until ca. 0.75 V. An anodic, peak-shaped wave (A) was produced at $E > 0.75$ V and is attributed to three concurrent processes: 1) oxidation of the Pt surface, 2) oxidation of adsorbed As(III), and 3) oxidation of As(III) transported to the electrode surface by convective-diffusion. Note that oxide formation was suppressed by ca. 150 mV due to the presence of adsorbed As(III). Maximum current was obtained during the positive scan of potential at ca. 0.85 V. A steady decrease in anodic current was observed for $E > 0.85$ V owing principally to the loss of current produced by the oxidation of adsorbed As(III). Upon reversal of the potential scan at $E_a = 1.3$ V, an anodic current plateau was observed in the region $1.2 \text{ V} < E < 0.7$ V. Peak B corresponds to the reduction of Pt oxide. The shoulder on the falling edge of the oxide reduction peak (C) is due to the underpotential deposition of As(V).

Current-potential curves recorded as a function of ω at a constant value of ϕ indicated that the oxidation of As(III) was dependent upon ω, although plots of I vs. $\omega^{\frac{1}{2}}$ were nonlinear. A series of I-E curves was recorded while varying ϕ at a constant value of ω. The height of peak A varied with changes in ϕ; hence, surface-controlled reactions, i.e., oxide formation and oxidative desorption of As(III), are occurring simultaneously with the transport-coupled oxidation of As(III). The magnitude of the current plateau observed in the region $1.2 \text{ V} < E < 0.7$ V during the negative scan of potential was independent of ϕ; however, the

Figure V-5: I-E and ΔI-E curves of 0.5 mM As(III) in 0.5 M H_2SO_4 at a Pt RDE

a. I-E curve

Electrode rotation speed (W): 1000 rpm

Potential scan rate (ϕ): 6 V/min

b. ΔI-E curve

Lower rotation speed (W_l): 1000 rpm

Upper rotation speed (W_u): 4000 rpm

Potential step increment (ΔE): 5 mV

Time delay (t_d): 150 ms

Number of data points (N): 10

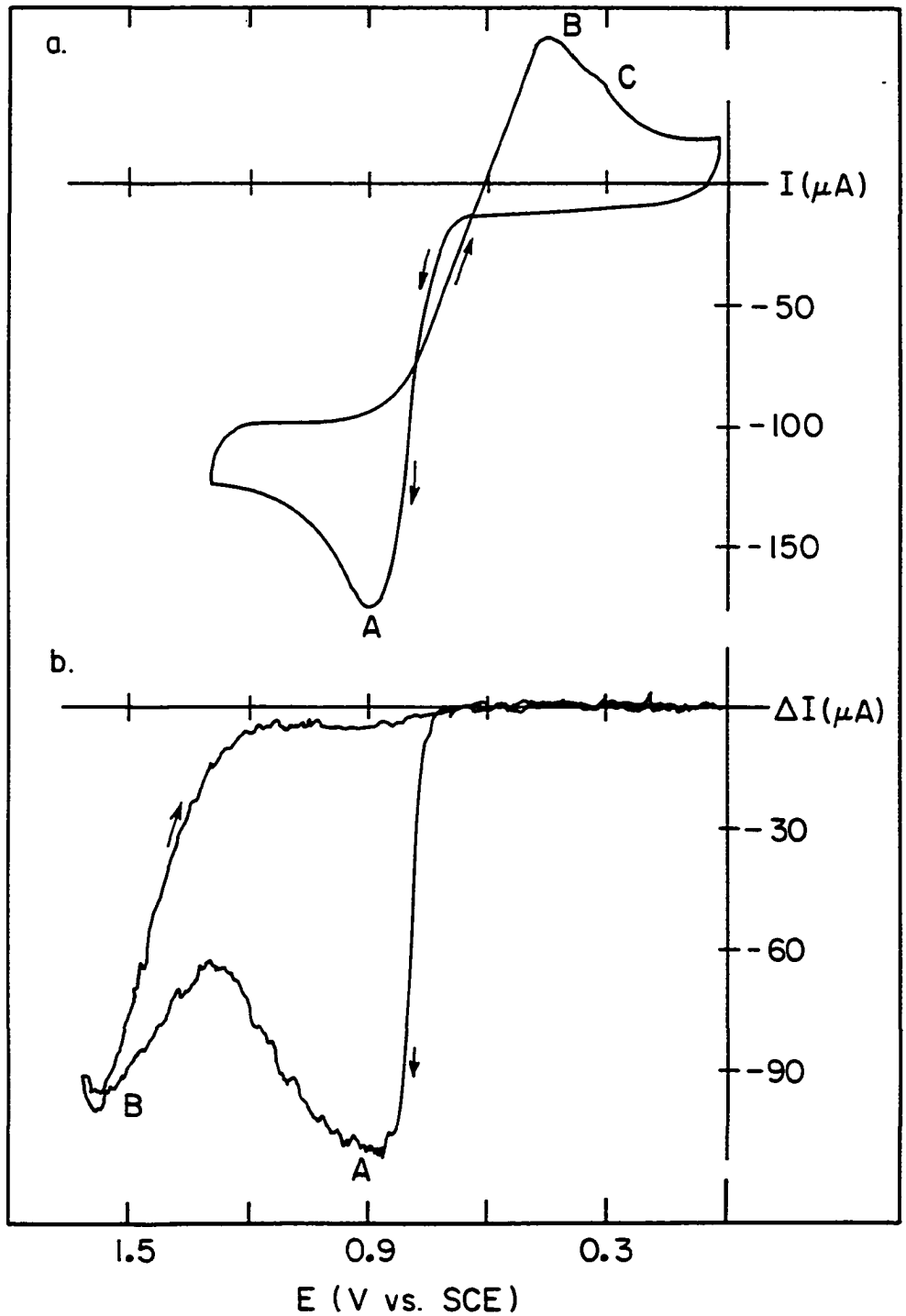
a.
B
C
I (μA)
-50
-100
-150
A
b.
ΔI (μA)
-30
-60
-90
B
A
1.5
0.9
0.3
E (V vs. SCE)

current magnitude was much less than the predicted transport-limited value. Hence, the reaction is under mixed transport and kinetic control.

Wave A is comprised of three simultaneous processes, two of which are independent of ω; hence, the transport-coupled component of total current can be extracted by the application of QHMV (Figure V-5b). During the positive scan of potential, a large anodic wave (A) was observed corresponding to the oxidation of As(III) to As(V) with a maximum value attained in the region 0.8 V < E < 0.9 V. As the positive scan of potential continued, ΔI decreased steadily; however, as the potential was increased beyond 1.25 V, ΔI in region B increased and approached the maximum value observed for wave A. Upon reversal of the potential scan, the mass-transport coupled oxidation of As(III) continued as long as O_2 was being evolved. A ΔI plateau was observed in the region 1.2 V < E < 0.9 V for the oxidation of As(III). The magnitude of ΔI in this region was dependent upon E_a; as E_a became more positive, ΔI decreased.

The rising portion of the anodic wave was analyzed by measuring the value of $E_{2/3} - E_{1/3}$. The predicted value for a reversible reaction is $E_{2/3} - E_{1/3} = 0.0356/n$. Therefore, if n = 2, a value of 17.8 mV is expected. The observed value of $E_{2/3} - E_{1/3}$ was 20 mV; hence, the reaction of As(III) to As(V) is virtually reversible. However, recall that the theoretical E^0 for the As(V)/As(III) half reaction is 0.32 V. A reaction appearing to be reversible but occurring at an overpotential (η) of 400 mV can only be rationalized in terms of electrocatalysis caused by a potential dependent change in activity of the electrode

surface. The anodic formation of surface oxide is inhibited by the presence of adsorbed As(III). Adsorbed As(III) is oxidatively desorbed by a mechanism concluded to involve O-atom transfer from PtOH to the As-species (25, 48). When a small amount of the adsorbed As(III) is desorbed, corresponding bare Pt sites are rapidly converted to PtOH which has a consequential accelerating effect on the reaction of the remainder of adsorbed As(III). Furthermore, oxidation of As(III) from the bulk solution is initiated also by the production of PtOH.

The oxidation of As(III) at a Au electrode has been examined by Zakharov et al. (41) and Loucka (99). Arsenic(III) adsorbs on Au; however, not to the extent of the adsorption on Pt. The I-E curve for As(III) on Au is shown in Figure V-6a. Wave A ($E_{\frac{1}{2}}$ = 0.82 V) was the result of oxidation of As(III) to As(V). A limiting current plateau was observed in the region 0.9 V < E < 1.1 V. The small peak observed at E_p = 0.85 V was the result of the oxidative desorption of As(III). At E > 1.1 V, oxidation of the Au surface, i.e., the formation of AuO, occurred followed by a decrease in anodic current below the limiting value for As(III). When the scan direction was reversed, anodic current rapidly decreased; no current plateau was observed for As(III) oxidation on Au as was observed for As(III) oxidation during the negative scan on Pt. Reduction of Au oxide commenced at ca. 0.95 V.

The ΔI-E curve obtained for As(III) oxidation at a Au electrode is shown in Figure V-6b. During the positive scan of potential, an anodic wave (A) was observed. A limiting value of current was attained in the region 0.95 V < E < 1.15 V. At E > 1.15 V, ΔI decreased rapidly to a

Figure V-6: I-E and ΔI-E curves of 0.5 mM As(III) in 0.5 M H_2SO_4 at a Au RDE

a. I-E curve

Electrode rotation speed (W): 1000 rpm

Potential scan rate (ϕ): 6 V/min

b. ΔI-E curve

Lower rotation speed (W_l): 1000 rpm

Upper rotation speed (W_u): 4000 rpm

Potential step increment (ΔE): 5 mV

Time delay (t_d): 150 ms

Number of data points (N): 10

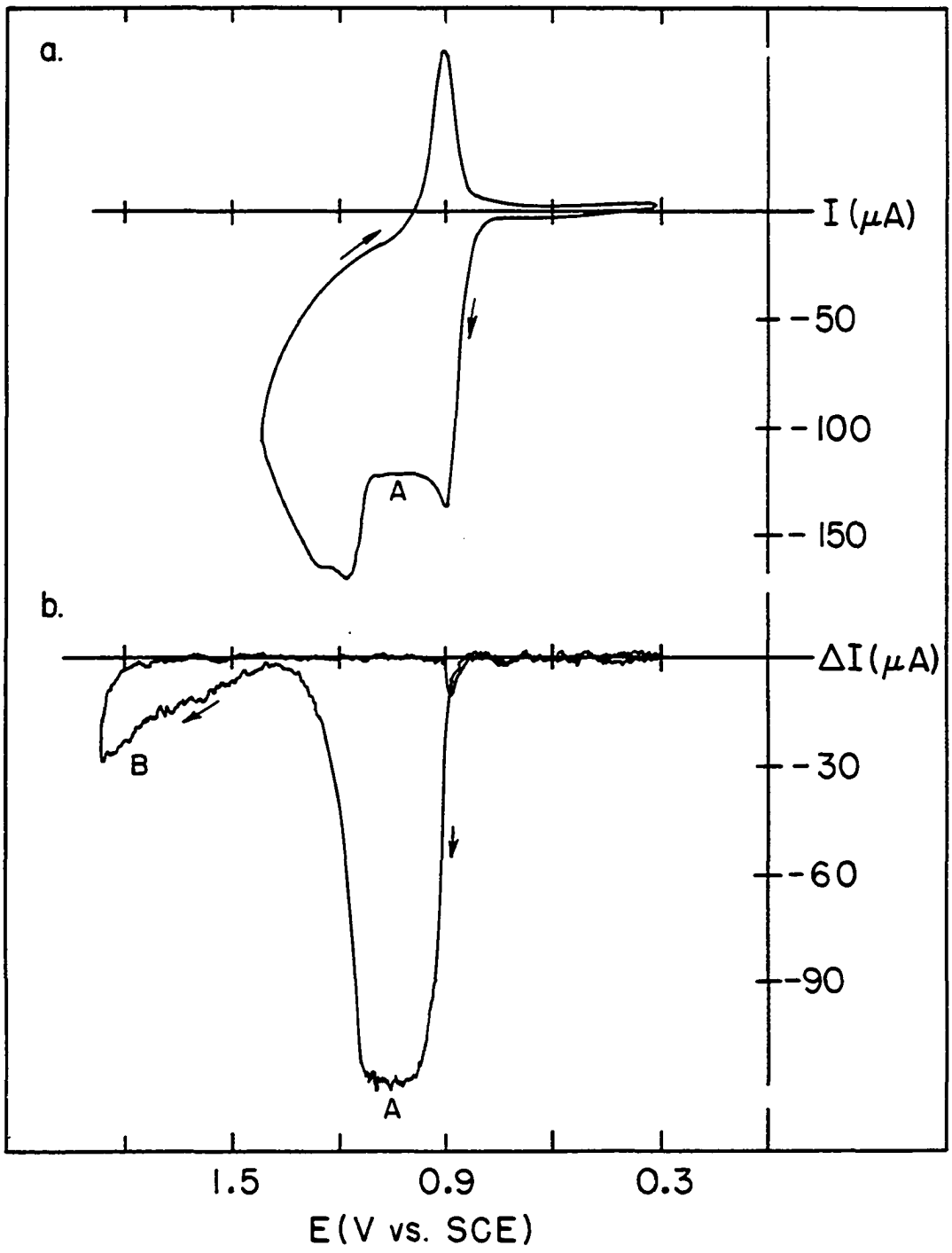
a.
I (μA)
-50
-100
-150
A
b.
ΔI (μA)
-30
-60
-90
B
A
1.5
0.9
0.3
E (V vs. SCE)

near-zero value. However, at E > 1.40 V, ΔI increased linearly with potential (region B). The maximum ΔI attained at 1.85 V was ca. 23% of the theoretical value of ΔI_{lim} observed in region A. Upon reversal of the potential scan, ΔI decreased rapidly to zero. Anodic ΔI was observed following the reduction of Au oxide, the magnitude of which was dependent upon E_a.

The electro-oxidation of As(III) at a Au electrode produced an anodic wave with $E_{2/3} - E_{1/3} = 10$ mV; hence, the reaction was concluded to be virtually reversible. However, the reaction does not occur until the potential is 150 mV more positive than the E^0 for this reaction. Once again, electrocatalysis of the reaction is concluded to occur, presumably through the involvement of adsorbed OH radicals on Au. The formation of AuOH proceeds at E > 0.8 V. The value of ΔI remained at the mass-transport limited value until the formation of AuO occurred at E > ca. 1.1 V. The inhibitory effect exhibited by AuO is much greater than the inhibitory effect observed for As(III) oxidation at a Pt electrode. The observed difference in behavior of As(III) at Au and Pt may be attributed to a low surface density of OH species adsorbed on AuO. Also, the strength of the Au-O bond may preclude direct O-atom transfer and AuO cannot participate in the oxidation of As(III). An increase in ΔI was observed concurrently with an increase in surface density of $(OH)_{ads}$, i.e., as O_2 evolution commenced at ca. 1.4 V and subsequently, as the formation of a highly hydrated Au(III) species, $Au(OH)_3$, occurred. Upon scan reversal, ΔI rapidly diminished to zero and remained at zero until Au oxide was reduced ca. 0.88 V, giving a

small anodic ΔI.

2. Nitrite

The I-E curves for NO_2^- at Pt and Au (Figures V-7 and V-8) appear, at first glance, quite similar to the I-E curves obtained for As(III) at Pt and Au (see Figures V-5 and V-6). Further voltammetric investigation of NO_2^- oxidation demonstrated both similarities and differences with the anodic behavior of As(III). Nitrite oxidation during the positive scan of potential occurred concomitantly with the initial stage of surface oxidation. No mass-transport coupled oxidation of NO_2^- occurred simultaneously with O_2 evolution on Pt; however, renewal of the oxidative process for NO_2^- occurred concurrently with O_2 evolution at a Au electrode. The literature available for the electro-oxidation of NO_2^- on Pt and Au is sparse. However, Guidelli et al. (100), who examined the oxidation of NO_2^- on Pt, and Erlikh et al. (42), who studied NO_2^- on Au, concluded that NO_2^- oxidation involves the interaction of active surface oxygen (PtOH and AuOH) and passivation is due to further oxidation of the oxides to a less active form (PtO and AuO).

No current was observed for oxidation of NO_2^- for $E < 0.8$ V at a Pt electrode (Figure V-7a) due to the suppression of oxide formation caused by the presence of adsorbed NO_2^-. At $E > 0.8$ V on the positive scan, a large, anodic, peak-shaped wave (A) was observed with maximum current at $E =$ ca. 1.03 V. The anodic wave is comprised of three components: 1) oxidation of the Pt surface, 2) oxidation of adsorbed NO_2^-, and 3) oxidation of NO_2^- transported to the electrode by convective-diffusion. As the positive scan of potential was continued,

Figure V-7: I-E and ΔI-E curves of 0.5 mM NO_2^- in 0.5 M H_2SO_4 at a Pt RDE

a. I-E curve

Electrode rotation speed (W): 1000 rpm

Potential scan rate (ϕ): 6 V/min

b. ΔI-E curve

Lower rotation speed (W_l): 1000 rpm

Upper rotation speed (W_u): 4000 rpm

Potential step increment (ΔE): 5 mV

Time delay (t_d): 150 ms

Number of data points (N): 10

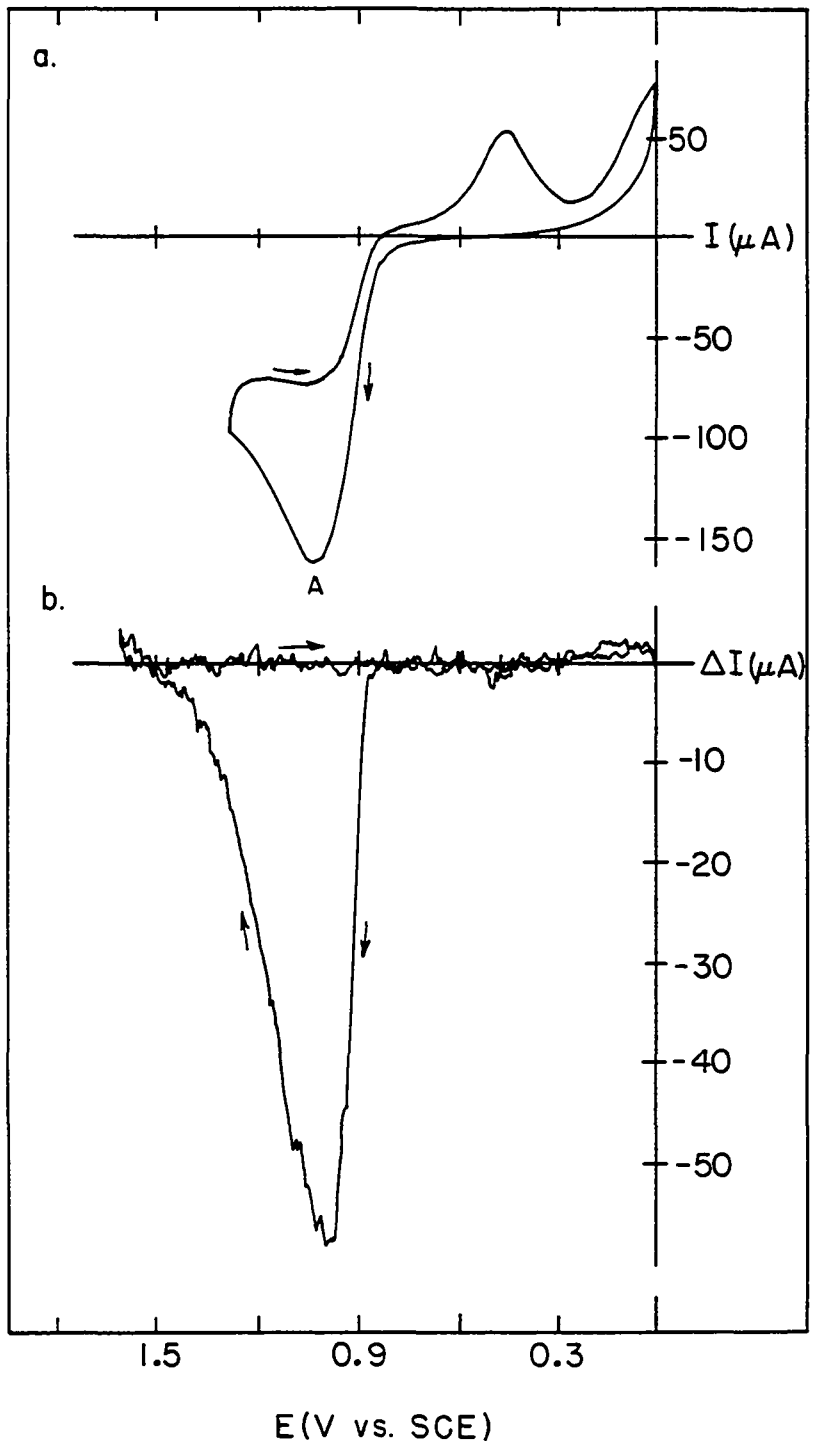
a.
50
I (μA)
-50
-100
-150
A
b.
ΔI (μA)
-10
-20
-30
-40
-50
1.5
0.9
0.3
E(V vs. SCE)

Figure V-8: I-E and ΔI-E curves of 0.5 mM NO_2^- in 0.5 M H_2SO_4 at a Au RDE

a. I-E curve

Electrode rotation speed (W): 1000 rpm

Potential scan rate (ϕ): 6 V/min

b. ΔI-E curve

Lower rotation speed (W_l): 1000 rpm

Upper rotation speed (W_u): 4000 rpm

Potential step increment (ΔE): 5 mV

Time delay (t_d): 150 ms

Number of data points (N): 10

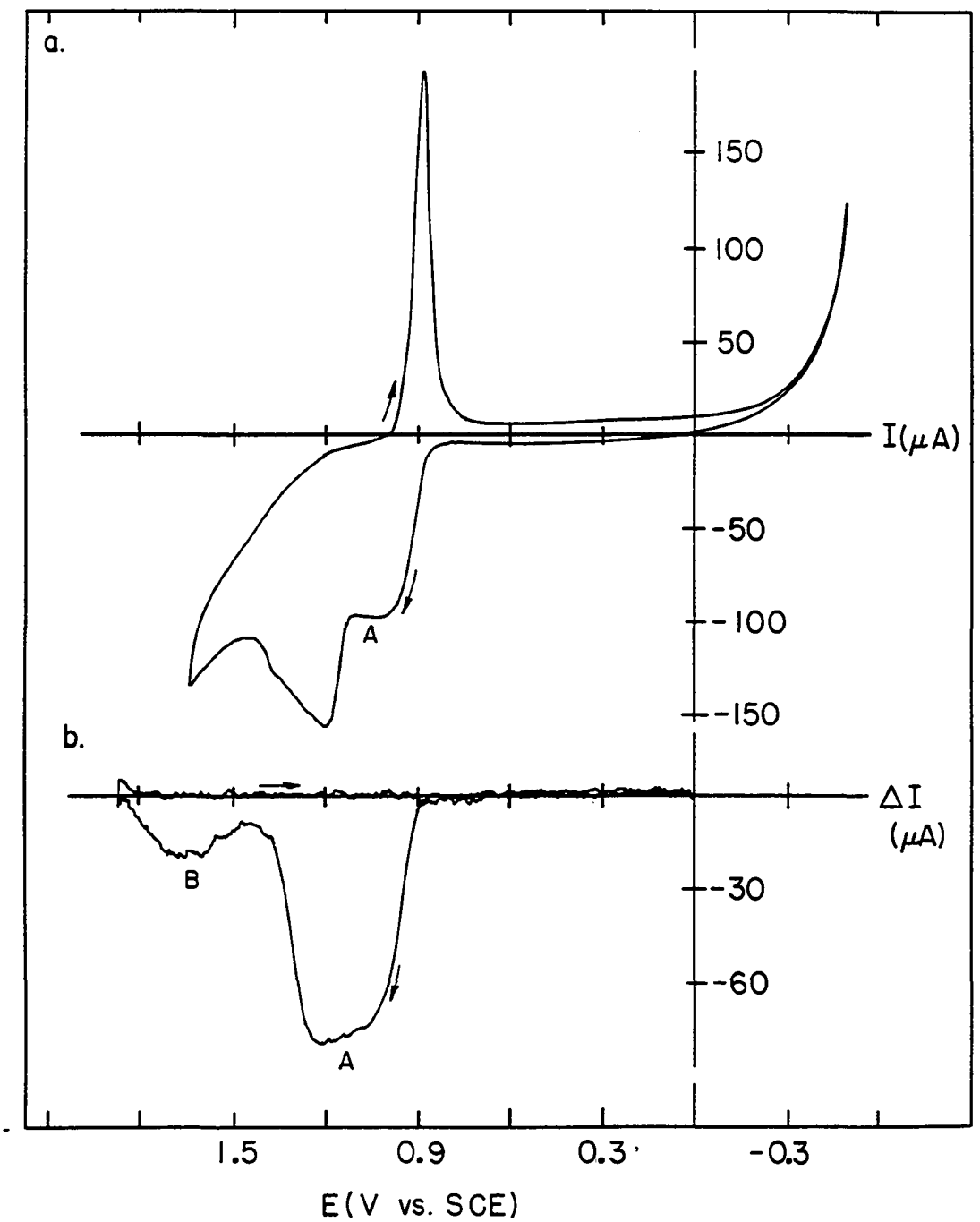
a.
150
100
50
I(μA)
-50
-100
-150
A
b.
ΔI
(μA)
B
-30
-60
A
1.5
0.9
0.3
-0.3
E(V vs. SCE)

anodic current decreased steadily caused by the loss of the contribution from the oxidation of adsorbed NO_2^-. The anodic current observed in the region 1.2 V > E > 1.0 V during the negative scan of potential was less than the value predicted by the Levich equation.

A series of I-E curves was recorded as a function of ω at a constant value of ϕ. The oxidation of NO_2^- was dependent upon the value of ω; however, a plot of I vs. $\omega^{\frac{1}{2}}$ was not linear. Current-potential curves were also recorded at various values of ϕ for a given value of ω. Wave A was dependent upon ϕ, as well as ω, indicating that surface-controlled reactions were occurring simultaneously with NO_2^- oxidation.

The ΔI-E curve obtained by QHMV is shown in Figure V-7b. A large anodic wave was observed during the positive scan of potential which reached a maximum value at E = ca. 1.0 V. At E > 1.0 V, ΔI steadily decreased, reaching zero at ca. 1.5 V. No additional transport-coupled current occurred during the remainder of the positive potential scan. The magnitude of ΔI observed during the subsequent negative scan was highly dependent upon E_a. For E_a > 1.45 V, ΔI was zero throughout the negative potential scan. For E_a < 1.45 V, an anodic ΔI was observed in the region 1.45 V > E > 0.90 V. The value of ΔI increased as E_a was made more negative.

The oxidation of NO_2^- has been concluded to occur by the electrocatalytic involvement of OH radicals on the Pt surface. The E^0 value for the NO_3^-/NO_2^- half reaction is 0.70 V. No appreciable current was observed until η > 150 mV. Nitrite ions adsorb on Pt and inhibit the formation of surface oxides. Adsorbed NO_2^- is oxidatively desorbed by

a mechanism concluded to involve O-atom transfer from PtOH to the NO_2^- species. When a small amount of adsorbed NO_2^- is desorbed, the associated Pt sites are rapidly converted to PtOH. An accelerating effect then is exhibited on the reaction of the remainder of adsorbed NO_2^-. In addition, the oxidation of NO_2^- from the bulk solution is initiated by the presence of PtOH. Conversion of PtOH to PtO results in a decrease of NO_2^- oxidation at E > ca. 1.0 V. Oxygen evolution appears to have no catalytic effect on the mass-transport coupled anodic reaction of NO_2^-.

The I-E curve obtained for NO_2^- at a Au electrode is shown in Figure V-8a. An anodic wave (A) was produced during the positive scan at E > 0.9 V, as the result of the oxidation of NO_2^- to NO_3^-, and a limiting current plateau was attained in the region 0.95 V < E < 1.1 V. At E > 1.1 V, bulk oxidation of the Au surface occurred simultaneously with NO_2^- oxidation. Upon reversal of the potential scan, the anodic current steadily decreased. The Au oxide was reduced with E_p = 0.88 V.

A series of curves recorded as a function of ω at a given value of ϕ demonstrated that the anodic current plateau was dependent upon ω; however, the plot of I vs. $\omega^{\frac{1}{2}}$ was not linear. Variation of ϕ at a constant value of ω demonstrated that the anodic current plateau was independent of ϕ.

Two anodic waves were observed upon application of QHMV (Figure V-8b). The first wave (A) corresponded to the production of NO_3^-; however, the predicted ΔI_{lim} was not attained. At E > 1.25 V, ΔI decreased; however, at E > 1.45 V an increase in ΔI was observed (B)

but which did not exceed 23% of the value for wave A. For E = 1.85 V, no ΔI was observed during the negative scan of potential; however, at less positive E_a values, a small increase in anodic ΔI was observed at E < 0.95 V, i.e., NO_2^- oxidation was renewed upon reduction of Au oxide.

The E^0 for the NO_3^-/NO_2^- half reaction is 0.70 V. No current for the oxidation of NO_2^- was observed, however, until E > 0.8 V which corresponds with the potential at which the formation of AuOH proceeds. Hence, NO_2^- oxidation is concluded to be catalyzed by AuOH. The formation of AuO at ca. 1.1 V inhibits the oxidation of NO_2^-. This observation is in agreement with the results reported by Erlikh et al. (42). In contrast to the behavior observed at a Pt electrode, renewed oxidation was observed at a Au electrode simultaneously with O_2 evolution. Furthermore, an interesting similarity was observed in comparison to As(III) oxidation at a Au electrode. The anodic ΔI observed for both NO_2^- and As(III) concomitantly with O_2 evolution was 23% of the anodic ΔI value attained in the region 0.95 V < E < 1.1 V. The resulting increase in anodic ΔI may be attributed to flaking of Au_2O_3 from the electrode surface exposing Au metal sites. Reformation of Au_2O_3 and/or evolution of O_2 would occur at these sites which would be expected to have a similar catalytic effect on the oxidation of NO_2^- and As(III).

3. Iodide

Since the oxidation of I^- at a Pt electrode was chosen to be studied in greater detail, only a brief summary will be presented here to facilitate the discussion of results obtained for I^- at other noble

metal electrodes. For I-E and ΔI-E curves, see Figures VI-2 and VI-5; for a complete discussion see section VI.

The mass-transport limited production of I_2 occurs with apparent reversibility at $E_{\frac{1}{2}}$ = 0.48 V, as predicted thermodynamically. The anodic formation of surface oxide on a Pt electrode during the positive scan of potential is significantly inhibited by the presence of adsorbed I (see Figure VI-1). Adsorbed I is oxidatively desorbed as IO_3^- in the region 1.0 V < E < 1.2 V by a mechanism concluded to involve O-atom transfer from PtOH to the I species. When a small amount of adsorbed I is desorbed, the corresponding bare Pt sites are rapidly converted to more PtOH which has a consequential accelerating effect on the reaction of the remaining adsorbed I. Furthermore, oxidation of I^- from the bulk solution to IO_3^- is initiated by the production of PtOH. Unfortunately, the potential range is quite narrow over which the oxidation of I^- to IO_3^- is thermodynamically allowed, and in which PtOH exists in an appreciable quantity at the electrode surface. Rearrangement of PtOH to OHPt and further oxidation to PtO occur rapidly at E > 1.2 V and IO_3^- production is sharply suppressed. As the potential is increased beyond 1.25 V, the mass-transport limited production of IO_3^- proceeds simultaneously with O_2 evolution. The formation of IO_3^- at E > 1.25 V is attributed to the catalytic involvement of OH radicals produced on the electrode surface during O_2 evolution. Upon reversal of the potential scan, IO_3^- production proceeds as long as O_2 was evolved. At E < 1.3 V, only the transport-limited oxidation of I^- to I_2 occurs.

The oxidation of I^- in basic media at a Pt electrode was investi-

gated briefly. No anodic wave was observed for the oxidation of I^- to I_2. The simultaneous formation of IO_3^- and surface oxide produced a peak at E_p = 0.37 V. The height of this peak varied nonlinearly with $\omega^{\frac{1}{2}}$ as the result of surface-controlled reactions, i.e., the formation of surface oxide and the possible oxidative desorption of I occurring concomitantly with the mass-transport coupled production of IO_3^-. A small, single, anodic peak (E_p = 0.37 V) was observed upon application of QHMV for I^- in basic media. However, no mass-transport coupled formation of IO_3^- was observed simultaneously with O_2 evolution.

No study of the voltammetric response of I^- at Au, Ir, or Pd electrodes has been reported in the literature. The initial observations obtained upon application of CV and QHMV will be described briefly. Of major significance is the mass-transport coupled production of IO_3^- occurring simultaneously with O_2 evolution.

The I-E and ΔI-E curves for I^- at a Au electrode are shown in Figure V-9. Several anodic waves and peaks were observed during the positive scan of potential. The oxidation of I^- to I_2 proceeds with the thermodynamically predicted value of $E_{\frac{1}{2}}$ = 0.48 V to yield an anodic current plateau (A) in the region 0.58 V < E < 0.88 V. The second anodic wave (B) was observed in the region 0.88 V < E < 1.12 V and is attributed to the oxidation of I^- to HIO. Peak C is produced as the result of the anodic formation of Au oxide and, possibly, the formation of a gold-iodide surface species. Peak D is attributed to the formation of IO_3^- concomitantly with surface oxidation. Current in the region 1.4 V < E < 1.6 V corresponds to the formation of IO_3^- (E). Oxygen

Figure V-9: I-E and ΔI-E curves of 0.5 mM I^- in 0.5 M H_2SO_4 at a Au RDE

a. I-E curve

Electrode rotation speed (W): 1000 rpm

Potential scan rate (ϕ): 6 V/min

b. ΔI-E curve

Lower rotation speed (W_l): 1000 rpm

Upper rotation speed (W_u): 4000 rpm

Potential step increment (ΔE): 5 mV

Time delay (t_d): 150 ms

Number of data points (N): 10

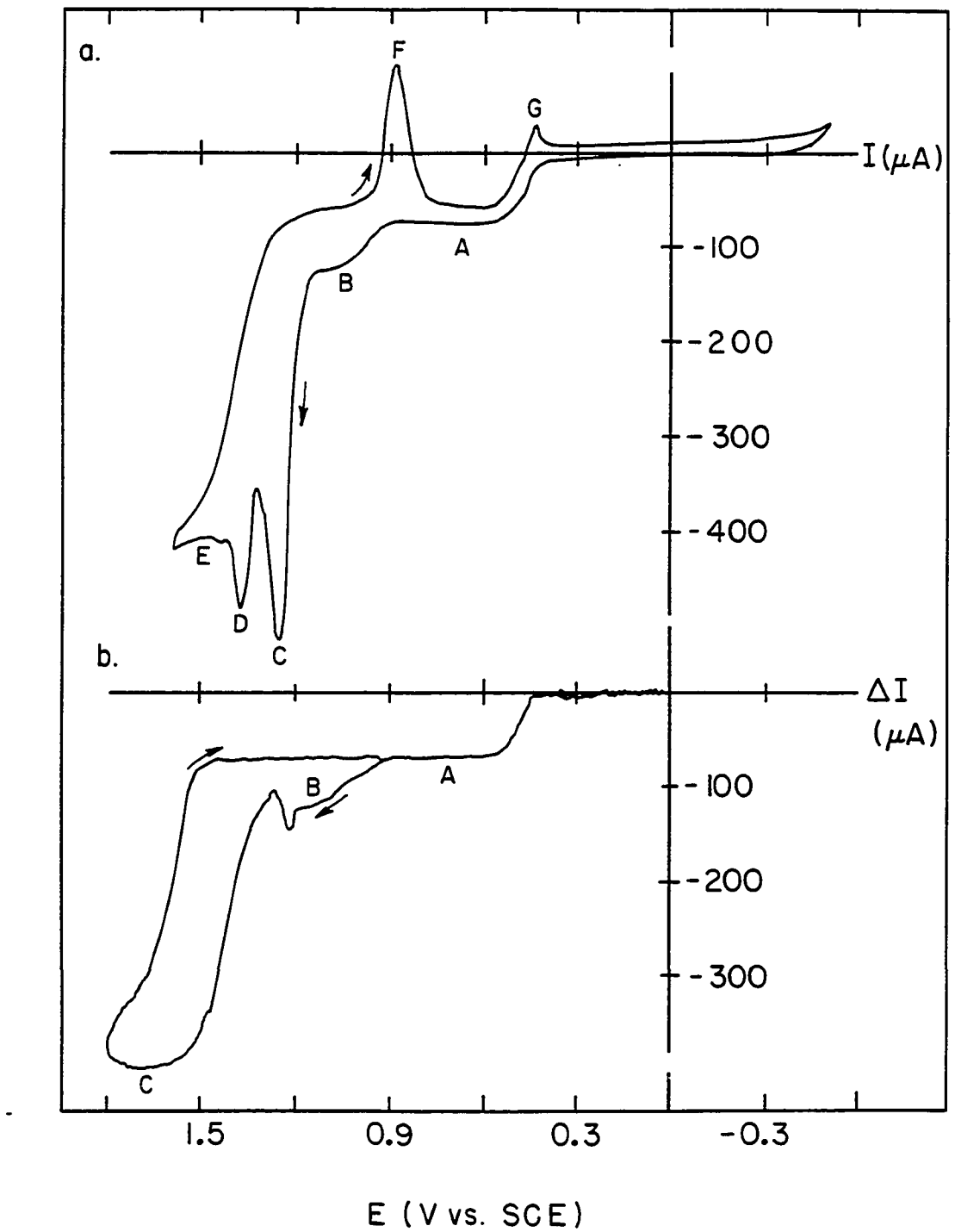
a.
F
G
I(μA)
A
B
-100
-200
-300
-400
E
D
C
b.
ΔI
(μA)
A
B
-100
-200
-300
C
1.5
0.9
0.3
-0.3
E (V vs. SCE)

evolution increased rapidly at E > 1.6 V; therefore, the potential scan was reversed at E = 1.6 V. Upon reversal of the potential scan, the formation of IO_3^- was observed in the region 1.6 V > E > 1.45 V. At E < 1.45 V, current decreased to the current plateau value attained for the oxidation of I^- to I_2 (A). The reduction of Au oxide (F) occurred with E_p = 0.88 V. Peak G is attributed to the reduction of reversibly adsorbed I_2.

Results for the variation of ω at a constant value of ϕ demonstrated that the anodic current plateau (A) varied linearly with $\omega^{\frac{1}{2}}$, as predicted by the Levich equation; hence, I_2 formation is a mass-transport limited reaction. Current owing to the oxidation of I^- to HIO (B) reached a plateau value at progressively more positive values of $E_{\frac{1}{2}}$ as ω was increased. Current in the region 1.15 V < E < 1.6 V increased nonlinearly with $\omega^{\frac{1}{2}}$ due to the surface-controlled oxidation of Au which occurred simultaneously with the transport-coupled formation of IO_3^-.

A series of I-E curves was recorded as a function of ϕ at a constant value of ω. Wave A was independent of ϕ which is the expected behavior of a mass-transport limited reaction. The $E_{\frac{1}{2}}$ of wave B shifted to more positive potential values at low ω. The height of peaks C and D varied with ϕ which is the typical response for reactions under surface control. At ϕ < 0.5 V/min, peak D was not observed. Current in the region of wave E was dependent upon ϕ because of the simultaneous formation of Au_2O_3.

The application of QHMV produced a ΔI-E curve less complex than

the corresponding I-E curve for CV. Three anodic waves were observed during the positive scan of potential. The mass-transport limited formation of I_2 (A) was observed in the region 0.55 V < E < 0.95V. The oxidation of I^- to HIO produces wave B. Wave C was observed for the oxidation of I^- to IO_3^-. A limiting value of ΔI was attained in the region 1.55 V < E < 1.75 V. The ratio of $\Delta I_C/\Delta I_A$ is 6.0 as expected based on the assigned reactions. Upon reversal of the potential scan, ΔI decreased to the limiting value observed for wave A. The limiting ΔI value for the production of I_2 was observed in the region 1.5 V > E > 0.55 V. As in the case of Pt, I_2 formation is not inhibited by the presence of surface oxides.

The oxidation of I^- at an Ir electrode was examined briefly. An electrolyte solution of 5 M H_2SO_4 was utilized to minimize the continuous buildup of oxide with repetitive potential scanning that is observed in less concentrated acidic solutions. The I-E curve obtained is shown in Figure V-10a. The anodic formation of Ir oxide commenced at E = 0.16 V. The anodic wave (A), $E_{\frac{1}{2}}$ = 0.37 V, is attributed to the oxidation of I^- to I_2. Zakharov and Songina (101) also observed that the oxidation of I^- to I_2 occurred at $E < E^0$ in highly acidic media at a Pt electrode; however, they did not offer an explanation for the phenomenon. Since this behavior is not unique to the Ir electrode, it is concluded that the highly acidic media is responsible for the observed anodic response. The cause of this behavior requires further investigation. The large residual current obscured the observation of a limiting current plateau for the production of I_2 at this concentration

Figure V-10: I-E and ΔI-E curves of 0.5 mM I^- in 5.0 M H_2SO_4 at an Ir RDE

a. I-E curve

Electrode rotation speed (W): 1000 rpm

Potential scan rate (ϕ): 6 V/min

b. ΔI-E curve

Lower rotation speed (W_l): 1000 rpm

Upper rotation speed (W_u): 4000 rpm

Potential step increment (ΔE): 5 mV

Time delay (t_d): 200 ms

Number of data points (N): 25

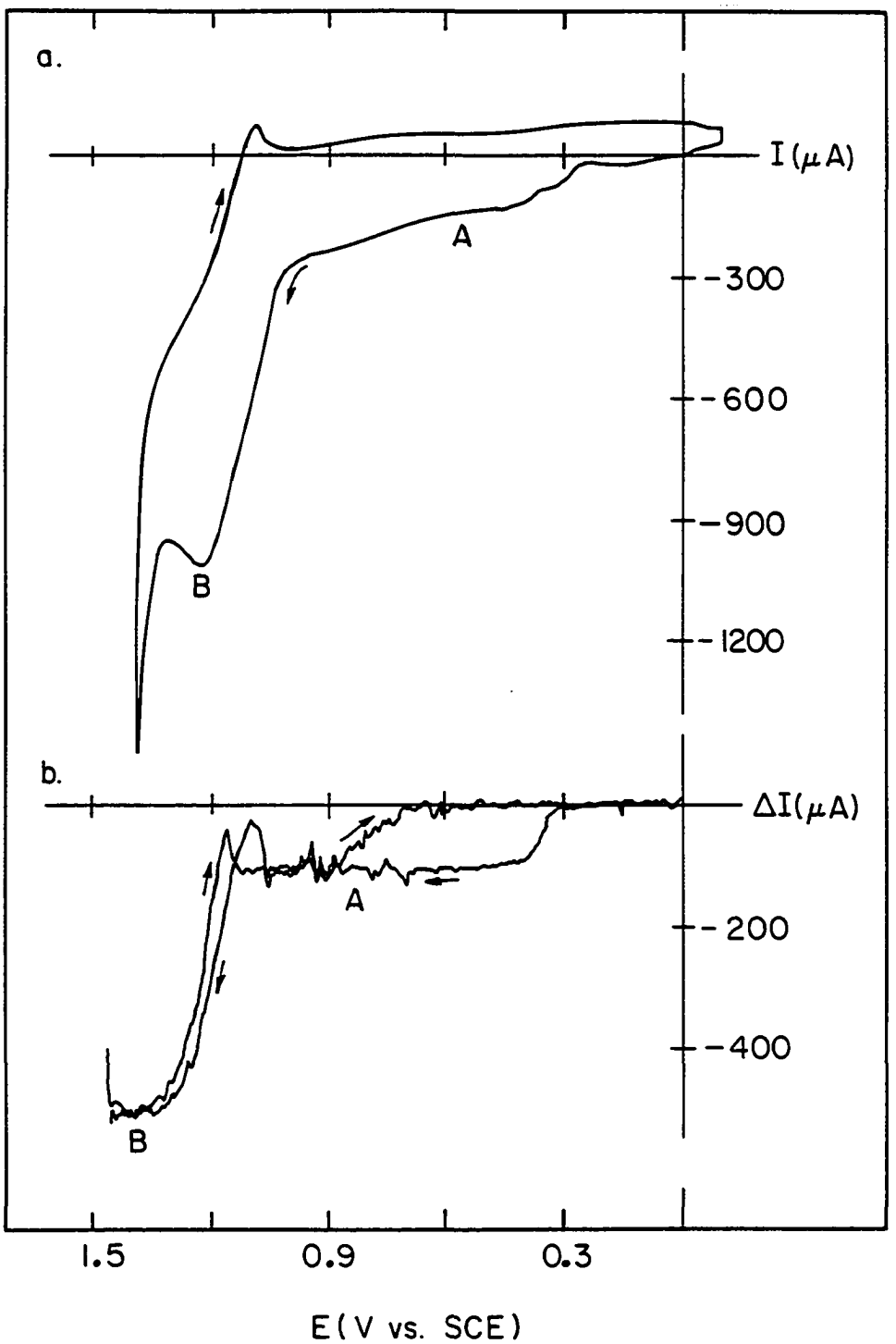
a.
I(μA)
A
-300
-600
-900
-1200
B
b.
ΔI(μA)
A
-200
-400
B
1.5
0.9
0.3
E(V vs. SCE)

of I^-. At E > 1.0 V, anodic current increased producing peak B which corresponds to the oxidation of I^- to a mixture of HIO and IO_3^-. At E > 1.28 V, anodic decomposition of the solvent became significant, therefore, the anodic potential limit was established.

Current-potential curves, recorded as a function of ϕ while holding ω constant, were not particularly informative for the evaluation of the surface dependence of the oxidative reactions of I^- since Ir oxidation occurred over the whole potential range of I^- oxidation. A series of I-E curves was recorded as a function of ω at a constant value of ϕ. Although both anodic waves were dependent upon ω, precise rotation speed data could not be obtained due to the large contribution to the total current from the formation of Ir oxide.

The application of QHMV was advantageous since the contribution to the total current from the mass-transport coupled oxidation of I^- could be isolated from the large background current produced during the formation of Ir oxide. The ΔI-E curve is shown in Figure V-10b. During the positive scan of potential, an anodic ΔI plateau (A) was observed in the region 0.3 V < E < 1.0 V corresponding to the oxidation of I^- to I_2. At E > 1.0 V, ΔI decreased; however, ΔI increased abruptly at E > 1.05 V. A limiting ΔI plateau was attained in the region 1.25 V < E < 1.45 V (B). The ratio of $\Delta I_B/\Delta I_A$ was 4.26. The ratio of ΔI values was less than 6, as predicted for the formation of IO_3^-, and was concluded to be the result of the concomitant formation of IO_3^- and an I species with a lower oxidation state than IO_3^-, presumably HIO. Upon reversal of the potential scan, the limiting value of ΔI was observed in the region

1.45 V > E > 1.3 V. The value of ΔI decreased to a minimum at ca. 1.15 V. The limiting ΔI value for the formation of I_2 was observed during the negative scan of potential in the region 1.0 V > E > 0.9 V. For E < 0.9 V, ΔI decreased to zero current at 0.6 V.

Anodic response of I^- at a Pd electrode was observed, as shown in Figure V-11a (curve 1), provided that the electrode was not anodized at E > 1.3 V. The oxidation of I^- to I_2 (A) occurred at E > 0.45 V with a limiting current plateau attained in the region 0.55 V < E < 0.9 V during the positive scan of potential. At E > 1.05 V, a sharp increase in current was observed which reached a maximum value at E_p = 1.19 V (B). This peak is produced by the concurrent oxidation of Pd and the oxidative desorption of I. Oxygen evolution was significant at E > 1.25 V. Upon reversal of the potential sweep, current decreased to a plateau in the region 1.1 V > E > 0.7 V which corresponds to the oxidation of I^- to I_2. The reduction peak (C) observed at E_p = -0.05 V is due to the reduction of irreversibly adsorbed I_2.

Current-potential curves were recorded as a function of ω while holding ϕ constant. Anodic current observed in the region of wave A increased linearly with $\omega^{\frac{1}{2}}$; therefore, the production of I_2 is a mass-transport limited reaction. The anodic current observed for E > 0.9 V was dependent upon ω as the result of the mass-transport limited formation of I_2 which occurred simultaneously with the surface-controlled formation of Pd oxide and oxidative desorption of I. Peak C was independent of ω which is indicative of a surface-controlled process.

A series of I-E curves was also recorded as a function of ϕ at a

Figure V-11: I-E and ΔI-E curves of 0.5 mM I^- in 0.5 M H_2SO_4 at a Pd RDE

a. I-E curves

Electrode rotation speed (W): 1000 rpm

Potential scan rate (ϕ): 6 V/min

1) ——— Electrode anodized at E ≤ 1.3 V

2) ----- Electrode anodized at E > 1.3 V

b. ΔI-E curve

Lower rotation speed (W_l): 1000 rpm

Upper rotation speed (W_u): 4000 rpm

Potential step increment (ΔE): 5 mV

Time delay (t_d): 150 ms

Number of data points (N): 10

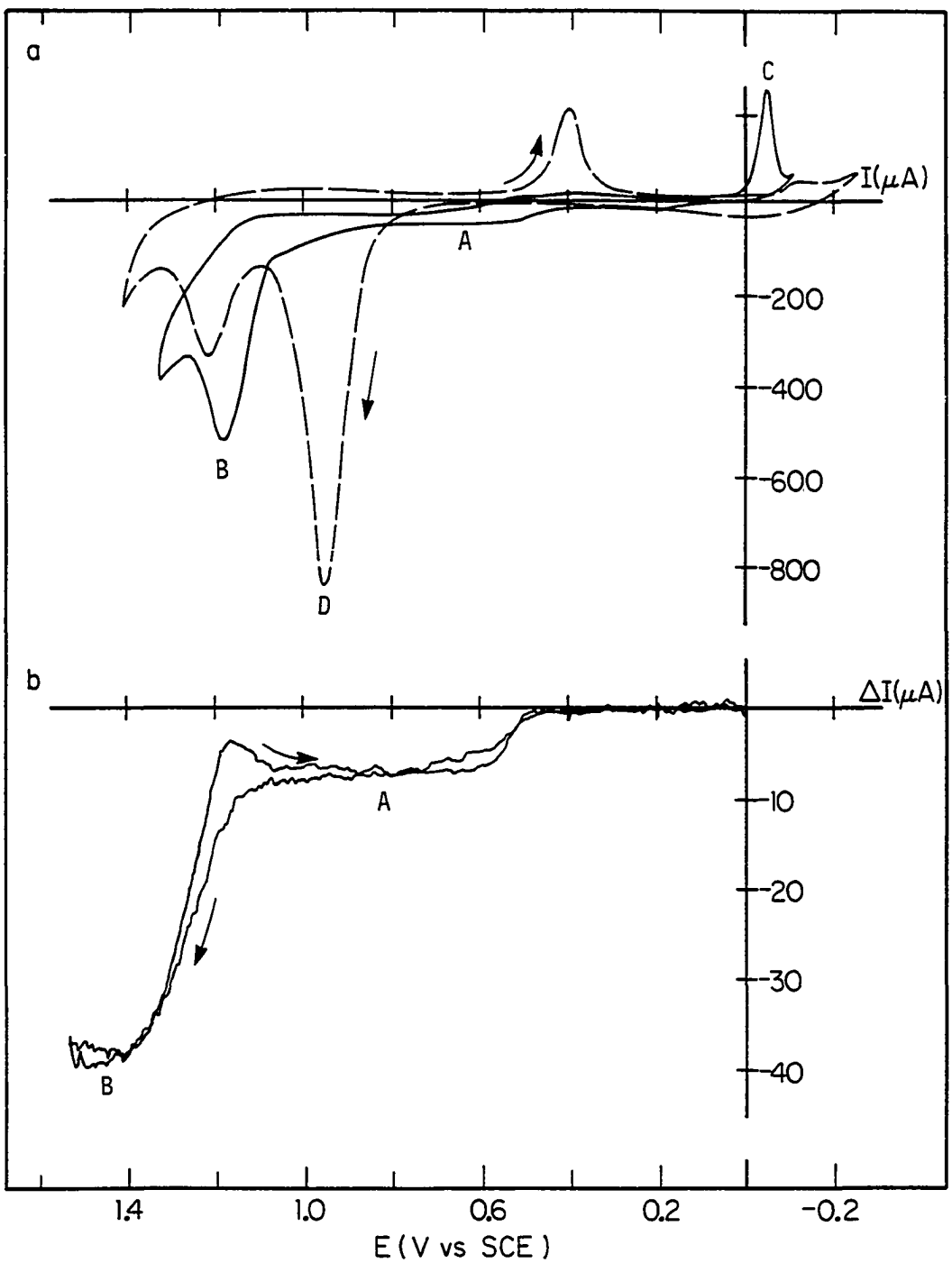
a
C
I(μA)
A
B
D
-200
-400
-600
-800
b
ΔI(μA)
A
B
-10
-20
-30
-40
1.4
1.0
0.6
0.2
-0.2
E (V vs SCE)

constant value of ω. Wave A, produced as the result of the formation of I_2, was independent of ϕ as expected for a mass-transport limited reaction. The height of peak B decreased rapidly as ϕ was decreased and, appeared only as a small shoulder on a rising wave at $\phi < 0.5$ V/min. Hence, the reaction producing IO_3^- in the potential region of peak B is a surface-controlled reaction. The height of peak C decreased and the value of E_p shifted more positive as ϕ was decreased.

The ΔI-E curve recorded for I^- at a Pd electrode is shown in Figure V-11b. A ΔI plateau (A) was observed in the region 0.55 V < E < 1.1 V which corresponds to the production of I_2. At E > 1.1 V, ΔI increased to a plateau ΔI value (B) in the region 1.4 V < E < 1.55 V. The ratio of $\Delta I_B/\Delta I_A$ was 4.74 indicating that a mixture of IO_3^- and an I species with a lower oxidation state is produced simultaneously with O_2 evolution. This behavior is similar to that observed for the further oxidation of I^- at an Ir electrode.

The anodic response of I^- at a Pd electrode is highly dependent upon the pretreatment of the electrode. If the Pd electrode was anodized at E > 1.3 V prior to cycling the potential (-0.2 V < E < 1.3 V), the I-E curve shown in Figure V-11a (curve 2) was obtained. The mass-transport limited oxidation of I^- to I_2 was not observed in the region 0.55 V < E < 0.9 V during the positive scan of potential. However, a peak (D) was produced at E_p = 0.95 V which corresponds, presumably, to the formation of PdI_2. Peak D increased with each repetitive scan of potential as the result of continuous roughening of the electrode surface through the oxidation and desorption of Pd metal which produced Pd black and thereby

increased the effective surface area of the working electrode. Anodization at E > 1.3 V provided the initial Pd black. Evidently, the mechanism of reaction changed in the presence of Pd black and the formation of PdI_2 is favored over the production of I_2. The position of peak B shifted 35 mV more positive and the height of this peak decreased gradually with repetitive scans of potential. During the negative scan of potential, peak E was observed as the result of the reduction of Pd oxide. Peak C, produced by the reduction of irreversibly adsorbed I_2, was not observed. Rotation speed and scan rate studies did not provide useful information since the height of peaks B and D changed with each consecutive scan of potential even at constant ω and ϕ.

4. Chloride

The industrial interest in chlor-alkali technology has prompted the study of the electrocatalytic effect of various noble metals and noble metal oxides on the Cl_2 evolution reaction (15, 102-117). The fundamental and applied aspects of anodic Cl_2 production are discussed by Novak, Tilak, and Conway (118). Chlor-alkali technology is reviewed by Caldwell (119), and by Venkatesh and Tilak (120).

Chloride ions strongly adsorb on Pt (15, 103, 104, 121) with retention of the negative charge. Adsorbed ions have been shown to exhibit an inhibitory effect on the anodic formation of surface oxide on Pt (53, 122, 123). Novak and Conway (104) observed that the adsorption of Cl^- preferentially blocks the formation of PtOH by competing with hydroxyl radicals for adsorption sites on the electrode surface. However, at chloride concentrations greater than $10^{-4.8}$ M, competitive

adsorption is observed at E > 0.86 V where the second stage of Pt oxidation occurs, i.e., the formation of PtO.

Two mechanisms have been proposed for the evolution of Cl_2:

$$\text{I.}\quad Cl^-_{(aq)} + S \longrightarrow SCl\cdot_{(ads)} + e^- \qquad \text{(Volmer)}$$

$$2SCl\cdot_{(ads)} \longrightarrow 2S + Cl_2\uparrow \qquad \text{(Tafel)}$$

$$\text{II.}\quad Cl^-_{(aq)} + S \longrightarrow SCl\cdot_{(ads)} + e^- \qquad \text{(Volmer)}$$

$$SCl\cdot_{(ads)} + Cl^-_{(aq)} \longrightarrow S + Cl_2\uparrow + e^- \qquad \text{(Heyrovsky)}$$

where S designates an oxidized or partially oxidized Pt surface. The second step in each mechanism is the rate determining step. Most researchers agree that Cl_2 evolution occurs by a recombination-controlled mechanism (mechanism I). A nondiffusion limited current (I_{ndl}) is attained as the coverage of Cl^- approaches unity. Since no oxide formation occurs on Pt in anhydrous trifluoroacetic acid (TFA), the evolution of Cl_2 has been investigated in TFA/H_2O mixtures (0-100% H_2O) to evaluate the effect which surface oxides exhibit on the production of Cl_2 (102, 124). In all TFA/H_2O mixtures, Cl_2 evolution proceeds by a recombination-controlled mechanism; therefore, solvation effects are secondary. For the case of anhydrous TFA, S (mechanism I) represents an unoxidized Pt electrode surface. The limiting current (I_{ndl}) obtained at an oxide-covered surface is 45 times larger than that observed at an unoxidized Pt surface. Since the mechanism is the same in both solvents, the observed increase in current indicates that substantial electrocatalytic

enhancement of the recombination rate for $Cl\cdot_{(ads)}$ exists for an oxidized Pt surface. The increase in the rate of recombination is due to weaker binding of Cl· on an oxidized Pt surface than on the Pt metal surface; consequently, a lower activation energy exists for the recombination step.

The I-E curve recorded for Cl^- at a Pt electrode is shown in Figure V-12a. The anodic formation of surface oxide on a Pt electrode during the positive scan of potential is inhibited by the presence of adsorbed Cl^-. The formation of Cl_2 commenced at the thermodynamically predicted value of 1.11 V. A decrease in the height of the oxide reduction peak was observed during the negative scan of potential in the presence of Cl^- indicating that adsorbed Cl^- influences not only the potential at which oxide formation begins but also the quantity of oxide which forms. Adsorbed Cl^- also affects the adsorption of H on Pt. Although a monolayer of H is adsorbed regardless of the coverage by Cl^-, the adsorbed Cl^- affects the energy distribution of adsorbed H by decreasing the Pt-H bond energy (121). Therefore, the H adsorption waves were shifted to more negative potentials.

Current-potential curves recorded at different values of ϕ, while holding ω constant, indicated that the evolution of Cl_2 is a surface-dependent process. The anodic production of Cl_2 exhibited minimal dependence upon ω as observed by recording I-E curves at different ω while holding ϕ constant. Hence, the evolution of Cl_2 occurs predominantly by a surface-controlled process which is consistent with the proposed recombination-controlled mechanism.

Figure V-12: I-E and ΔI-E curves of 0.5 mM Cl^- in 0.5 M H_2SO_4 at a Pt RDE

a. I-E curves

Electrode rotation speed (W): 1000 rpm

Potential scan rate (ϕ): 6 V/min

----- Pt residual

——— 0.5 mM Cl^-

b. ΔI-E curve

Lower rotation speed (W_l): 1000 rpm

Upper rotation speed (W_u): 4000 rpm

Potential step increment (ΔE): 5 mV

Time delay (t_d): 150 ms

Number of data points (N): 10

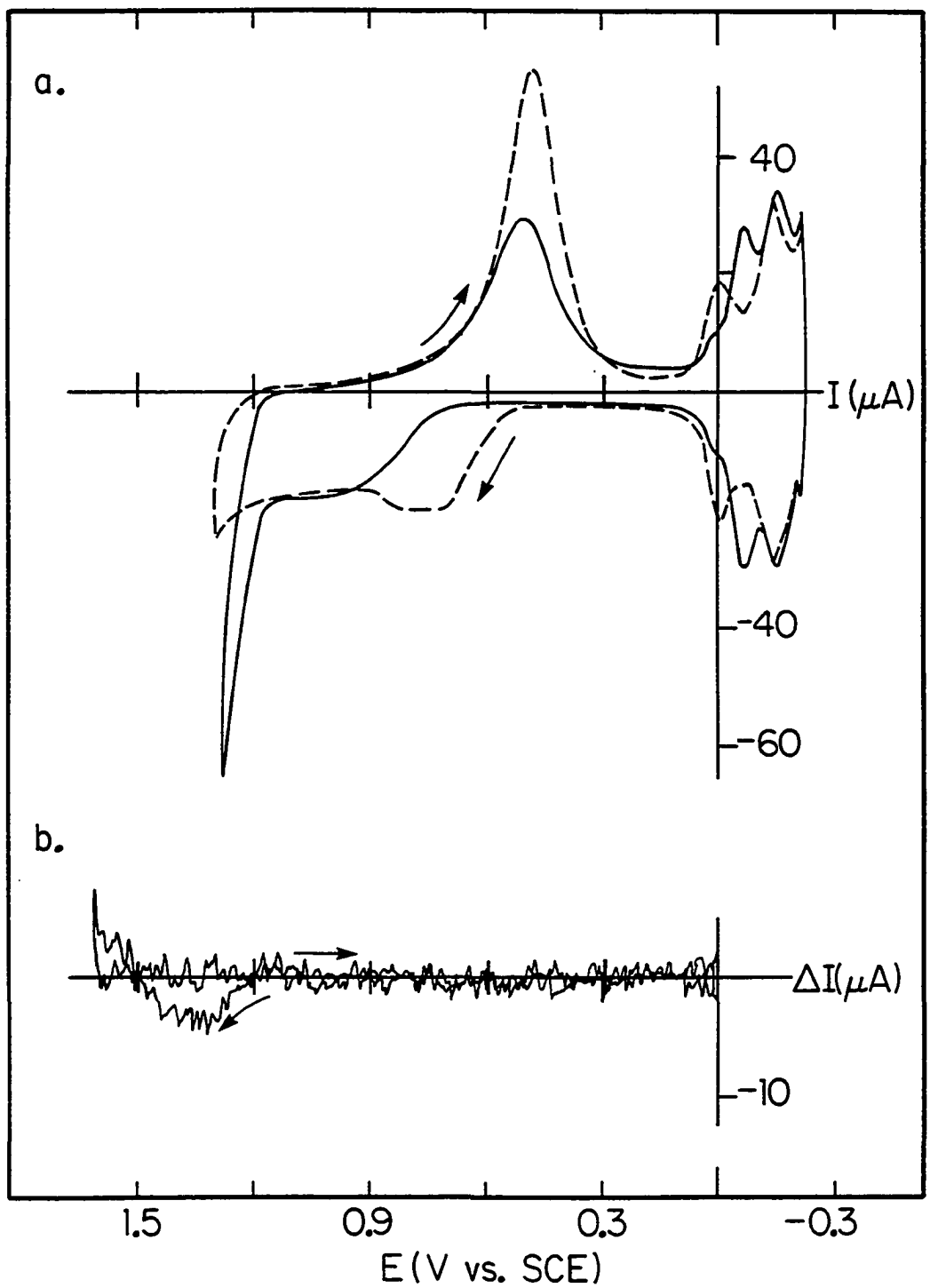
a.
40
I (μA)
-40
-60
b.
ΔI(μA)
-10
1.5
0.9
0.3
-0.3
E (V vs. SCE)

The ΔI-E curve obtained by QHMV is shown in Figure V-12b. There is a finite contribution to the total current by a mass-transport coupled process during the positive scan of potential. Perhaps, the formation of Cl_2 occurs to a small extent by an alternate pathway (mechanism II) as proposed by Burrows, Entwisle, and Harrison (111). Since the rate determining step involves the reaction of $Cl^-_{(aq)}$ with $Cl\cdot_{(ads)}$, the reaction is dependent upon the transport of Cl^- to the surface; therefore, current is a function of ω. The anodic current will become limiting provided the kinetics of the second step is fast. The observed ΔI_{lim} was approximately 5% of the theoretical ΔI_{lim} therefore, the kinetics of the second step are quite slow. The anodic formation of Cl_2 occurs predominately by a surface-controlled reaction.

Currently, the anode material of choice in the chlor-alkali industry is a mixed oxide electrode of RuO_2 and TiO_2 coated on a Ti substrate. This electrode was first patented by Beer (125) in the late 1950s. Although the exact composition of commercial cells is proprietary, increased production of Cl_2 is observed upon doping the electrode with various nonnoble metals e.g., Sn, Bi, or Co. The composition of the coating also affects the rate of undesired side reactions such as O_2 evolution or the formation of ClO_3^-. The RuO_2/TiO_2 anode has a low overpotential for Cl_2 evolution; commercial chlorine cells operate at an anodic overpotential of ca. 50 mV (119). Unlike the graphite anode, which is consumed by physical wear and electrochemical oxidation (service time of 6-24 months), the RuO_2/TiO_2 anode has a service time of 8-10 years.

Because RuO_2/TiO_2 is an efficient electrocatalyst for Cl_2 evolution, the reaction mechanism has been investigated by numerous researchers (111, 113, 116, 126, 127). Comparison of results must be done cautiously due to the variation in coating composition and the difficulty in reproducibly preparing the electrode surface. Both the Volmer-Heyrovsky and Volmer-Tafel mechanisms have been proposed for Cl_2 evolution on RuO_2/TiO_2 electrodes. Ardizzone et al. (127) reported that the mechanism is dependent upon the macroscopic defect structure of the electrode surface. At highly compact electrodes, the Volmer-Heyrovsky mechanism predominates (113, 127) whereas at highly cracked electrodes, the mechanism changes to the Volmer-Tafel pathway. The slow step in both pathways is the removal of the adsorbed intermediate therefore the transition between mechanisms implies an increase in the metal-halogen surface bond strength. Burke and O'Neill (128) suggest that the reaction mechanism may involve the participation of surface oxygen species although the precise nature of the surface species is uncertain. Based on the results obtained for Cl_2 evolution at a Pt electrode in mixtures of TFA/H_2O (0-100% H_2O) (102, 124), which demonstrate the enhanced electrocatalysis of Cl_2 evolution at an oxide covered electrode, the participation of a surface oxygen species is not an unreasonable hypothesis.

Preliminary results obtained by QHMV indicate that the production of Cl_2 is occurring by a surface-controlled mechanism since no mass-transport dependent current was observed in either acidic or basic media at concentrations as high as 0.1 M Cl^-.

Gold is not a practical anode for Cl_2 evolution owing to the

corrosive nature of the chloride solution; however, electrolytic refining of Au by the Wohlwill process takes advantage of the increased rate of dissolution of the metal through the formation of stable chloro-gold complexes. Therefore, the anodic dissolution of Au in Cl^- solutions has been the subject of fundamental electrochemical studies (129-137). Chloride ions adsorb on Au at a diffusion-limited rate (134). Dissolution of Au occurs at E > 0.8 V and approaches the theoretical limiting value. The formation of $AuCl_2^-$ proceeds by the mechanism (137)

$$Au + Cl^-_{(aq)} \longrightarrow AuCl^-_{(ads)}$$

$$AuCl^-_{(ads)} \longrightarrow AuCl_{(ads)} + e^-$$

$$AuCl_{(ads)} + Cl^- \longrightarrow AuCl_2^-{}_{(aq)}$$

where the third step is the rate determining step. Removal of an $AuCl_{(ads)}$ species exposes a bare metal site where adsorption of Cl^- occurs rapidly. However, if the Cl^- ions in the diffusion layer are consumed faster than they are replenished, i.e., the rate of transport becomes limiting, oxide formation is initiated. Passivation of the Au dissolution reaction occurs concomitantly with the formation of surface oxide (136). The potential at which the onset of passivation is observed corresponds to the potential at which sudden changes are observed by ellipsometry (135). As the Cl^- concentration increases, the potential at which passivation occurs shifts to more positive values.

The I-E curve obtained for Cl^- at a Au electrode is shown in Figure V-13a. Wave A corresponds to the formation of $AuCl_2^-$. The formation of

Figure V-13: I-E and ΔI-E curves of 0.5 mM Cl^- in 0.5 M H_2SO_4 at a Au RDE

a. I-E curve

Electrode rotation speed (W): 1000 rpm

Potential scan rate (ϕ): 6 V/min

b. ΔI-E curve

Lower rotation speed (W_l): 1000 rpm

Upper rotation speed (W_u): 4000 rpm

Potential step increment (ΔE): 5 mV

Time delay (t_d): 150 ms

Number of data points (N): 10

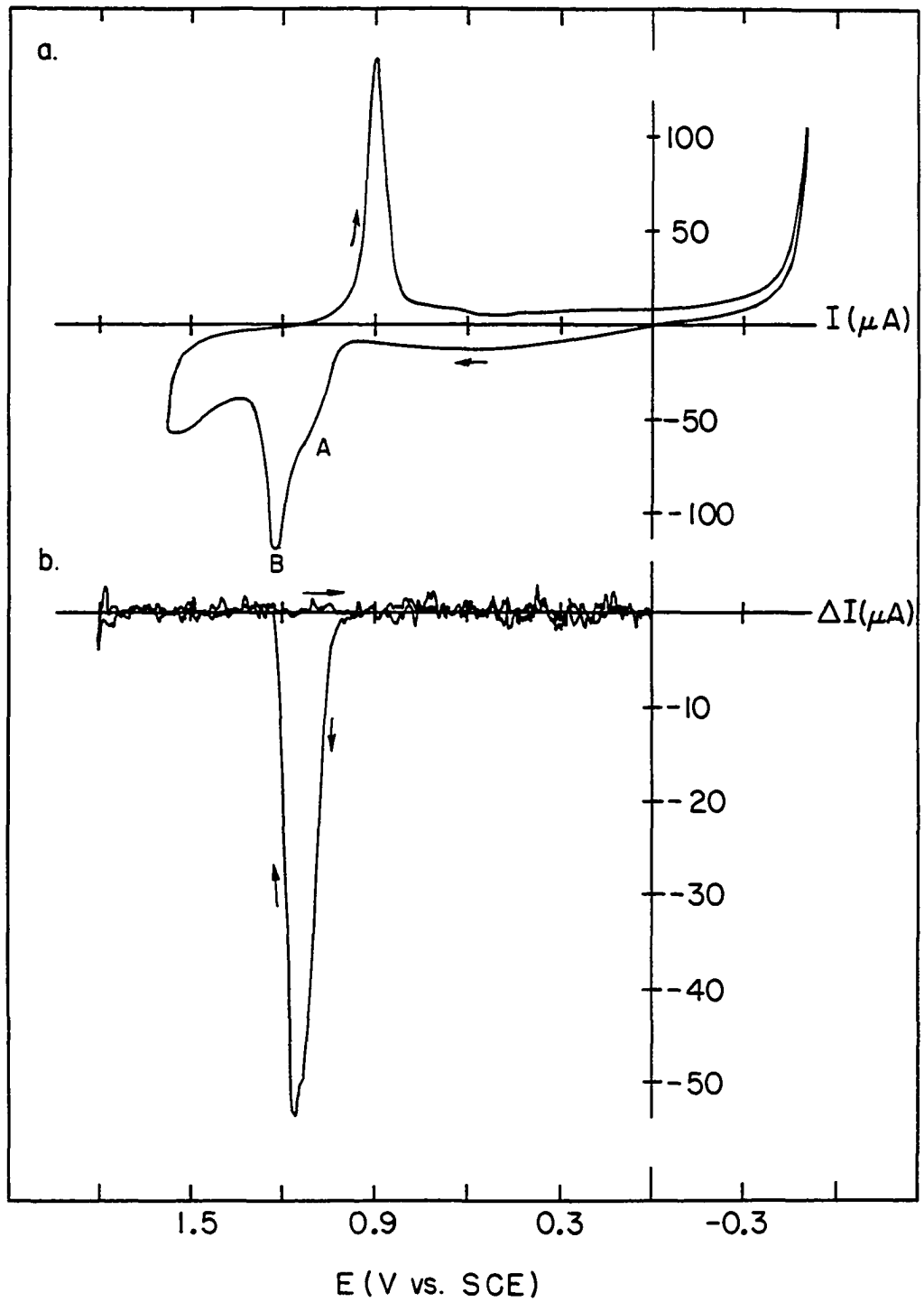
a.
100
50
I (μA)
-50
-100
A
B
b.
ΔI(μA)
-10
-20
-30
-40
-50
1.5
0.9
0.3
-0.3
E (V vs. SCE)

Au oxide was observed at ca. 1.2 V producing wave B. At E > 1.2 V, current sharply decreased owing to the passivation of Au dissolution which occurs as the formation of surface oxide commences.

Variation of the ϕ at a constant ω indicated that the formation of $AuCl_2^-$ is independent of ϕ. Current in the region 1.2 V < E < 1.6 V was dependent upon ϕ; therefore, surface-controlled processes are occurring at E > 1.2 V. The magnitude of waves A and B increased with increased ω at a constant ϕ. Since wave A was dependent solely upon ω, the formation of $AuCl_2^-$ is a mass-transport coupled process. Current in the region 1.2 V < E < 1.6 V was independent of ω; therefore, only surface-controlled processes are occurring. There was no evidence of Cl_2 evolution occurring at a Au electrode prior to the evolution of O_2.

The potential region over which corrosion of the Au surface occurs is clearly defined by the application of QHMV (Figure V-13b). A single, narrow anodic peak, corresponding to the production of $AuCl_2^-$, was observed during the positive scan of potential. The magnitude of ΔI rapidly declined to zero at E > 1.15 V. No transport-coupled current was observed throughout the remainder of the triangular potential sweep. If Cl_2 evolution occurs at an oxide covered Au electrode simultaneously with the evolution of O_2, the mechanism involves a surface-controlled rate determining step perhaps analagous to the mechanism on Pt, i.e., a recombination-controlled mechanism.

5. Bromide

The investigation of halide ions utilizing QHMV is completed with the discussion of the results obtained for the anodic oxidation of Br^-

at Pt and Au electrodes. The I-E and ΔI-E curves obtained for Br^- at Pt and Au are shown in Figures V-14 and V-15. The contribution to total current by the mass-transport coupled current is dramatically different for these electrode materials; however, the ΔI response can be rationalized based on specific properties of the surface oxides formed on Pt and Au.

Bromide ions adsorb on Pt in the H region (-0.2 V < E < 0.1 V) with substantial retention of charge (104, 121, 122). The adsorption of Br^- alters the energy distribution of adsorbed H; however, the total amount of H adsorbed does not change regardless of the extent of coverage by Br^- (104, 122). Partial charge transfer occurs as the potential is scanned in the positive direction (138). Unlike Cl^- which blocks the initially deposited OH monolayer at Pt, adsorbed Br^- blocks the formation of the surface oxide nonselectively over a wide potential range (0.55 V < E < 1.25 V) (104).

The mechanism for Br_2 evolution on Pt is dependent upon the oxidation state of the electrode surface (139). The change in mechanism is attributed to the ease of Br^- adsorption on an oxide-free or oxide-covered surface. Although Br^- strongly adsorbs on Pt metal, adsorption of Br^- on an oxide-covered Pt surface does not occur (20, 121, 140). The evolution of Br_2 was proposed to occur on a reduced Pt electrode by the mechanism

$$Br^-_{(aq)} \longrightarrow Br^-_{(ads)}$$

$$Br^-_{(ads)} \longrightarrow Br_{(ads)} + e^-$$

Figure V-14: I-E and ΔI-E curves of 0.5 mM Br^- in 0.5 M H_2SO_4 at a Pt RDE

a. I-E curve

Electrode rotation speed (W): 1000 rpm

Potential scan rate (ϕ): 6 V/min

b. ΔI-E curve

Lower rotation speed (W_l): 1000 rpm

Upper rotation speed (W_u): 4000 rpm

Potential step increment (ΔE): 5 mV

Time delay (t_d): 150 ms

Number of data points (N): 10

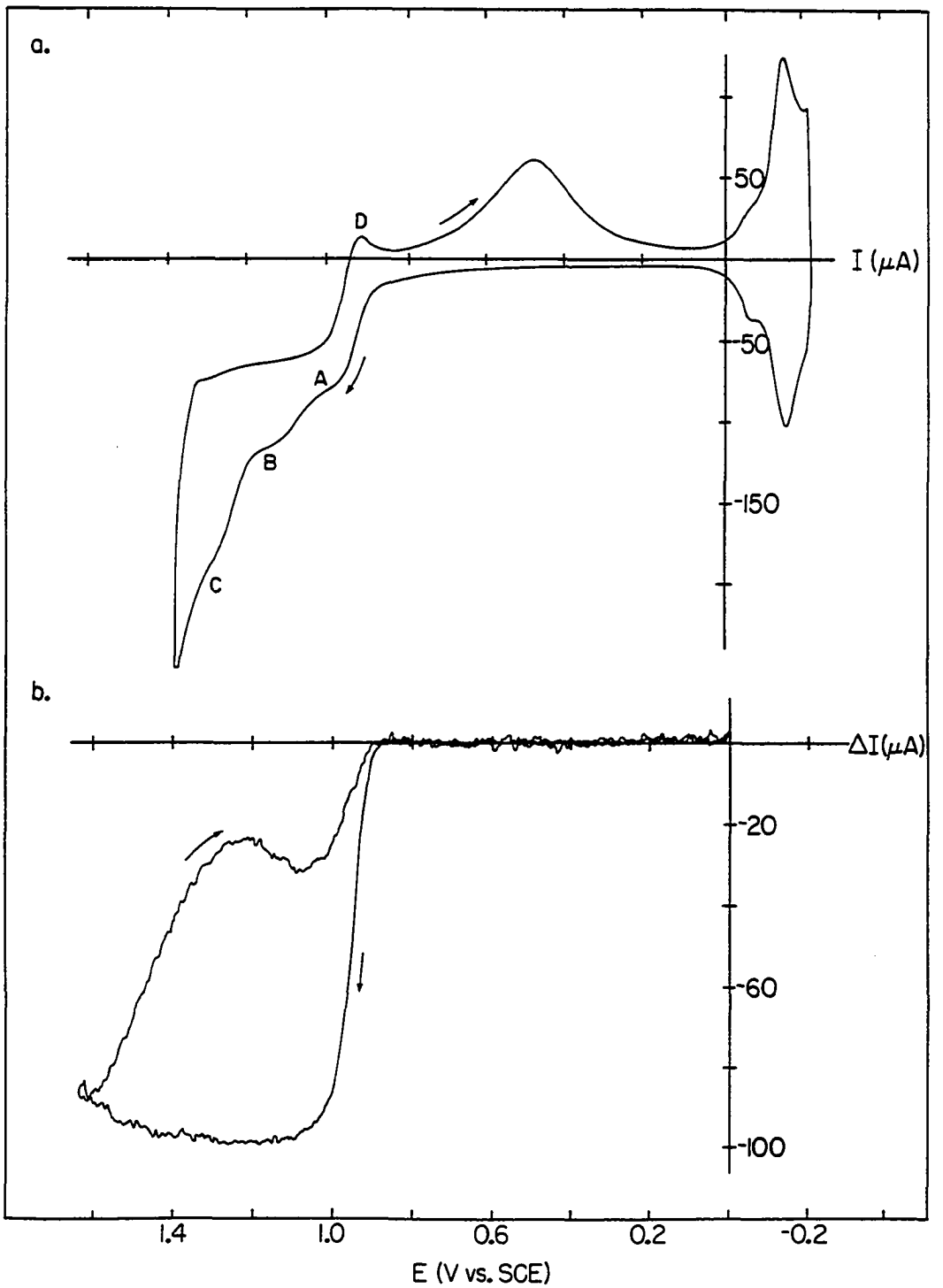
a.
50
D
I (μA)
A
-50
B
-150
C
b.
ΔI(μA)
-20
-60
-100
1.4
1.0
0.6
0.2
-0.2
E (V vs. SCE)

Figure V-15: I-E and ΔI-E curves of 0.5 mM Br^- in 0.5 M H_2SO_4 at a Au RDE

a. I-E curve

Electrode rotation speed (W): 1000 rpm

Potential scan rate (ϕ): 6 V/min

b. ΔI-E curve

Lower rotation speed (W_l): 1000 rpm

Upper rotation speed (W_u): 4000 rpm

Potential step increment (ΔE): 5 mV

Time delay (t_d): 150 ms

Number of data points (N): 10

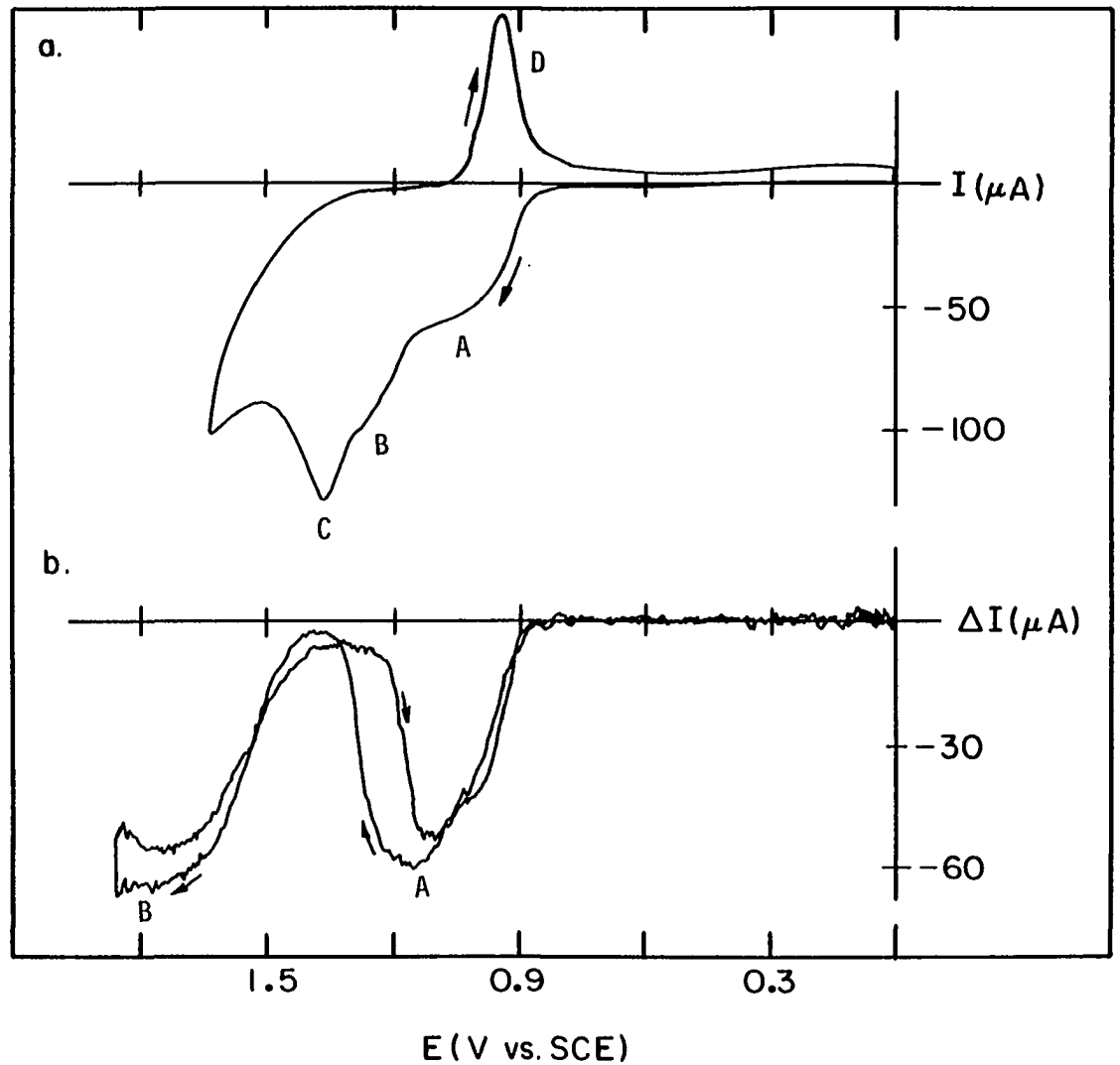
a.
D
I(μA)
A
-50
B
-100
C
b.
ΔI(μA)
-30
A
B
-60
1.5
0.9
0.3
E(V vs. SCE)

$$2Br_{(ads)} \longrightarrow Br_{2(aq)} \quad \text{or} \quad Br^-_{(aq)} + Br_{(ads)} \longrightarrow Br_{2(aq)} + e^-$$

with the rate determining step being the charge transfer from an adsorbed Br^- ion to form an adsorbed Br atom. If the rate determining step is fast, a limiting current will be observed. The mechanism for the production of Br_2 on an oxidized electrode occurs according to the scheme

$$Br^-_{(aq)} \longrightarrow Br_{(ads)} + e^-$$

$$2Br_{(ads)} \longrightarrow Br_{2(aq)}.$$

The rate determining step involves the discharge of Br^- from the solution. The anodic formation of Br_2 proceeds at a faster rate on a reduced Pt surface in comparison with an oxidized Pt surface (139), i.e., the discharge of Br^- from the solution occurs at a slower rate than the charge transfer from an adsorbed Br^- to form an adsorbed Br atom.

The I-E response of Br^- at a Pt electrode has been examined in detail by Johnson and Bruckenstein (20). Three anodic waves were observed when scanning the potential in the positive direction (Figure V-14a). The first anodic wave (A) is attributed to the oxidation of Br^- to Br_2 ($E_{1/2}$ = 0.90 V). The formation of Pt oxide during the positive scan of potential is inhibited by the presence of adsorbed Br^- and no oxide reduction peak was observed until E > 1.0 V. Wave B corresponds to the formation of Pt oxide. As E_a was increased beyond 1.0 V, the height of the oxide reduction peak increased and it was concluded that surface oxidation is occurring simultaneously with the production of HOBr (C). The small reduction peak D observed during the negative scan

of potential is attributed to the reduction of Br_2 present in the convective-diffusion layer. At higher ω and/or lower ϕ, peak D was not observed. The reduction of Pt oxide (E) occurred with E_p = 0.48 V.

Current-potential curves recorded as a function of ω at a low ϕ demonstrated that I_{lim} vs. $\omega^{\frac{1}{2}}$ is linear for wave A, i.e., the production of Br_2 is a mass-transport limited reaction. The height of waves B and C increased in a nonlinear fashion with increasing ω indicating that surface-controlled reactions are occurring or that the kinetics of a mass-transport coupled reaction are slow.

A single anodic wave was observed upon application of QHMV to a study of the oxidation of Br^- at a Pt electrode (Figure V-14b). In the region 1.05 V < E < 1.4 V, the value of ΔI is the theoretical value predicted from the Levich equation. However, at E > 1.4 V, ΔI decreased steadily. The decrease in ΔI corresponds to an increasing amount of surface oxidation. Upon reversal of the potential scan, ΔI decreased to a value less than the ΔI observed during the positive scan of potential; the value of ΔI is a function of E_a. The observed behavior of Br_2 production by QHMV is consistent with the results of mechanistic and kinetic studies reported by Rubenstein (139). At a reduced electrode, the charge transfer from an adsorbed Br^- ion to an adsorbed Br atom occurs rapidly and the predicted value of ΔI_{lim} is attained for the formation of Br_2. However, as the potential increases and the degree of surface oxidation increases, the reaction mechanism changes. The discharge of Br^- from solution is now the rate controlling step which proceeds more slowly than the charge transfer step at a reduced

electrode. Consequently, mass-transport coupled current is less than the predicted ΔI_{lim} value. There was no evidence of the transport-coupled production of HOBr or BrO_3^- occurring simultaneously with the evolution of O_2. Hence, HOBr is generated only by a surface-controlled reaction, i.e., the oxidative desorption of Br^-.

The E^0 value for the BrO_3^-/Br^- half reaction in base is 0.37 V. An I-E curve was recorded for Br^- in 0.1 M NaOH; however, no change in the response of current was observed. Nevertheless, QHMV was applied to determine if any transport-coupled reaction occurs simultaneously with O_2 evolution. No transport-coupled current was observed in the region of O_2 evolution.

The anodic reactions occurring at a Au electrode in the presence of Br^- have not been studied in detail. The formation of Br_2 is thermodynamically predicted to occur with $E_{1/2}$ = 0.94 V vs. SCE which is close to the values for the formation of the gold-bromo complexes $AuBr_2^-$ ($E_{1/2}$ = 0.92 V) and $AuBr_4^-$ ($E_{1/2}$ = 0.80 V). Early investigation of the oxidation of Br^- at a Au electrode by Gaur and Schmid (133) indicated that Au is dissolved and passivated in a dilute Br^- solution similarly to the dissolution and passivation of Au in Cl^- solutions. However, Gaur and Schmid did not consider the possible evolution of Br_2 until E > 1.0 V. More recently, Nicol (129) has reported preliminary results for the anodic behavior of Br^- at a Au electrode which were obtained by cyclic voltammetry at a RRDE. Experiments utilizing a RRDE provide additional information about the reactions occurring at the disk electrode (1, 141, 142). Soluble electroactive species which are

produced at the disk electrode, as well as electroactive species which are present in the bulk solution, are transported to the ring electrode where they can be detected at a constant potential value (E_r). By appropriate selection of the value of E_r, electroactive species can be detected selectively. Current produced at the ring electrode (I_r) is recorded as a function of the potential of the disk electrode (E_d). Hence, variations in I_r reflect a change in reactions that are occurring at the disk electrode. To study the oxidation of Br^- at a Au disk electrode, a Au electrode cannot be employed due to interfering reactions that occur at the Au electrode at potentials where the species of interest are detected. Therefore, a Au disk/Pt ring RRDE was utilized. Nicol observed that the quantity of Au(I), Au(III), and Br_2 produced at the anode was dependent upon potential and concentration of Br^-. The proportion of total current consumed in the production of Br_2 decreased with increasing Br^- concentration. Therefore, the competing reaction, presumably the formation of a gold-bromo complex, is favored at higher concentrations of Br^-. Cadle and Bruckenstein (143) reported that the formation of soluble gold(I)-aquo species and gold(III)-aquo species occurs upon oxidation and reduction of the Au electrode in the absence of electroactive species. Nicol (129) did not specify the Au species detected as gold-aquo of gold-bromo species, nor did he report the potential region over which each of the Au species was detected. Unfortunately, no detailed report of the anodic behavior of Br^- at a Au electrode or elucidation of the reaction mechanism has been found in the literature.

The I-E curve obtained in acidic solution at a Au electrode is shown in Figure V-15a. Three anodic waves were observed during the positive scan of potential. The production of Br_2 occurred with the thermodynamically predicted value of $E_{\frac{1}{2}}$ = 0.94 V (A). Wave B was produced upon formation of a gold-bromo complex which was concluded to be $AuBr_4^-$ which has an E^0 value slightly more negative than the E^0 for the formation of $AuBr_2^-$. Peak C consists of current resulting from the anodic formation of Au_2O_3 and concomitant formation of Br_2 and $AuBr_4^-$. At E > 1.5 V, O_2 evolution commences. During the negative scan of potential, anodic current decreased rapidly to a small, yet finite, value in the region 1.35 V < E < 1.05 V. The reduction of Au oxide (D) occurred at E_p = 0.95 V; however, the quantity of oxide formed in the presence of Br^- is diminished in comparison with the quantity formed in the absence of Br^-.

A series of I-E curves was recorded as a function of ϕ at a constant value of ω. The production of Br_2 (A) was independent of ϕ which is characteristic of a mass-transport coupled reaction, whereas, the height of peaks B and C varied with ϕ indicating that surface-coupled reactions are occurring in the potential region of peaks B and C. At high values of ϕ, peak B was indistinguishable from peak C; hence, the formation of $AuBr_4^-$ is inhibited at high values of ϕ.

Current-potential curves were recorded also as a function of ω while holding ϕ constant. All three anodic waves observed during the positive scan of potential increased with increasing ω. Current due to the production of Br_2 (A) increased in a nonlinear fashion with

increasing ω indicating that the formation of Br_2 proceeds under mixed kinetic and convective-diffusion control. In effect, the kinetics of the reaction are sufficiently fast to produce the theoretical, transport-limited current at low values of ω; however, at high values of ω, the rate of Br_2 production is comparatively slow and, therefore, the theoretical limiting current is not observed. At higher values of ω, peak B owing to the formation of $AuBr_4^-$ became more prominent and the $E_{\frac{1}{2}}$ shifted to less positive values. Formation of $AuBr_4^-$ occurred more readily than the production of Br_2 as the convective transport of Br^- increased. The height of peak C increased with increasing ω due to the mass-transport coupled formation of Br_2 and production of $AuBr_4^-$ simultaneously with oxide formation. During the negative scan of potential, anodic current observed at $E < 1.15$ V increased due to the production of Br_2. The increase in anodic current in the region $1.15 \text{ V} < E < 0.85$ V produced an anomalous decrease in the height of the oxide reduction peak (D) at higher values of ω.

The ΔI-E curve recorded for Br^- at a Au electrode is shown in Figure V-15b. Wave A corresponds to the mass-transport coupled production of Br_2. In the region $1.2 \text{ V} < E < 1.3$ V, there is an unresolvable, finite contribution to ΔI, as the result of the production of $AuBr_4^-$ which is the kinetically favored reaction at the higher flux of Br^-. At $E > 1.3$ V, oxide formation commences and the formation of $AuBr_4^-$ and Br_2 is inhibited; hence, ΔI decreased to a small value corresponding to the formation of only a small amount of Br_2. At ca. 1.5 V, O_2 evolution is initiated and renewed production of Br_2 was

observed. The theoretical ΔI_{lim} was observed in the region 1.7 V < E < 1.85 V (B). The renewed production of Br_2 which occurs simultaneously with O_2 evolution (B) resulted from the increased availability of Au metal sites. Gold(III) oxide, loosely held at the electrode surface, easily flakes off exposing bare Au sites (69-71). Bromide oxidation, as well as O_2 evolution and continued formation of Au_2O_3, can occur at the exposed Au sites (70-72). Upon reversal of the potential scan, ΔI decreased and a minimum value was attained in the region 1.4 V > E > 1.2 V. At E < 1.2 V, ΔI increased owing to the production of Br_2. No $AuBr_4^-$ was formed during the negative scan of potential. As the concentration of Br^- was increased, the ratio $\Delta I_A/\Delta I_B$ decreased indicating that the production of Br_2, in the region 0.9 V < E < 1.2 V, decreased and the formation of $AuBr_4^-$ increased as the concentration of Br^- increased. The transport-limited production of Br_2 (B) was attained regardless of the Br^- concentration since the formation of $AuBr_4^-$ is not a competing reaction at E > 1.7 V.

6. Hydroquinone

The oxidation of hydroquinone (HQ) on Pt and Au does not involve O-atom transfer; nevertheless, a brief discussion of the anodic behavior of HQ is included because of the interesting results which were obtained, in particular, at a Au electrode. The adsorption of numerous aromatic compounds at Pt electrodes has been investigated utilizing thin-layer electrochemical techniques (144-148). The results demonstrated that aromatic molecules adsorb in specific molecular orientations. The molecular orientation is a function of the structure and the concen-

tration of the adsorbate, the strength of adsorption of the supporting electrolyte, and the pH of the solution. At millimolar concentrations in aqueous 0.1 M $HClO_4$, HQ adsorbs with the plane of the ring parallel to the electrode surface. At concentrations exceeding 10^{-3} M, HQ adsorbs with an edgewise orientation.

Hydroquinone adsorbs irreversibly on Pt (144, 148, 149) and is not removed upon rinsing with a HQ-free electrolyte solution. Oxidative desorption of the chemisorbed species occurs at E > 0.6 V. Complete conversion to CO_2 occurs if HQ is adsorbed in the parallel orientation whereas, if HQ is adsorbed in an edgewise manner, complete conversion to CO_2 does not occur. Minimal oxidation of the Pt surface occurs prior to the complete oxidative desorption of adsorbed HQ (150). Soriaga and Hubbard (151) concluded that Pt is ultimately oxidized to the same extent regardless of whether HQ had been previously adsorbed based on the observation that the area of the oxide reduction peaks is equal in the absence or presence of HQ. Adsorbed HQ suppresses the underpotential deposition of H in the region 0.15 V < E < -0.2 V (152). The adsorption of aromatic molecules is sufficiently strong to displace adsorbed HQ (145). Recently, Soriaga et al. (153) have examined the effects of halogens upon the adsorption of HQ. They observed that I^- quantitatively displaced HQ, on the other hand, HQ did not displace adsorbed I. Bromide and Cl^- displace HQ to some extent (Br^- > Cl^-) whereas adsorbed HQ is uneffected by F^-. The oxidation of unadsorbed HQ has been observed to occur reversibly at a Pt electrode at E > 0.46 V vs. SCE (151).

The I-E curve obtained for HQ in 0.5 M H_2SO_4 at a Pt electrode is

shown in Figure V-16a. An anodic wave (A) was observed for the oxidation of HQ to quinone (Q) at the thermodynamically predicted value $E_{1/2}$ = 0.46 V vs. SCE during the positive sweep of potential. The formation of Pt oxide was inhibited by the presence of adsorbed HQ. Wave B, observed at E > 0.7 V, consists of current produced as the result of the oxidation of adsorbed HQ and that which is transported to the electrode surface. At E > 0.9 V, the anodic formation of Pt oxide occurred concomitantly with the anodic reactions of HQ. Upon reversal of the potential scan, an anodic current plateau (C) was observed in the region 1.2 V > E > 0.8 V for the oxidation of unadsorbed HQ. Reduction of Pt oxide occurred at E_p = 0.45 V. The characteristic H adsorption and H desorption peaks were not observed in the H region (0.1 V < E < -0.2 V) owing to the presence of adsorbed HQ which suppresses the underpotential deposition of adsorbed H.

A series of I-E curves were recorded as a function of ϕ at a constant value of ω. After correcting for double-layer charging current, the anodic current produced upon oxidation of unadsorbed HQ (A) was independent of ϕ which is indicative of a mass-transport controlled reaction. Current in the region of peak B was dependent upon ϕ. The variation in current with changes in ϕ is attributed to the surface-controlled reactions which occur at E > 0.7 V, i.e., the oxidation of adsorbed HQ and the oxidation of Pt. The current plateau (C) observed during the negative scan of potential was independent of ϕ which is characteristic of a convective-controlled reaction.

Current-potential curves were recorded at a constant value of ϕ

Figure V-16: I-E and ΔI-E curves of 0.5 mM hydroquinone in 0.5 M H_2SO_4 at a Pt RDE

a. I-E curve

Electrode rotation speed (W): 1000 rpm

Potential scan rate (ϕ): 6 V/min

b. ΔI-E curve

Lower rotation speed (W_l): 1000 rpm

Upper rotation speed (W_u): 4000 rpm

Potential step increment (ΔE): 5 mV

Time delay (t_d): 150 ms

Number of data points (N): 10

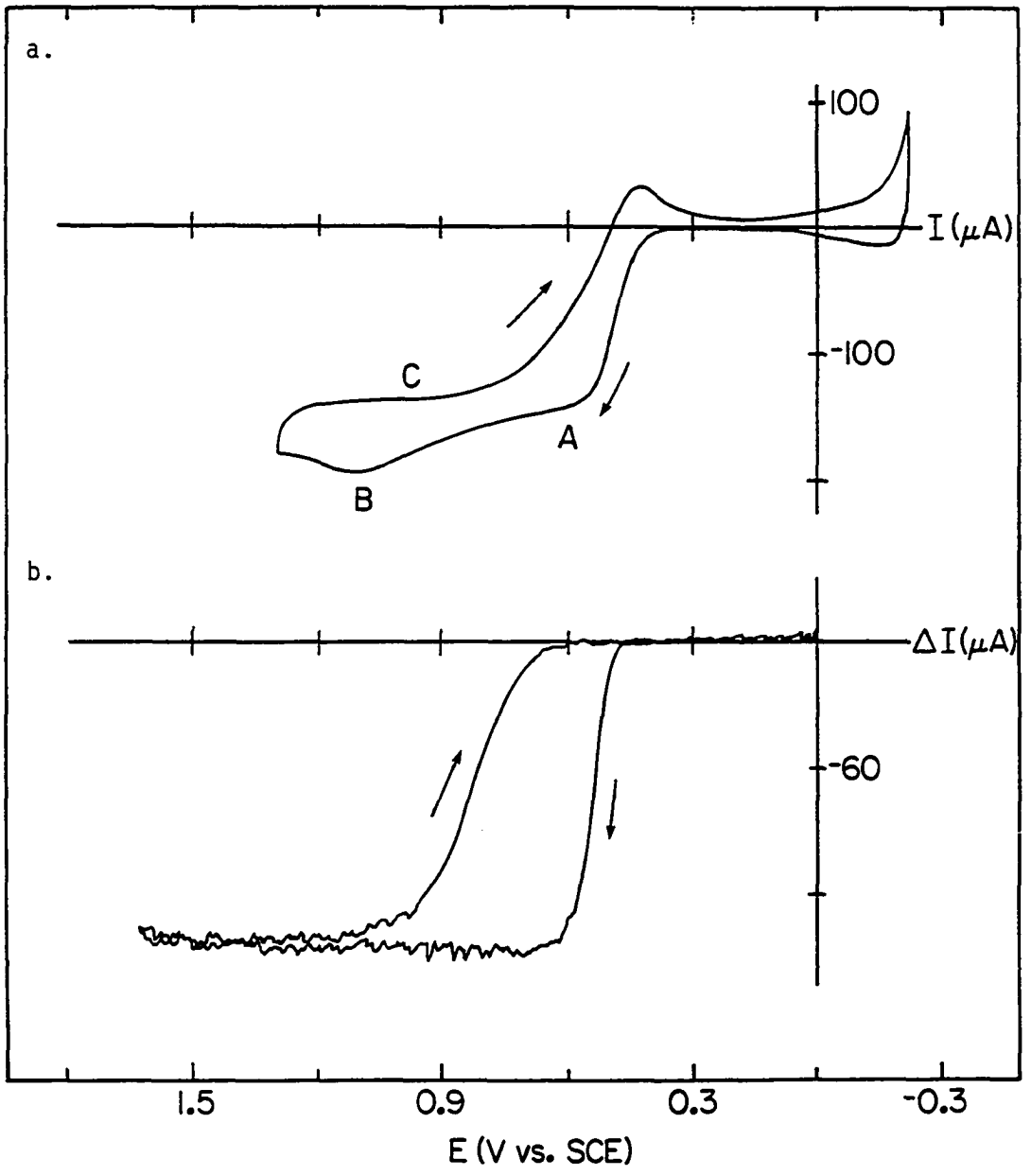
a.
100
I (μA)
-100
C
A
B
b.
ΔI (μA)
-60
1.5
0.9
0.3
-0.3
E (V vs. SCE)

while varying ω. Both anodic waves observed during the positive scan of potential were a function of ω indicating that the transport-dependent oxidation of HQ is occurring in the region 0.46 V < E < 1.3 V. During the negative scan of potential, the magnitude of the current plateau (C), observed in the region 1.2 V > E > 0.8 V, increased linearly with $\omega^{\frac{1}{2}}$.

The ΔI-E curve recorded for HQ at a Pt electrode is shown in Figure V-16b. A ΔI plateau was observed in the region 0.6 V < E < 1.65 V during the anodic scan of potential corresponding to the transport-coupled oxidation of HQ. Upon reversal of the potential scan at E_a = 1.65 V, an anodic ΔI plateau was observed in the region 1.65 V > E > 1.05 V. However, at E < 1.05 V, ΔI decreased to zero at ca. 0.6 V. The difference between the $E_{\frac{1}{2}}$ for the anodic wave observed during the positive scan of potential and the $E_{\frac{1}{2}}$ observed for the anodic wave during the negative scan decreased as the potential scan was reversed at successively less positive values of E_a. For E_a < 0.9 V, the $E_{\frac{1}{2}}$ values are equal for the two scan directions. No oxide formation occurred at E < 0.9 V, therefore, the observed irreversibility of HQ oxidation during the negative scan of potential is attributed to the presence of Pt oxide. The oxidation of HQ proceeded at a limiting value during the negative scan of potential provided that η was sufficiently large.

In sharp contrast to the numerous investigations of the adsorption and oxidation of HQ on Pt, the characterization of the adsorption and anodic behavior of HQ on Au has not been described in the literature. The I-E curve recorded for HQ at a Au electrode is shown in Figure

V-17a. The oxidation of HQ to Q proceeded with the thermodynamically predicted value $E_{\frac{1}{2}}$ = 0.46 V producing an anodic current plateau (A) in the region 0.55 V < E < 1.05 V. The small peak (B) observed prior to the establishment of the limiting current plateau is attributed to the slow depletion of species in the diffusion layer. At E > 1.05 V, formation of Au oxide occurred simultaneously with the anodic oxidation of HQ. The formation of oxide was not inhibited in the presence of HQ nor does the formation of oxide exhibit an inhibitory effect on the oxidation of HQ. During the negative scan of potential, anodic current owing to the oxidation of HQ was observed in the region 1.6 V > E > 0.46 V. The reduction of Au oxide occurred at E_p = 0.88 V concurrently with the oxidation of HQ.

Current-potential curves were recorded as a function of ϕ while holding ω constant. The magnitude of the anodic current plateau (A), corresponding to the oxidation of HQ, was independent of ϕ after correcting for double-layer charging current. This behavior is indicative of a mass-transport controlled process. At low values of ϕ, peak B was not observed since the sufficient time elapsed at that scan rate for the depletion of species in the diffusion layer to occur during the rising portion of the oxidation wave. Current due to the formation of Au oxide and the reduction of Au oxide varied with ϕ, which is characteristic of surface-controlled processes. Variation of ω at a constant value of ϕ demonstrated that the anodic plateau current increased nonlinearly with $\omega^{\frac{1}{2}}$. Since no surface-controlled reactions occurred simultaneously with HQ oxidation in the region 0.46 V < E <

Figure V-17: I-E and ΔI-E curves of 0.5 mM hydroquinone in 0.5 M H_2SO_4 at a Au RDE

a. I-E curve

Electrode rotation speed (W): 1000 rpm

Potential scan rate (ϕ): 6 V/min

b. ΔI-E curve

Lower rotation speed (W_l): 1000 rpm

Upper rotation speed (W_u): 4000 rpm

Potential step increment (ΔE): 5 mV

Time delay (t_d): 150 ms

Number of data points (N): 10

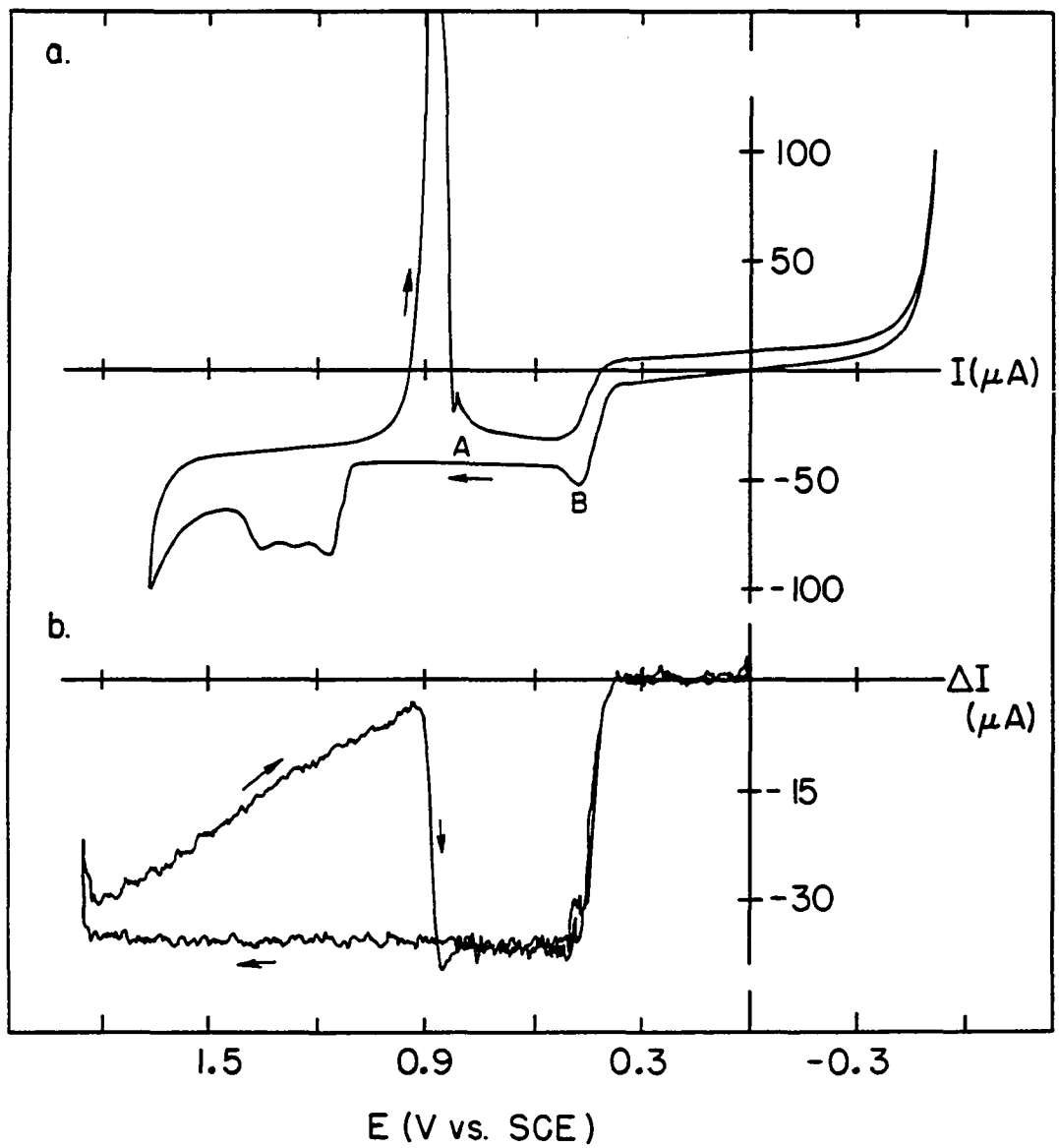
a.
100
50
I(μA)
A
B
-50
-100
b.
ΔI
(μA)
-15
-30
1.5
0.9
0.3
-0.3
E (V vs. SCE)

1.05 V, it was concluded that the kinetics for the anodic oxidation of HQ at a Au electrode are the controlling factor at large ω.

The anodic oxidation of HQ at a Au electrode was investigated further by application of QHMV. For $E_a \leq 1.8$ V, a reversible anodic wave was observed for the mass-transport coupled oxidation of HQ. The ΔI-E curve obtained for $E_a = 1.85$ V is shown in Figure V-17b. An anodic current plateau was observed during the positive scan of potential; however, upon reversal of the potential scan direction, ΔI decreased linearly in the region 1.85 V > E > 0.9 V at a rate of 31.2 μA/V. At E < 0.9 V, Au oxide was reduced and ΔI rapidly increased to the anodic value observed during the positive scan of potential. The linear decrease in ΔI in the region 1.85 V > E > 0.9 V may be attributed to a change in the properties of the oxide-covered Au electrode upon anodization at E > 1.8 V. Kim et al. (68) reported that a highly-hydrated oxide $Au(OH)_3$ is formed at E > 1.8 V. Perhaps the formation of $Au(OH)_3$ forms a protective layer over the existing oxide; hence, less Au_2O_3 flakes off of the electrode surface. Since Au_2O_3 is known to be a poor electronic conductor, an ohmic drop may occur across the layer of Au_2O_3. It is also possible that by decreasing the amount of Au_2O_3 which flakes from electrode surface, the number of available oxide-free Au sites decreases; hence, the observed value of ΔI decreases. Cadle and Bruckenstein (143) have observed that anodization of a Au electrode at E > 1.8 V increases the surface roughness of the electrode. A two-fold increase in the roughness factor was observed upon potentiostating the electrode at E = 1.9 V for 2 min; whereas, no increase in

the roughness factor was observed upon potentiostating the electrode at E = 1.7 V for as long as an hour even though Au dissolution occurred at E = 1.7 V. The rate of Au dissolution increased at E > 1.8 V which corresponds to the potential at which $Au(OH)_3$ formation commences. Cadle and Bruckenstein concluded that the rate of dissolution, not the quantity of Au dissolved, controls the extent of roughening. The oxidation of HQ may be sterically hindered at a Au electrode roughened at the atomic level. Another possible explanation is that the reaction may be kinetically slower at an electrode which has been anodized at E > 1.8 V until the oxide layer is reduced from the electrode surface. Further investigation of this phenomenon may provide novel information about the oxide which forms on Au at E > 1.8 V.

D. Summary

In this section, data obtained by CV and QHMV has been presented for several analyte/electrode combinations. The results demonstrate the complementary nature of the two techniques. The ability of QHMV to extract the mass-transport coupled current from the total current produced in the potential region of O_2 evolution has proven to be the most informative attribute of QHMV. Tables V-2 and V-3 summarize the results obtained by QHMV for the anodic reactions discussed. Table V-4 summarizes the results obtained by QHMV at a Pt electrode for other reactions briefly examined but not discussed here.

Table V-2. Mass-transport dependent reactions observed by QHMV simultaneously with O_2 evolution

Reaction	Electrode Material			
	Pt	Au	Pd	Ir
$As(III) \longrightarrow As(V)$	mtc	mtc	-	-
$I^- \longrightarrow IO_3^-$	mtl	mtl	mtc	mtc
$Br^- \longrightarrow Br_2$	mtc	mtl	-	-
$Cl^- \longrightarrow Cl_2$	mtc	nc	-	-
$NO_2^- \longrightarrow NO_3^-$	nc	mtc	-	-
$HQ \longrightarrow Q$	mtl	mtl	-	-

mtc mass-transport coupled current was observed

mtl mass-transport limited current was observed

nc no coupling of the reaction to mass-transport was observed

- reaction was not studied

Table V-3. General trends of electrocatalysis observed for mass-transport coupled reactions

Reaction	Electrode Material			
	Pt	Au	Pd	Ir
$As(III) \longrightarrow As(V)$	1	1	-	-
$I^- \longrightarrow IO_3^-$	1	1	2	2
$Br^- \longrightarrow Br_2$	4	2	-	-
$Cl^- \longrightarrow Cl_2$	2	4	-	-
$NO_2^- \longrightarrow NO_3^-$	3	1	-	-
$HQ \longrightarrow Q$	4	4	-	-

1 catalyzed by lower oxide, inhibited by higher oxide, catalyzed during O_2 evolution

2 catalyzed only during O_2 evolution

3 catalyzed by lower oxide, inhibited by higher oxide, not catalyzed during O_2 evolution

4 the mass-transport coupled reaction does not involve electrocatalysis

- reaction was not studied

Table V-4. Mass-transport dependent reactions observed by QHMV occurring simultaneously with O_2 evolution at a Pt electrode

Reaction	Electrode Material Pt
Ce(III) ⟶ Ce(IV)	1
Cr(III) ⟶ Cr(VI)	3
Mn(II) ⟶ Mn(III) or Mn(II) ⟶ Mn(VII)	2
Sb(III) ⟶ Sb(V)	3
Se(IV) ⟶ Se(VI)	3
Sn(II) ⟶ Sn(IV)	3
V(III) ⟶ V(V)	1

1 mass-transport limited reaction occurring simultaneously with O_2

2 mass-transport coupled reaction occurring simultaneously with O_2 evolution

3 no mass-transport coupled reaction observed

VI. THE ANODIC OXIDATION OF IODIDE IN ACIDIC MEDIA AT A Pt ELECTRODE

A. Literature Review

The survey of anodic reactions utilizing CV and QHMV demonstrated the complimentary nature of the two techniques and illustrated that QHMV is an invaluable technique for the study of mass-transport coupled reactions that are occurring simultaneously with surface oxidation and O_2 evolution. Of particular interest are the results obtained for the oxidation of I^- at a Pt electrode in acidic media. The following observations promoted further study of the oxidation of I^- which involves the uptake of O atoms: 1) The surface-coupled, oxidative desorption of I to IO_3^- is initiated at the potential where PtOH formation commences. 2) The transport-coupled oxidation of I^- to IO_3^- proceeds concomitantly with the formation of PtOH. 3) The transport-limited production of IO_3^- occurs simultaneously with O_2 evolution.

Iodide is strongly adsorbed on an oxide-free Pt surface with complete loss of the negative charge (16, 104, 122). Adsorption of I^- as I^0 is irreversible and desorption does not occur upon thorough rinsing with I^--free solutions. The maximum coverage by I atoms was observed to be ca. $\theta = 0.5$ (16), implying one adsorbed I per two Pt surface atoms. Lane and Hubbard (16) suggested that the adsorption of I^- proceeds through the formation of dissociated HI. However, based on the results of recent studies utilizing low energy electron diffraction (LEED), Auger electron spectroscopy (AES), and thermal

desorption mass spectrometry (TDMS), it has been concluded that the adsorption of I^- on Pt is limited only by the size of the I atom (154, 155). Felter and Hubbard (154) examined the adsorption of gaseous I_2 on Pt(100) and Pt(111) single crystals. They concluded that I_2 dissociatively adsorbs to form a hexagonal or near-hexagonal lattice with a maximum coverage of $\theta = 0.56$. The adsorption of gaseous HI on Pt(100) and Pt(111) single crystals has been investigated by Garwood and Hubbard (155). The maximum coverage by I atoms on Pt(111) is $\theta = 0.43$; whereas a maximum coverage of $\theta = 0.54$ is attained on Pt(100). For $\theta < 0.50$, at either Pt(111) or Pt(100), I atoms are desorbed exclusively. However, at Pt(100), HI is desorbed exclusively in the transition from $\theta = 0.54$ to $\theta = 0.50$; hence, adsorption in excess of $\theta = 0.50$ occurs as HI. The stability of the Pt-I adsorption bond was demonstrated by the high temperature required for desorption to occur in vacuum. Thermal desorption of I from Pt(111) produced a peak at 735 K followed by a broad maximum for temperatures of 800-1000 K. At Pt(100), the transition from $\theta = 0.54$ to $\theta = 0.50$ produced a desorption peak at 620 K corresponding to the desorption of HI which is more weakly bonded than I atoms. Two desorption peaks were observed at temperatures of 735 K and 980 K, as the result of the desorption of I atoms from Pt(100). The contrasting thermal desorption behavior of I atoms from Pt(111) and Pt(100) parallels the dissimilar reactivity of these surfaces toward electrochemical oxidative desorption. Current-potential curves were recorded for the oxidative desorption of I which was deposited under vacuum on Pt(111) and Pt(100) single crystals.

The oxidative desorption of I from Pt(111) produced a single peak, whereas the oxidative desorption from Pt(100) produced two anodic peaks. Comparison of the I-E curve obtained for the oxidative desorption of I from Pt(100) deposited under vacuum with that for deposition from an aqueous solution indicated that the peak occurring at the more positive potential is unique to the adsorbed layer produced under vacuum. The differences in reactivity of adsorbed I are being investigated further by Felter and Hubbard (154).

The effects of adsorbed I upon the anodic formation of surface oxide and the underpotential deposition of H have been studied in detail (53, 104, 121, 122) and are illustrated in Figure VI-1. Adsorbed I suppresses the anodic formation of surface oxide on Pt nonselectively over the region 0.55 V < E < 1.0 V. However, at E > 1.0 V, adsorbed I is removed from the electrode surface by oxidative desorption to IO_3^- with concurrent formation of surface oxide. No I adsorbs on an oxide-covered Pt surface (12, 17). Unlike adsorbed Br^- and Cl^-, adsorbed I alters the quantity of H adsorbed in the region 0.1 V > E > -0.2 V; hence, the current observed progressively diminishes as the concentration of I^- increases in the solution.

Iodine atoms adsorbed on a Pt surface influence the rate of many electrochemical reactions (14, 156-158). Upon adsorption of I, the electrostatic charge distribution of the solution-electrode interface is altered. Oppositely charged reactants are attracted to the diffuse layer, thus facilitating their reaction; whereas, the reaction of like-charged species is not facilitated by adsorbed I on a Pt surface. The

Figure VI-1: I-E curves of I^- in 0.5 M H_2SO_4 at a Pt RDE as a function of I^- concentration

Electrode rotation speed (W): 400 rpm

Potential scan rate (ϕ): 4 V/min

····· 0.0 μM I^-

——— 1.1 μM I^-

------- 3.1 μM I^-

— · — 8.1 μM I^-

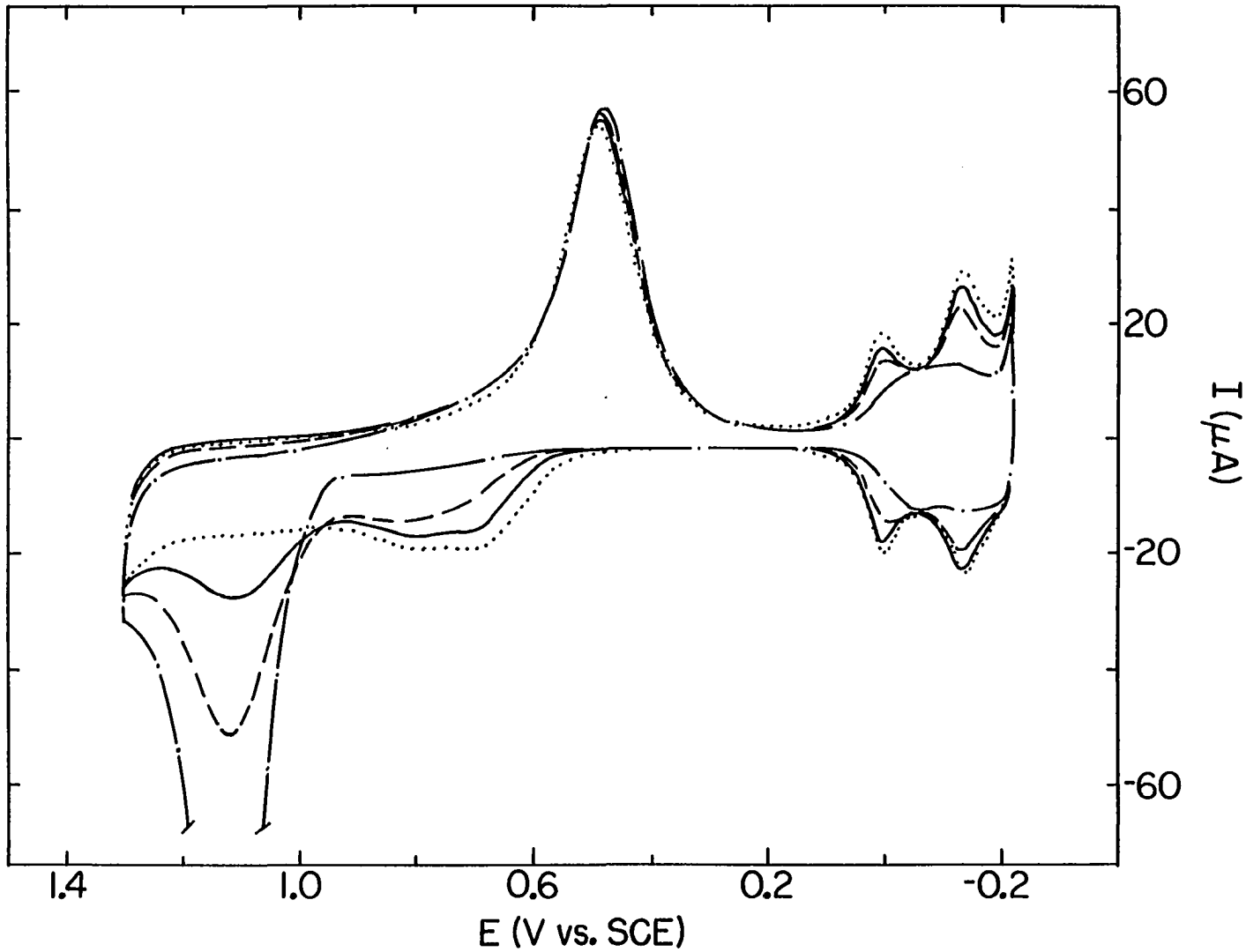
60
20
-20
-60
I (μA)
1.4
1.0
0.6
0.2
-0.2
E (V vs. SCE)

following examples illustrate the affect which I adsorbed on a Pt substrate exhibits on several electrochemical reactions: 1) Adsorbed I accelerates the reaction of anionic Pt(II) complexes, e.g., $PtCl_4^{2-}$ (156). On the other hand, deceleration of the reaction of cationic Pt complexes, e.g., $Pt(NH_3)_4^{2+}$ (156) occurs, as expected from electrostatic considerations. 2) The oxidation of Sb(III) in acidic Cl^- media is irreversible at a Pt electrode; however, upon pretreating the electrode with I, the oxidation of Sb(III) is reversible (157). 3) The *in vivo* voltammetric detection of catecholamines can be achieved without interference from oxide formation at a Pt electrode pretreated with I^- (14). In the absence of adsorbed I, no oxidation peak is discernible for the catecholamines. 4) The reduction of Cr(VI), which is irreversible at a Pt electrode untreated with I, is reversible at a Pt electrode on which I is adsorbed (158).

The anodic behavior of I^- on Pt in acidic media has been described previously (11, 12, 17, 101). The first step in the oxidation of I^- is the production of I_2. The mechanism of this reaction, as proposed by Newson and Riddiford (159), Jordan and Javick (160, 161), and Dane *et al.* (162), involves the adsorption of I^-. A more recent investigation by Osteryoung and Anson (11) indicated that the mechanism of I_2 formation does not require adsorbed I, e.g., when occurring at an oxide-covered electrode. However, they did not postulate specific mechanisms for the formation of I_2 at oxide-free or oxide-covered electrodes. The product of further oxidation of I^- is IO_3^- (12, 101, 163). Zakharov and Songina (101) concluded that the oxidation of I^- to IO_3^- takes place by the

direct participation of O atoms of the surface oxide of Pt as indicated schematically by

$$PtO[O]_n + I^- \longrightarrow PtO[O]_{n-3} + IO_3^- + 6e^-$$

No other mechanism has been reported in the literature.

A. Voltammetric Studies

1. Cyclic voltammetry

An I-E curve for 0.5 mM I^- in 0.5 M H_2SO_4 is shown in Figure VI-2. During the positive scan of potential, I^- is oxidized to I_2 ($E_{\frac{1}{2}}$ = 0.48 V) to yield an anodic wave (A) with a limiting current plateau in the region 0.55 V < E < 0.95 V. Peak B, observed at E > 0.95 V, is the result of the production of IO_3^- and surface oxide. A significant part of the IO_3^- produced has been concluded to originate from adsorbed I with oxidative desorption occurring simultaneously with the anodic formation of surface oxide (12, 17). A limiting current plateau was not attained for the production of IO_3^- in the region of peak B; apparently, the production of IO_3^- is inhibited by the rapid conversion of the lower oxide (PtOH) to the higher oxide (PtO) in the potential region of peak B. At E > 1.3 V, the large current resulting from the anodic decomposition of the solvent to produce O_2 serves as a practical limit for the positive scan of potential. Two cathodic peaks were observed during the subsequent negative scan of potential. Peak C at E_p = 0.45 V is the result of the reduction of the surface oxide formed during the positive scan for E > 1.0 V. The electrochemical reduction of I_2 irreversibly adsorbed at

Figure VI-2: I-E curve of 0.5 mM I^- in 0.5 M H_2SO_4 at a Pt RDE

Electrode rotation speed (W): 1000 rpm

Potential scan rate (ϕ): 6 V/min

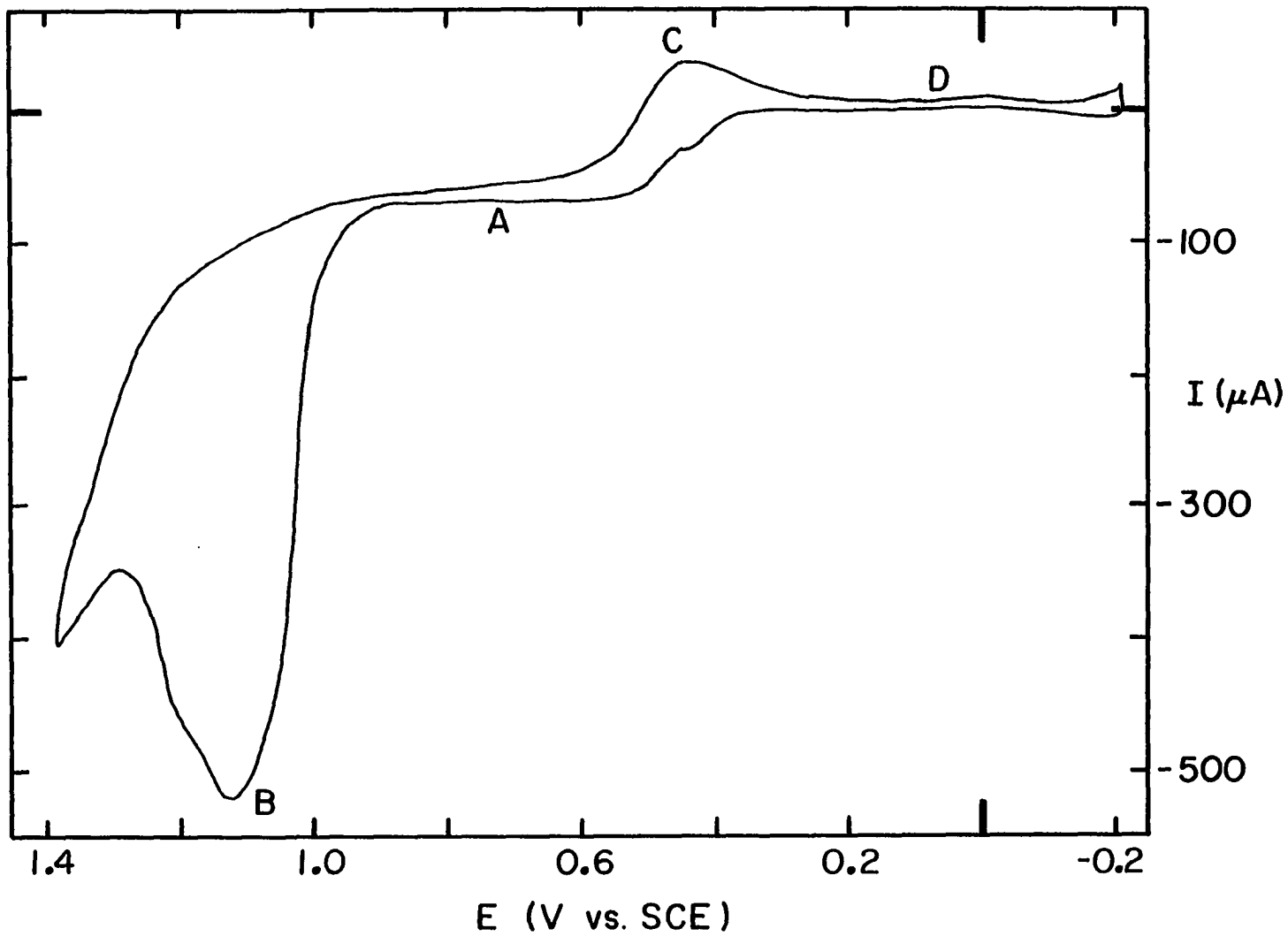
C
D
A
B
-100
-300
-500
I (μA)
1.4
1.0
0.6
0.2
-0.2
E (V vs. SCE)

the surface produces peak D at 0.0 V (17).

Current-potential curves were recorded as a function of ϕ for a constant value of ω. The height of peak B varied with changes in ϕ as expected for a surface-controlled process. The faradaic signal corresponding to the oxidation of I^- to I_2 (A) was independent of ϕ which is the typical behavior of a transport-controlled reaction. The I-E curves obtained at a single value of ϕ, while varying ω, demonstrated that the electrode current for both anodic reactions (A and B) increased as ω was increased. The oxidation of I^- to I_2 (A) is a mass-transport limited reaction, i.e., a plot of I_{lim} vs. $\omega^{\frac{1}{2}}$ is linear. The height of peak B varied nonlinearly with $\omega^{\frac{1}{2}}$, since peak B consists of currents resulting from the formation of surface oxide and the anodic production of IO_3^- from I (i.e., surface-controlled reactions), in addition to any transport-coupled oxidation of I^- from the bulk solution.

A series of I-E curves was recorded as a function of E_a (Figure VI-3). The anodic formation of surface oxide does not occur for $E_a \leq 1.0$ V, because of the presence of adsorbed I. The reduction peak observed during the negative scan for $E_a \leq 1.0$ V (A) is attributed to the reduction of reversibly adsorbed I_2. For $E_a = 1.1$ V, formation of PtOH proceeds with a minimal amount of place exchange to give OHPt or further oxidation to PtO. Therefore, upon reversal of the potential scan, PtOH is available to catalyze the oxidation of I^- to IO_3^-. The $E_{\frac{1}{2}}$ observed for the formation of IO_3^- during the negative scan of potential is 35 mV more negative than the $E_{\frac{1}{2}}$ observed for this reaction during the preceding positive scan of potential. In a thermodynamic

Figure VI-3: I-E curves of 0.5 mM I^- in 0.5 M H_2SO_4 at a Pt RDE as a function of E_a

Electrode rotation speed (W): 1000 rpm

Potential scan rate (ϕ): 6 V/min

——— 1.0 V

------- 1.1 V

····· 1.2 V

— · — 1.3 V

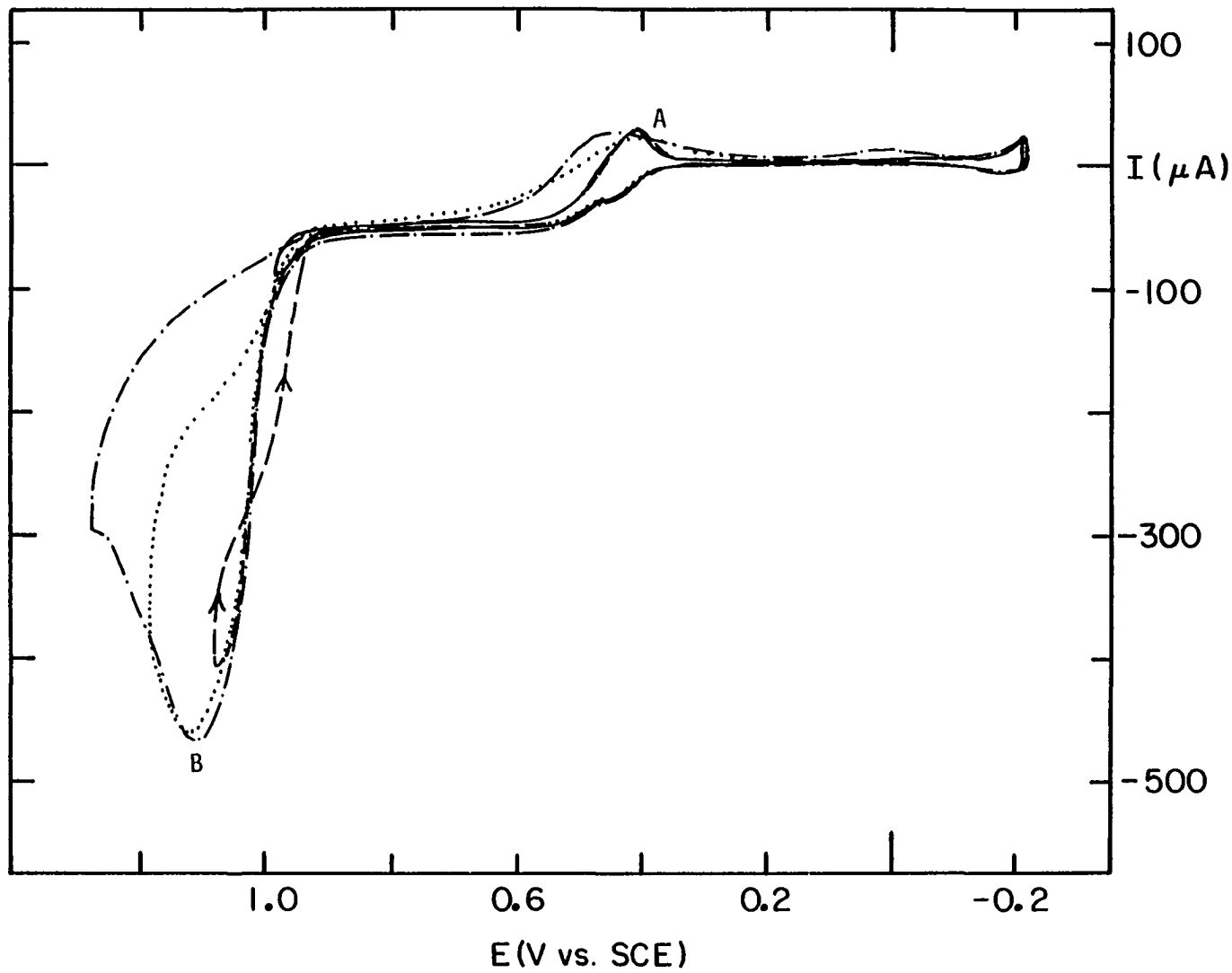
100
I(μA)
-100
-300
-500
A
B
1.0
0.6
0.2
-0.2
E(V vs. SCE)

sense, the oxidation reaction is more reversible in the presence of a small amount of surface oxide, specifically PtOH. At $E_a \geq 1.2$ V, an anodic peak (B) was attained for the oxidation of I^- to IO_3^- during the positive scan of potential. The anodic formation of IO_3^- did not occur during the negative scan of potential for $E_a \geq 1.2$ V because of the presence of OHPt and PtO on the electrode surface which do not catalyze the reaction.

The transition between reversibly adsorbed I_2 and irreversibly adsorbed I_2 was observed by close examination of the reduction reactions occurring in the region 0.7 V > E > -0.22 V (Figure VI-4). Peak A at $E_p = 0.45$ V corresponds to the reduction of reversibly adsorbed I_2 (17). As long as $E_a < 1.02$ V, i.e., no oxide formation occurred, only peak A was observed. However, for $E_a > 1.02$ V, a reduction peak at $E_p = 0.0$ V was produced which is attributed to the reduction of irreversibly adsorbed I_2 (17). The height of peak B, i.e., the amount of irreversibly adsorbed I_2, increased to a constant value as E_a became more positive. Hence, the I_2, once reversibly adsorbed, is converted to irreversibly adsorbed I_2 as Pt oxide is formed on the electrode (17). The change in the height of peak A was obscured by the overlapping oxide reduction peak.

2. Square-wave hydrodynamically modulated voltammetry

The investigation of the transport-coupled process of IO_3^- formation required the measurement of the convective component of the total current, as can be achieved by QHMV. The production of IO_3^- by oxidative desorption of adsorbed I does not contribute to the ΔI signal.

Figure VI-4: I-E curves of 0.5 mM I^- in 0.5 M H_2SO_4 at a Pt RDE as a function of E_a

Electrode rotation speed (W): 1000 rpm

Potential scan rate (ϕ): 6 V/min

——— 1.0 V

------- 1.1 V

····· 1.2 V

— · — 1.3 V

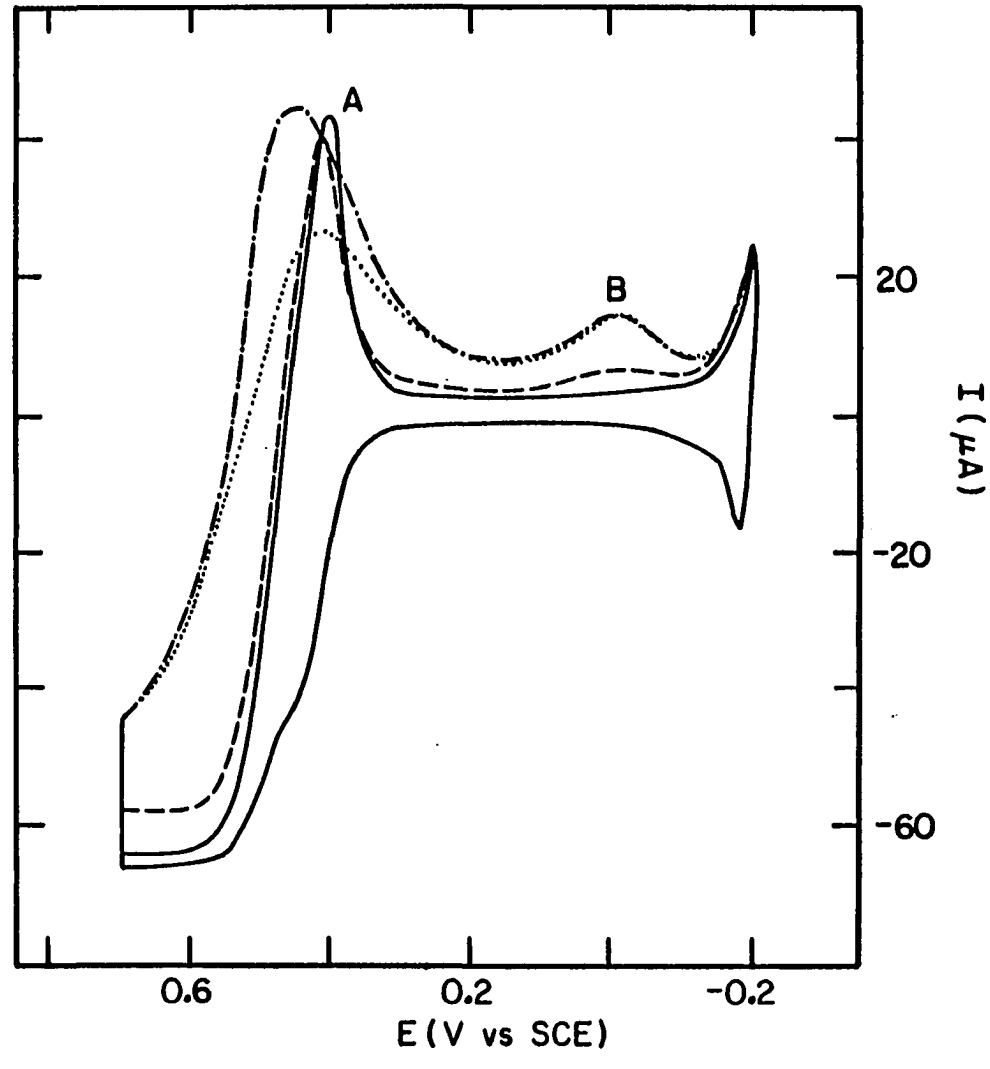
A
B
20
-20
-60
I (μA)
0.6
0.2
-0.2
E (V vs SCE)

a. Staircase potential waveform The electrochemical response of I^- at a Pt electrode was characterized by QHMV utilizing the staircase potential waveform illustrated in Figure IV-1. The resultant ΔI-E curve is shown in Figure VI-5. The reaction $I^- \longrightarrow \frac{1}{2}I_2 + e^-$ occurred with the thermodynamically predicted value of $E_{\frac{1}{2}} = 0.48$ V and the transport-limited current was observed in the region 0.55 V < E < 0.95 V (A). The value of ΔI (67 μA) corresponds closely to the theoretical value (69 μA) predicted from the linear Levich plot (I vs. $\omega^{\frac{1}{2}}$) constructed for this anodic process from data obtained by cyclic voltammetry. Peak B at ca. 1.05 V corresponds to the oxidation of I^- transported from the bulk solution to IO_3^-. The height of peak B was significantly less than the transport-limited value predicted for this reaction (i.e., 6·69 μA); however, ΔI is greater than the value expected for the transport-limited oxidation of I^- to HIO (i.e., 2·69 μA). The appearance of a peak signal for the oxidation of I^- to IO_3^- can be explained on the basis of the catalytic properties of the surface oxide. Oxidation of I^- to IO_3^- is thermodynamically allowed in this solution for E > 0.84 V; however, the reaction was not observed to occur until E > 1.0 V, corresponding to the onset of the formation of surface oxide. It was concluded that the production of IO_3^- from I^-, as well as adsorbed I, is initiated by the generation of PtOH as the first step in the formation of the surface oxide (PtO). Unfortunately, the adsorbed I suppresses the onset of oxide formation (see Figure VI-1); hence, the potential range is quite narrow over which the production of IO_3^- is thermodynamically allowed, and in which PtOH exists in an appreciable quantity at the electrode

Figure VI-5: ΔI-E curve of 0.5 mM I^- in 0.5 M H_2SO_4 at a Pt RDE

Lower rotation speed (W_l): 1000 rpm

Upper rotation speed (W_u): 4000 rpm

Potential step increment (ΔE): 5 mV

Time delay (t_d): 150 ms

Number of data points (N): 10

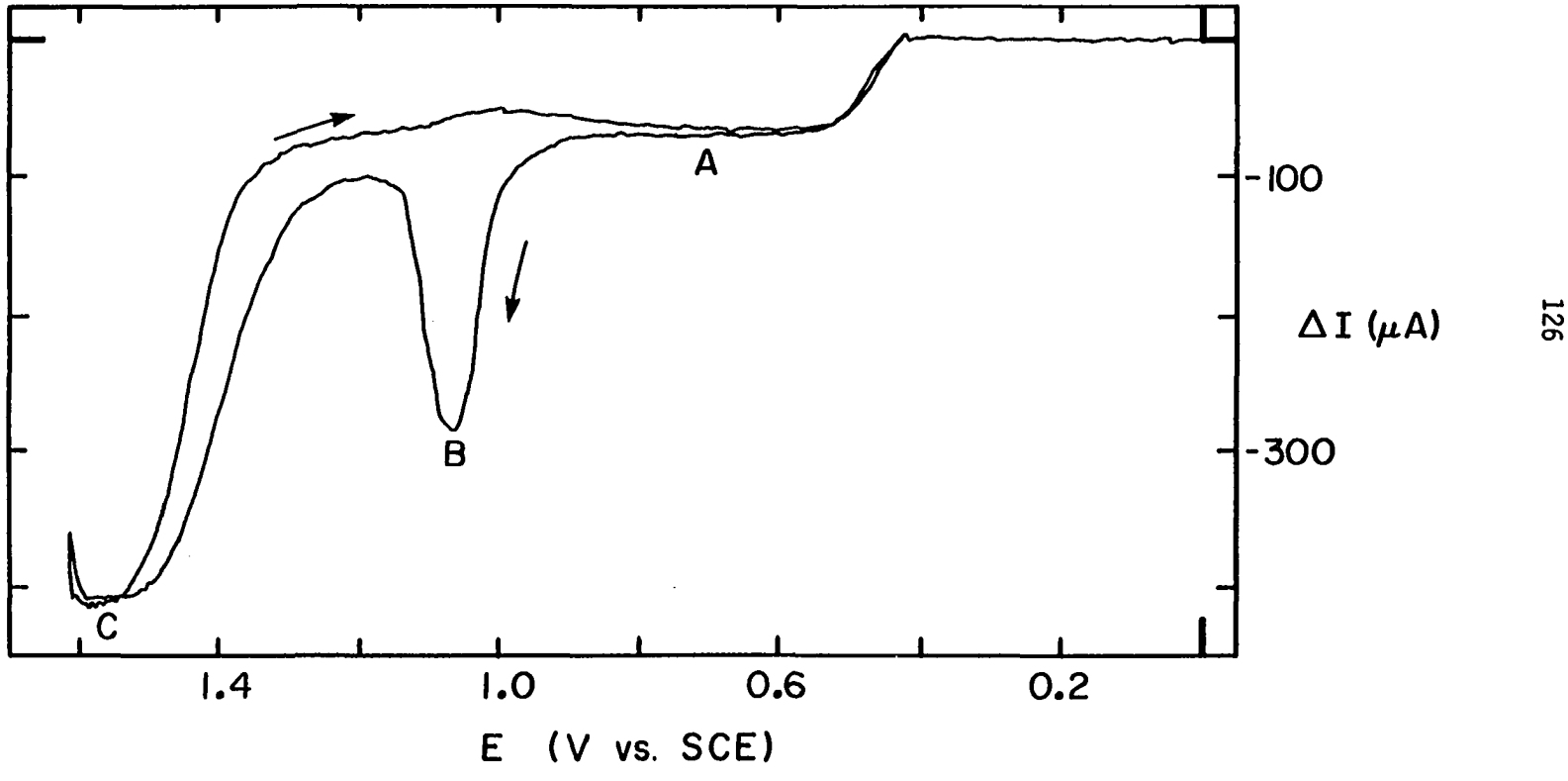
A
B
C
-100
-300
ΔI (μA)
1.4
1.0
0.6
0.2
E (V vs. SCE)

surface. Rearrangement of PtOH to the catalytically inactive OHPt, and further oxidation to PtO, occur rapidly for E > 1.2 V and the production of IO_3^- is suppressed sharply. As the potential increased beyond 1.3 V, ΔI increased to a limiting current plateau for E > 1.5 V (C) and is attributed to the production of IO_3^-. The ratio of ΔI for the two limiting values of current for waves C and A ($\Delta I_C/\Delta I_A$) is 6.0 as expected on the basis of the assigned reactions. The renewed formation of IO_3^- occurring concomitantly with O_2 evolution is attributed to the catalytic involvement of the OH radical generated on the PtO surface as the first step in the production of O_2. In addition, the evolution of O_2 involves the abstraction of O-atoms in the oxide film (54, 56); therefore, when O_2 molecules leave the surface of the electrode, the oxide must be reformed. Since the formation of oxide involves OH radicals as an intermediate product, there is an abundance of OH radicals present on the electrode surface during O_2 evolution which exhibit an electrocatalytic effect on IO_3^- formation. Upon reversal of the potential scan, the transport-limited production of IO_3^- proceeded as long as O_2 was evolved. At E < 1.3 V, only the oxidation of I^- to I_2 occurred, since virtually no PtOH is generated during the negative scan of potential. These results are consistent with the conclusion that the oxidation of I^- to IO_3^- requires the electrocatalytic benefit of the OH radical, whether adsorbed on the metal surface (PtOH) or the oxide (PtOOH).

b. Triple-step potential waveform QHMV was applied utilizing the triple-step potential waveform illustrated in Figure IV-2. The potential waveform consisted of an initial potential value (E_1) which

resulted in the reduction of PtOH and PtO on the electrode surface, an oxidizing potential (E_2) for which surface oxidation was initiated, and a sampling potential ($E_3 < E_2$) at which the faradaic signal was measured. This particular sequence of potential values effectively "freezes" the oxide layer, for the sampling period, in the state which is characteristic of the oxide formed at E_2 for the time period t_2. For a small value of t_2 (e.g., 50 ms), production of the catalytically active oxide (PtOH) is maximized with relatively little conversion to the less active OHPt and PtO. The driving force for the formation of additional oxide no longer exists at $E < E_2$; therefore, anodic reactions which occur will tend to be characteristic of the catalytic activity of the oxide formed at E_2. It should be noted that catalytically active PtOH generated at E_2 will undergo conversion to the inactive OHPt at $E_3 < E_2$. Since PtOH is not reduced until $E < 0.7$ V, use of this waveform results in the availability of PtOH produced at the electrode surface for a limited time during the sampling period with $E_3 > 0.7$ V. The results for E_2 = 1.1 V, 1.2 V, and 1.6 V are shown in Figure VI-6. The oxidation of I^- to I_2 (A) for $0.45 \text{ V} < E < 0.95$ V proceeded regardless of the value of E_2, i.e., the formation of I_2 is not inhibited by the presence of surface oxide. As E_2 was increased from 1.1 V to 1.2 V, the value of ΔI in the region of peak B decreased significantly and the $E_{1/2}$ of the wave shifted 25 mV in the positive direction; these changes demonstrate that the formation of OHPt and PtO is more irreversible than the formation of PtOH at less positive potentials. Current in the region of peak B continued to decrease as E_2 was increased and the $E_{1/2}$ of the

Figure VI-6: ΔI-E_3 curve of 0.5 mM I^- in 0.5 M H_2SO_4 at a Pt RDE utilizing the triple-step potential waveform illustrated in Figure IV-2

Lower rotation speed (W_l): 1000 rpm

Upper rotation speed (W_u): 4000 rpm

Potential step increment (ΔE): 20 mV

Number of data points (N): 50

E_1 = 0.0 V t_1 = 250 ms

E_3 = variable t_3 = 200 ms

values of E_2 (t_2 = 200 ms) were as follows:

- • 1.10 V
- x 1.20 V
- \+ 1.60 V

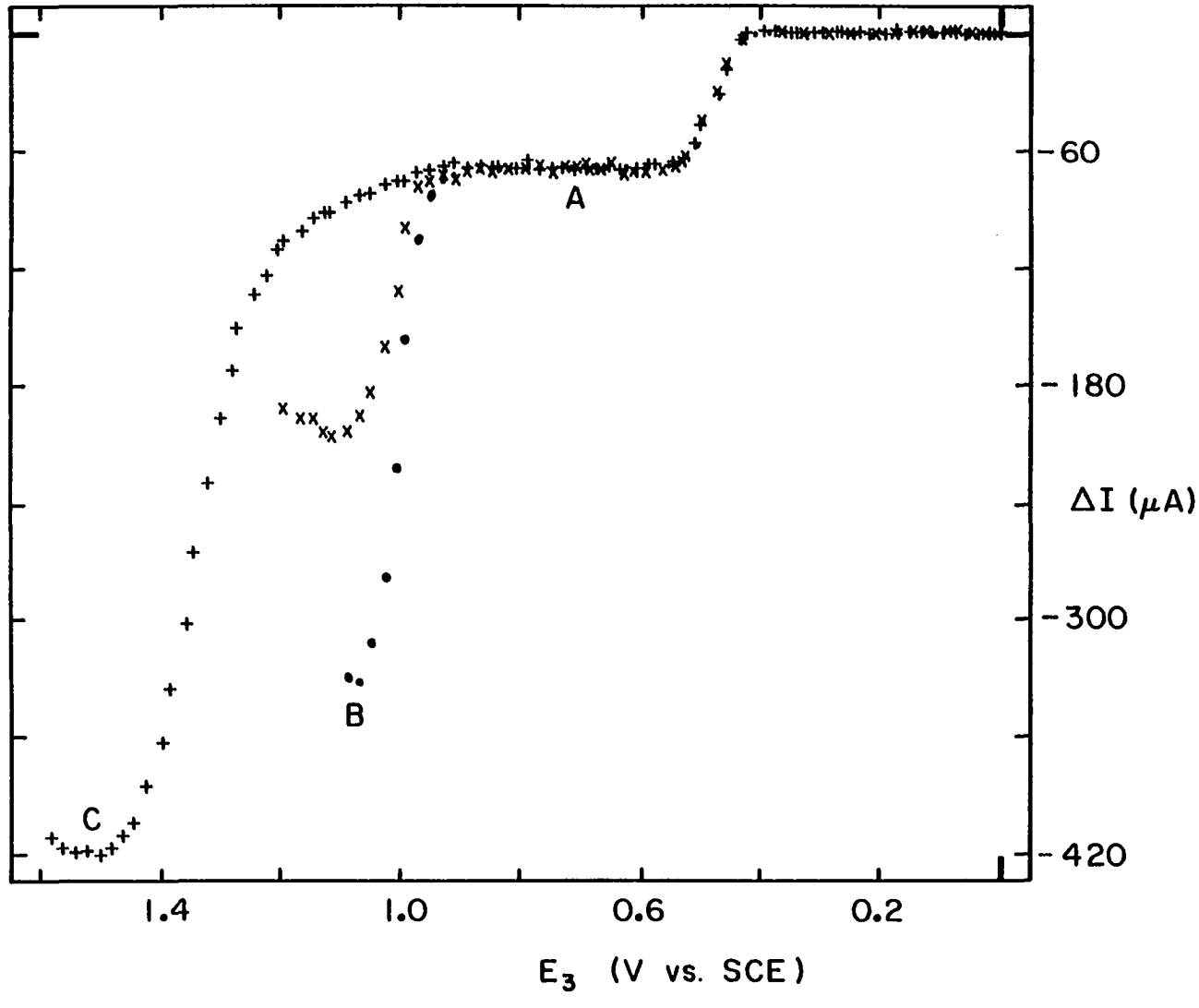
-60
-180
-300
-420
ΔI (μA)
A
B
C
1.4
1.0
0.6
0.2
E3 (V vs. SCE)

reactions shifted to more positive values. However, values of ΔI, obtained for 1.3 V < E < 1.6 V (C), correspond to the limiting current for the oxidation of I^- to IO_3^-. The ratio of ΔI for the two limiting currents ($\Delta I_C/\Delta I_A$) is 6.0.

The time dependence for conversion of active PtOH to the inactive OHPt and PtO is illustrated by plots of ΔI as a function of t_2 for several values of E_2 in the range 1.1 V < E < 1.6 V (Figure VI-7). For E_2 = 1.1 V, ΔI was essentially constant throughout the range of values of t_2 tested. For E_2 = 1.2 V, the catalytic activity of the electrode surface, as measured by ΔI, decreased with increasing t_2, approaching the limiting value for the oxidation of I^- to I_2 observed for t_2 > ca. 400 ms. For $E_2 \geq$ 1.3 V, ΔI corresponded approximately to the transport-limited value for the oxidation of I^- to I_2 at all values of t_2.

3. Summary

The oxidative reactions of I^- in acidic media at a Pt electrode were examined in detail. The convective components of the total electrode current include: 1) the mass-transport limited formation of I_2 at E > 0.45 V; 2) the mass-transport coupled oxidation of I^- to IO_3^-, which is catalyzed by the anodic formation of PtOH; and 3) the mass-transport limited production of IO_3^-, which is concluded to be electro-catalyzed by OH, an intermediate product of O_2 evolution. Observation of the latter two components was possible only upon application of QHMV.

Figure VI-7: Plots of ΔI vs. t_2 as a function of E_2 for 0.5 mM I^- in 0.5 M H_2SO_4 at a Pt RDE

Lower rotation speed (W_l): 1000 rpm

Upper rotation speed (W_u): 4000 rpm

Number of data points (N): 10

E_1 = 0.00 V t_1 = 250 ms

E_2 = variable t_2 = variable

E_3 = 1.05 V t_3 = 20 ms

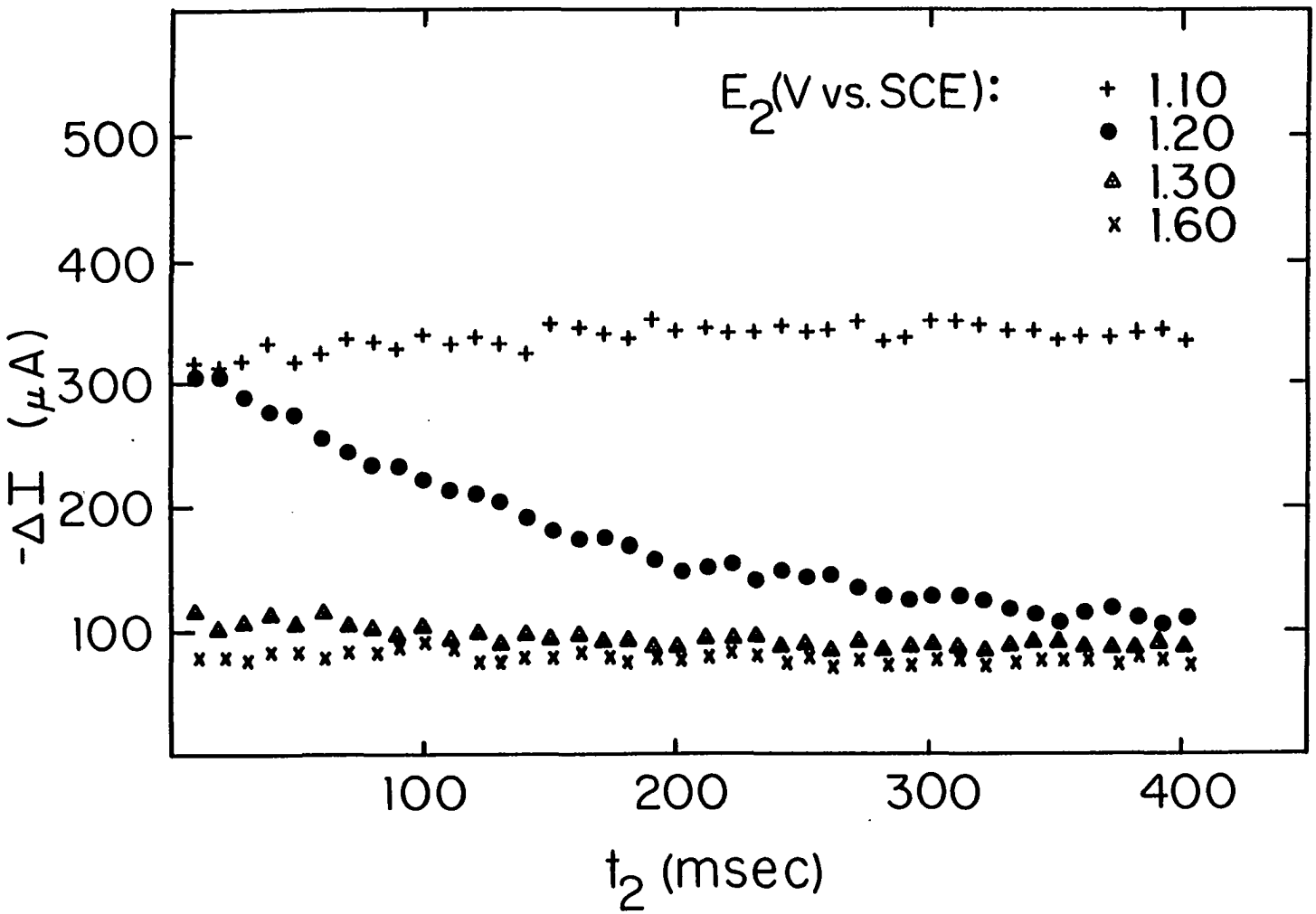
E_2(V vs. SCE):
1.10
1.20
1.30
1.60
500
400
300
200
100
$-\Delta I$ (μA)
100
200
300
400
t_2 (msec)

C. Flow Injection Detection

Constant potential amperometry is applicable for the detection of numerous electroactive species; however, the loss of electrode activity at noble metal electrodes frequently is observed. The loss of electrode activity can be attributed to 1) the formation of a passivating oxide or 2) fouling of the electrode surface by residual products which remain strongly adsorbed on the electrode surface. In either case, continued oxidation of the analyte is inhibited and the analytical signal rapidly diminishes. Amperometric detection utilizing a stepped potential waveform has been developed which leads to greater stability of the electrochemical response. Results obtained by application of a double-step potential waveform have been reported (164-167), noting the observed increase in stability of the electrochemical response. However, recently, triple-step amperometric detection has received much attention (168-173) particularly for the anodic detection of organic compounds, e.g., alcohols (168), carbohydrates (169-172), amino acids (171, 173), and sulfur-containing organic compounds (173). Triple-step amperometry utilizes a potential waveform which incorporates voltammetric cleaning and reactivation of the electrode surface together with the amperometric measurement. Reproducible electrode activity is achieved during each cycle of the potential waveform, therefore, the value of current measured for a given concentration of analyte is constant.

Amperometric detection of compounds, whose oxidation is catalyzed by anodic formation of PtOH, is greatly enhanced through the application

of triple-step amperometry. The electrocatalyzed response is short-lived due to the transient lifetime of PtOH. Therefore, by application of a triple-step potential waveform, the surface is reproducibly regenerated and current is measured when the electrocatalyzed response is near its maximum value. The amperometric detection of I^- was examined utilizing single (dc) and multi-step potential waveforms to illustrate the enhanced sensitivity of the measured signal in the potential region where the electrocatalyzed oxidation of I^- to IO_3^- occurs.

The response of electrode current to a step change in potential will be considered in general terms so that the choice of the multi-step potential waveform and the observed analytical signal for specific reactions are more easily understood. In all instances, the contribution of double-layer charging current is ignored for simplicity.

The Cottrell equation, $I = nFAD^{\frac{1}{2}}C^b/\pi^{\frac{1}{2}}t^{\frac{1}{2}}$, describes the response of current as a function of time following a step in potential under the condition of no convection. The observed electrode current approaches zero as time approaches infinity (Figure VI-8-A). If the potential is stepped to a region where a mass-transport limited reaction occurs, the Cottrell equation is valid at short t, regardless of the geometric shape of the electrode or the existence and nature of convection. However, for long t, current deviates from the Cottrell equation and approaches a steady state value which is a function of the geometry of the electrode and the rate of convection (Figure VI-8-B). At a rotating disk electrode, the magnitude of the steady-state current is described

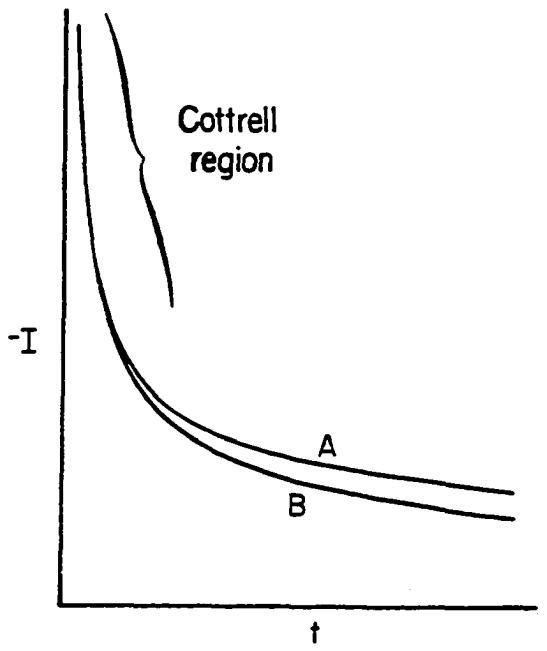

Figure VI-8: Expected anodic response following a positive potential step into a region where a transport-limited reaction is occurring. [A-no convection. B-with convection.]

by the Levich equation and is independent of time.

When the potential is stepped to a region where surface oxide formation is the only faradaic reaction occurring, current (I_{ox}) decays according to the equation $I_{ox} = c\eta/t$ where η is the applied overpotential, t is time, and c is a constant (174, 175) (Figure VI-9-A). In the presence of an irreversibly adsorbed, electroinactive species, I_{ox} is decreased at all values of t (Figure VI-9-B).

If a change in applied potential results in the desorption of an electroinactive species concomitantly with formation of oxide, the value of I_{ox} is decreased significantly at small t. However, at longer t,

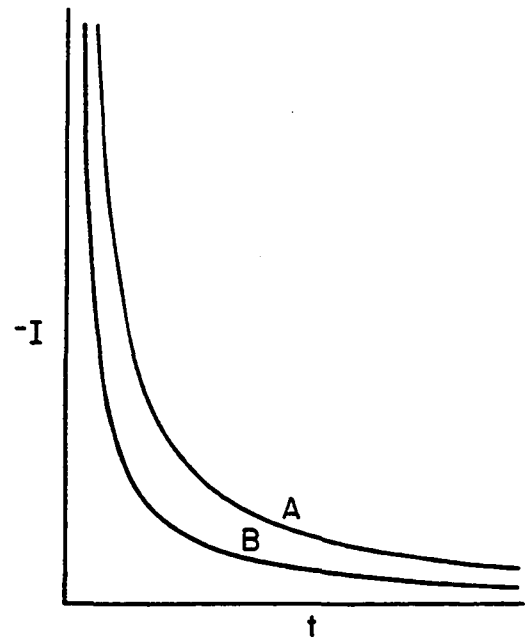

Figure VI-9: Expected anodic response following a positive potential step into a region where oxide formation occurs. [A-oxide formation in the absence of analyte, $\theta_A = 0$. B-oxide formation in the presence of an irreversibly adsorbed analyte $\theta_A = 0.5$.]

current is larger than the value of I_{ox} observed in the absence of an adsorbed species, since the total charge passed for oxide formation over an extended period of time must be virtually the same regardless of the initial coverage by an electroinactive species. The I-t response for this case is shown in Figure VI-10.

Oxidative desorption of an electroactive adsorbate by a process electrocatalyzed by the formation of surface oxide produces a I-t curve shown in Figure VI-11. Current is inhibited at short t for $\theta > 0$ but enhancement of the current is observed at longer t. The total

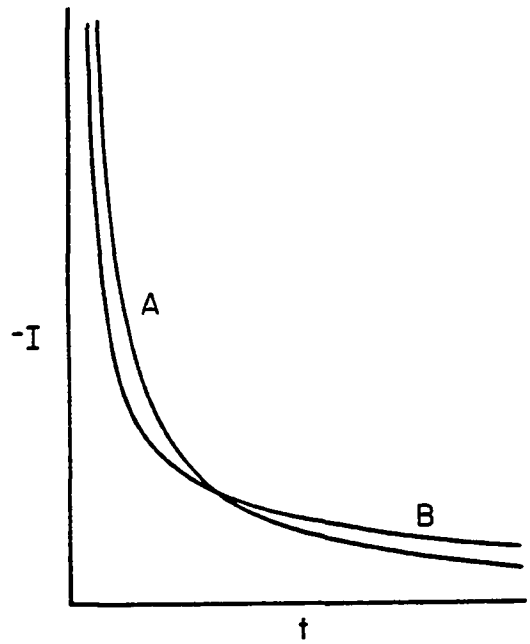

Figure VI-10: Expected anodic response following a positive potential step into a region where oxide formation occurs. [A-oxide formation in the absence of analyte, $\theta_A = 0$. B-oxide formation in the presence of reversibly adsorbed analyte, $\theta_A = 0.5$.]

charge passed upon electro-oxidative desorption over a long time period will exceed the charge passed for the formation of oxide because of the faradaic reaction of the analyte.

The magnitude of the current and the direction of deflection of the signal in relation to the baseline for pulsed amperometric detection is dependent upon the processes occurring at the sampling potential and the value of t selected for measurement of I. Analytical application utilizing any of the responses is feasible provided that the electrode surface is reproducibly regenerated during each cycle of the applied

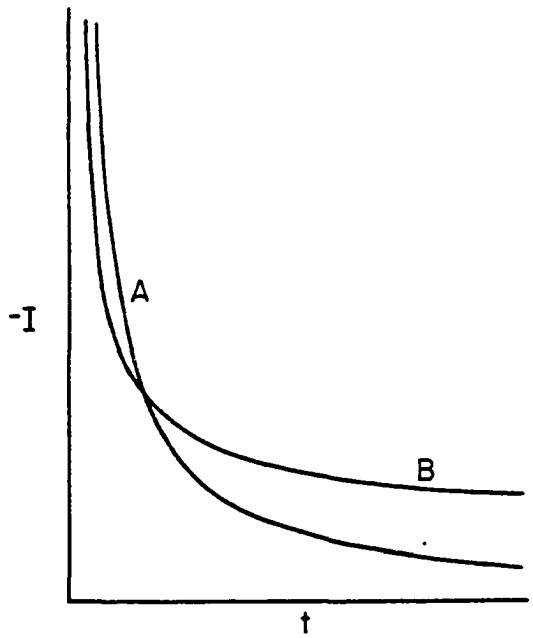

Figure VI-11: Expected anodic response following a positive potential step into a region where oxide formation occurs. [A-oxide formation in the absence of analyte, $\theta_A = 0$. B-oxide formation and concurrent oxidative desorption of the analyte. $\theta_A = 0.5$.]

waveform. Tailing of peaks is observed if the adsorbate is not completely removed from the electrode surface during the cleaning steps in the waveform.

The amperometric detection of I^- at a Pt electrode was investigated taking advantage of the following characteristics of the electrochemical response of I^-: 1) I^- is oxidized to I_2 by a mass-transport limited reaction in the region 0.55 V < E < 0.95 V; 2) I^- is strongly adsorbed on a reduced Pt surface, consequently, anodic formation of surface oxide is suppressed in the region 0.55 V < E < 1.0 V; and 3) adsorbed I

is oxidatively desorbed at E > 1.0 V through an electrocatalytic reaction producing IO_3^-. The multi-step potential waveforms applied for flow injection detection are listed in Table VI-1. The resultant flow injection peaks for single (dc) and multi-step amperometry are illustrated in Figure VI-12. Each case will be discussed briefly.

Table VI-1. Multi-step potential waveforms utilized for the amperometric detection of I^- at a Pt electrode

Waveform	E_1 (mV); t_1 (ms)	E_2 (mV); t_2 (ms)	E_3 (mV); t_3 (ms)
A	700; 100	1300; 200	200; 150
B	600; 100	1300; 200	200; 150
C	1150; 100	200; 150	none
D	1150; 100	1300; 200	200; 150

Constant potential amperometry can be employed for the detection of I^- by observing the mass-transport limited signal produced by the reaction $I^- \longrightarrow \frac{1}{2}I_2 + e^-$ in the region 0.55 V < E < 0.95 V without interference from surface oxide (Figure VI-12a). The electrode is pretreated by injecting a highly concentrated plug of I^- which establishes the maximum equilibrium coverage by I on the electrode surface. The equilibrium condition persists even for the absence of I^- in the electrolytic solution provided the potential does not exceed 1.0 V. Hence, reproducible anodic peaks were obtained upon subsequent injection of I^- into the I^--free carrier stream. If the maximum

Figure VI-12: Flow injection peaks for 100 μM I^- in 0.5 M H_2SO_4 at a Pt wire electrode

Flow rate: 1.1 ml/min

Sample volume: 50 μl

Constant potential amperometry

a. E = 700 mV

Triple-step potential amperometry

b. waveform A

c. waveform C

d. waveform D

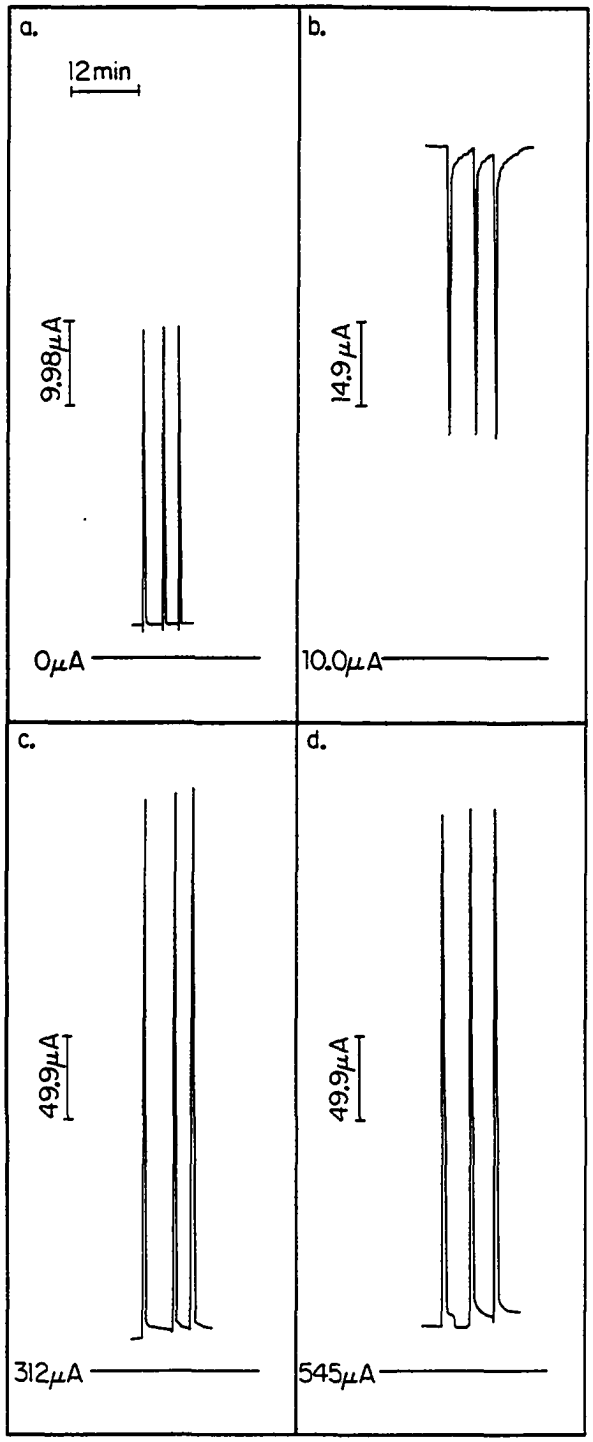
a.
12min
9.98μA
0μA
b.
14.9μA
10.0μA
c.
49.9μA
312μA
d.
49.9μA
545μA

equilibrium coverage does not exist on the surface, I^- will preferentially adsorb on the electrode surface resulting in irreproducible anodic peaks.

Because adsorbed ions suppress the formation of surface oxide on Pt, I^- can be detected indirectly on the basis of the suppressed oxide current utilizing waveforms A and B. This mode of detection is employed successfully for flow injection detection if all adsorbed I from one detection cycle is removed prior to the next detection cycle. The following processes occur sequentially during a single application of the waveform: 1) I is oxidatively desorbed (E_2 = 1300 mV) and surface oxide is formed; 2) the resulting surface oxide is cathodically reduced at E_3 = 200 mV and I^- is adsorbed from the solution; and 3) the current sampled at E_1 = 600 mV or 700 mV is less than the background signal for the absence of I^- in solution since adsorbed I suppresses the formation of surface oxide. Although the background signal for E_1 = 600 mV (waveform B) was slightly lower than for E_1 = 700 mV (waveform A), the height of the detection peak observed upon application of waveform A was approximately 3 times larger than the height of the detection peak observed upon application of waveform B. Hence, waveform A was preferred (Figure VI-12b).

Direct anodic detection of I^- can be accomplished by measuring the current produced as a result of the oxidative desorption of I (waveforms -C and D). Although a limiting current value was not attained for the production of IO_3^-, substantially increased sensitivity was observed. Application of a double-step potential waveform (C) resulted in

broadening of the detection peaks due to carry-over of adsorbed I from the previous detection cycle. Addition of a potential step for oxidative cleaning minimized peak broadening; however, sensitivity decreased. A larger quantity of oxide is formed during anodic cleaning which requires a larger cathodic current to reduce the surface oxide, thus, a longer time is required for the potentiostat to overcome the uncompensated value of iR_{cell}. As a result, a shorter effective time period in which the adsorption of I^- occurs and a decrease in sensitivity was observed. As the adsorption time for both waveforms (C and D) were increased, the analytical response became equivalent for the two waveforms (Figures VI-12c and VI-12d).

Examination of the relationship between the time spent at the adsorption potential and the height of the detection peak should provide information about the adsorption isotherm. Increased peak height should be observed with increasing adsorption time (t_{ads}, where $t_{ads} = t_3$ for waveforms A and D and $t_{ads} = t_2$ for waveform C) until equilibrium coverage is attained. Plots of peak height vs. t_{ads}, for waveforms A, C, and D, are shown in Figure VI-13. Equilibrium coverage by I was not attained for $t_{ads} \leq 500$ ms. An estimate of exposure time (τ) required for maximum coverage to occur, assuming transport-limited adsorption for $t < \tau$, was calculated in the following manner: 1) Flux (F_x) is defined as $F_x = I_{lim}/nF = A(D/\delta)C^b$. In this case, $A = 0.050\ cm^2$, $D = 6.95 \times 10^{-5}\ cm^2/s$, $\delta = 3.8 \times 10^{-3}$ cm, and $C^b = 1.0 \times 10^{-7}\ mol/cm^3$; therefore, $F_x = 9.1 \times 10^{-11}$ mol/s. 2) The value of Γ_{max} for I^- on Pt is $1 \times 10^{-9}\ mol/cm^2$ (16). 3) The exposure time (τ) is given by

Figure VI-13: Peak height vs. t_{ads} for triple-step amperometric detection of 100 μM I^- in 0.5 M H_2SO_4 at a Pt wire electrode

Flow rate: 1.1 ml/min

Sample volume: 50 μl

a. waveform A

b. waveform C

c. waveform D

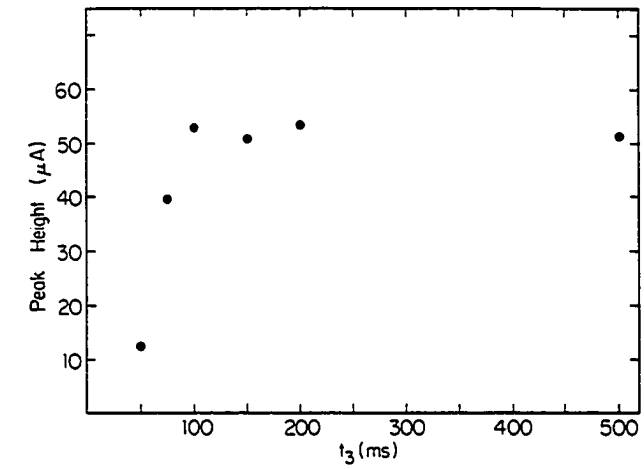
Peak Height (μA)
60
50
40
30
20
10
100
200
300
400
500
t_3 (ms)

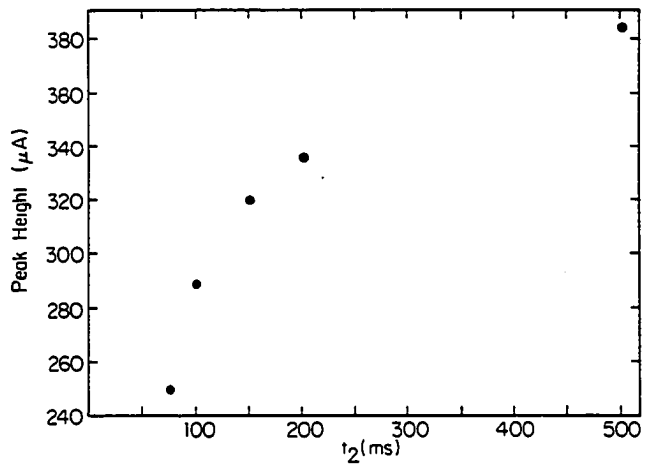
Peak Height (μA)
380
380
340
320
300
280
260
240
100
200
300
400
500
t_2 (ms)

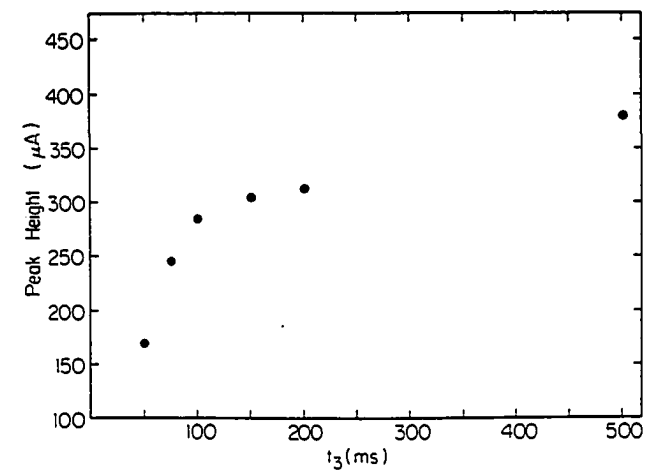
Peak Height (μA)
450
400
350
300
250
200
150
100
100
200
300
400
500
t_3 (ms)

$\tau = \Gamma_{max}/F_x$; hence, τ = 0.7 s. Additional data was collected to test this prediction; however, the observed value of t_{ads} was on the order of 10 s before maximum peak height was attained. Since these experiments were completed, it has been determined that all Pt oxide is not reduced under the conditions of these experiments (E_{ads} = 200 mV, $t_{ads} \leq$ 500 ms). Therefore, these results are not valid for the determination of adsorption isotherm parameters. Nevertheless, the data are useful in predicting conditions for maximum sensitivity vs. efficiency for the pulsed detection technique. Experiments which utilize a four-step potential waveform are currently in progress.[1] The processes occurring during the sequence of potential steps are as follows: 1) adsorbed I is oxidatively desorbed at E = 1300 mV; 2) the potential is stepped into the region of H_2 evolution (E < -0.2 V) which facilitates reduction of the surface oxide and no I^- is adsorbed; 3) I^- is adsorbed at E = 200 mV for various lengths of time (50-500 ms); and 4) current is sampled at E = 600 mV. A four-step potential waveform increases the sensitivity of the measured signal since more I^- adsorbs on the surface for shorter adsorption times and increases the reliability of adsorption isotherm data.

---

[1] Polta, J. A., unpublished results, Iowa State University, 1984.

VII. THE REDUCTION OF IODATE

A. Introduction

Based on the results obtained for the oxidation of I^- to IO_3^- at a Pt electrode, it was concluded that the formation of IO_3^- is catalyzed by the initial stage of Pt oxide formation (i.e., PtOH) but is inhibited by the more stable form of Pt oxide (PtO). Numerous reactions, e.g., the evolution of O_2 (54) and the reduction of Ce^{4+} (176, 177) at Pt electrodes, are inhibited by PtO. In sharp contrast, the reduction of O_2 (178), V^{5+} (178), H_2O_2 (75), and IO_3^- (179, 180) occur more readily at an oxidized Pt electrode than at a reduced Pt electrode. Therefore, the cathodic behavior of IO_3^- at a Pt electrode was investigated by application of CV and QHMV to evaluate further the effect that Pt oxide exhibits on the reduction of IO_3^-.

The electroreduction of IO_3^- has been studied by chronopotentiometric and voltammetric techniques (179, 180). Anson (179) observed that the reduction of IO_3^- at an oxidized Pt surface occurred at potentials from 200-600 mV more positive than the potential at which the reduction of IO_3^- occurred at a reduced Pt electrode. The decrease in η was attributed to catalysis of the cathodic reduction of IO_3^- when accompanied by the reduction of the oxide layer. A decrease in cathodic current owing to the reduction of IO_3^- was observed as the "catalyzing" oxide layer was removed from the electrode surface by reduction. Once the removal of the oxide layer was complete, no cathodic current was observed for IO_3^- until η was sufficiently large to cause the reduction

of IO_3^- to occur at the reduced Pt electrode. The rate of current decay increased as the potential was maintained at successively more negative values. In contrast, no decrease in current with time was observed for reactions such as Fe^{3+} or I_2 reduction which are not influenced by the oxide. Anson also observed that the peak for IO_3^- reduction shifted with changes in pH in accordance with that observed for the reduction of Pt oxide. Based on these observations, Anson concluded that the oxide layer is essential for the reduction of IO_3^- to proceed at $\eta < 750$ mV. Davis (180) also concluded that the reduction of IO_3^- is facilitated by the simultaneous reduction of Pt oxide. Current densities, measured at 0.45 V vs. SCE, increased as E_a became more positive. Davis also observed an abrupt change in the term $n\alpha$(n is the number of electrons and α is the transfer coefficient which is a measure of the symmetry of the reaction energy barrier) when the electrode had been reduced at $E < 0.25$ V. Therefore, he concluded that the reduction of IO_3^- occurs via a different mechanism on a reduced Pt surface than on an oxidized Pt surface.

The anodic formation and cathodic dissolution of Pt oxide, in the absence of electroactive species, has been investigated (50, 52, 178). The results of those studies will be summarized briefly. The early stage of oxide formation, i.e., the formation of PtOH with minimal place exchange ($\theta_{OH} < 0.15$), is electrochemically reversible. However, as E_a becomes more positive, the formation of a more stable oxide layer occurs as a result of place exchange between Pt and OH and, subsequently, further oxidation to PtO. Hence, the oxide formed at more positive

potentials is increasingly more irreversible and reduction occurs at more negative electrode potentials (Figure VII-1).

The mechanism of Pt oxide reduction is dependent upon the form of oxide. If the potential scan is reversed prior to the formation of PtO, the reductive process occurs according to the scheme (52)

$$OHPt \longrightarrow PtOH$$
$$PtOH + H^+ + e^- \longrightarrow Pt + H_2O$$

where place exchange is the rate determining step. The rate of the second step increases with increasingly negative values of potential. The reduction of PtO proceeds by the mechanism (52)

$$PtO + H^+ + e^- \longrightarrow PtOH$$
$$PtOH + H^+ + e^- \longrightarrow Pt + H_2O$$

where the formation of PtOH is the rate determining step. In either case, the existence of PtOH during the reduction of Pt oxide is only transient. Hence, PtOH is, perhaps, responsible for catalyzing cathodic reactions, as well as catalyzing oxidative processes.

B. Cyclic Voltammetry

The I-E curve obtained for IO_3^- at a Pt electrode is shown in Figure VII-2. A cathodic wave (A), for the reduction of IO_3^- to I^- at a reduced Pt surface, was observed in the region $-0.2\ V < E < 0.3\ V$ during the positive scan of potential. Iodide ions generated by this reduction reaction are adsorbed on the Pt surface and inhibit formation

Figure VII-1: I-E curves of Pt in 0.5 M H_2SO_4 as a function of E_a

Electrode rotation speed (W): 100 rpm

Potential scan rate (ϕ): 4 V/min

——— 0.74 V

- - - - - - - 0.83 V

····· 0.95 V

— · — 1.10 V

——— 1.25 V

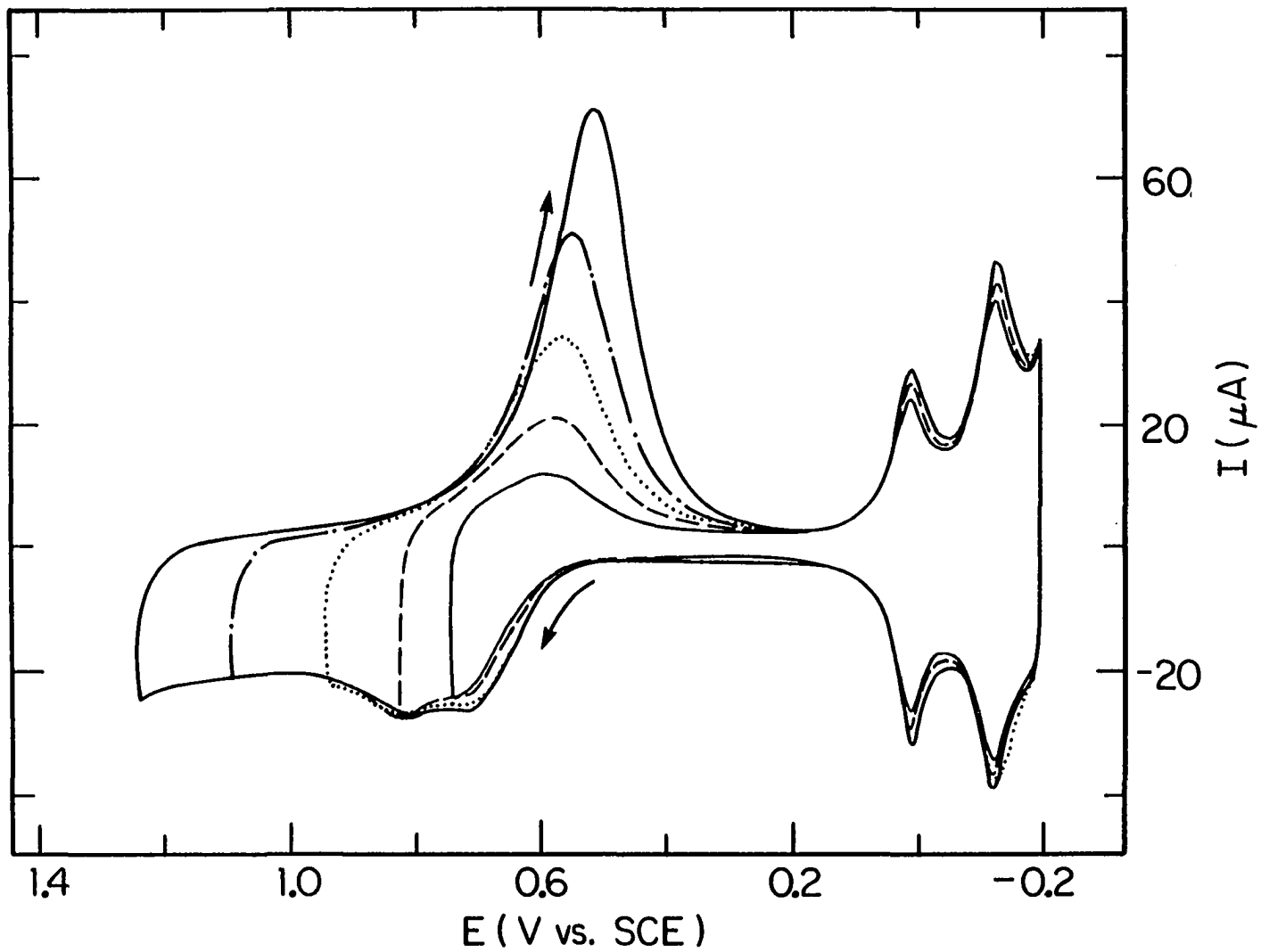
60
20
-20
I (μA)
1.4
1.0
0.6
0.2
-0.2
E (V vs. SCE)

Figure VII-2: I-E curve of 4×10^{-5} M IO_3^- in 0.5 M H_2SO_4 at a Pt RDE

Electrode rotation speed (W): 1000 rpm

Potential scan rate (ϕ): 6 V/min

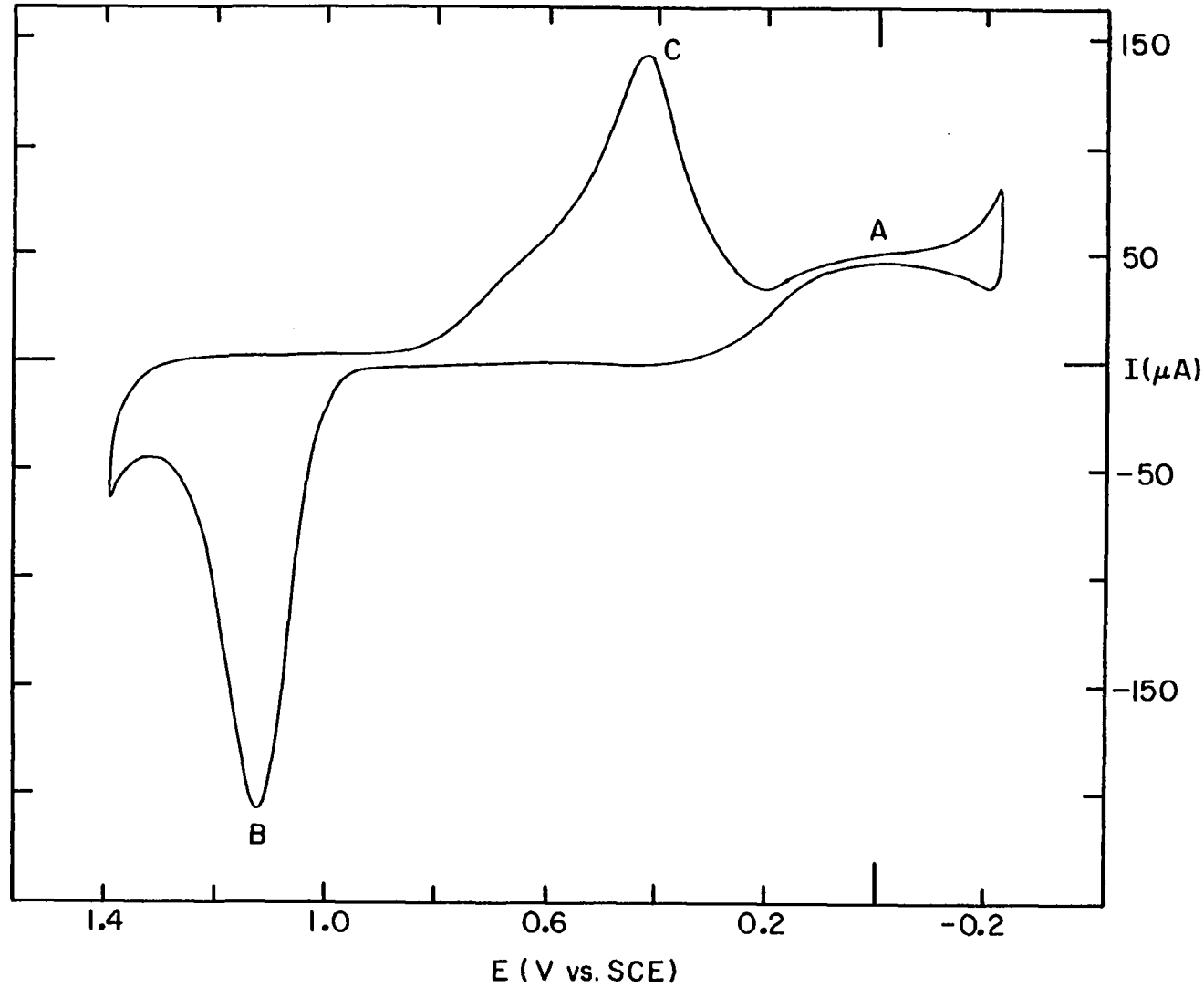
C
A
B
150
50
I(μA)
-50
-150
1.4
1.0
0.6
0.2
-0.2
E (V vs. SCE)

of PtOH during the subsequent positive scan of potential; therefore, only double layer charging current is observed in the region 0.3 V < E < 0.95 V. At E > 0.95 V, the anodic current increased rapidly and reached a maximum value at ca. 1.23 V (B). Peak B is the combination of current produced as the result of oxidative desorption of I and the formation of the surface oxide. For the negative scan of potential, the cathodic wave C corresponds to the reduction of Pt oxide and some reduction of IO_3^-. At E < 0.3 V, the cathodic wave A (already mentioned) was observed which corresponds to the reduction of IO_3^- to I^- on a reduced Pt surface with concurrent adsorption of I. Adsorption of H atoms is inhibited by the presence of adsorbed I therefore, the characteristic H adsorption and H desorption peaks are not observed.

Current-potential curves were recorded as a function of ϕ at a constant value of ω. The reduction of IO_3^- to I^- (wave A) at a reduced Pt electrode was independent of ϕ which is characteristic of a mass-transport controlled reaction. The height of peak B, the simultaneous oxidation of adsorbed I and the Pt surface, varied with ϕ which is the typical behavior observed for surface-controlled reactions. The height of peak C also varied with ϕ due to the contribution to the total current from the reduction of Pt oxide, a surface-controlled reaction.

Current-potential curves were recorded also as a function of ω while holding ϕ constant. Current resulting from the reduction of IO_3^- to I^- at a reduced Pt electrode (wave A) increased linearly with $\omega^{1/2}$, i.e., the reduction of IO_3^- is mass-transport limited at an overpotential of ca. 750 mV. Peak B, the combination of current due to surface oxide

formation and oxidative desorption of I, was independent of ω as expected for surface-controlled processes. The height of peak C increased nonlinearly with $\omega^{\frac{1}{2}}$ indicating that a surface-controlled reaction, i.e., oxide reduction, is occurring simultaneously with the transport-coupled reduction of IO_3^-.

Current-potential curves recorded as a function of E_a are shown in Figure VII-3. For $E_a \leq 1.0$ V, only the cathodic wave A was observed which corresponds to the reduction of IO_3^- at the reduced Pt electrode. The formation of Pt oxide is inhibited by adsorbed I produced during reduction of IO_3^- to I^-. Hence, no oxide formation occurs until $E > 1.0$ V. As E_a was made more positive than 1.0 V the height of peak C, obtained only for $E_a > 1.0$ V, increased. The increase in current is attributed to the greater quantity of oxide which is formed at more positive values of E_a. No conclusion can be made from these data as to whether the amount of IO_3^- reduction increased as E_a was made more positive and the quantity of oxide available to catalyze the reaction increased. Therefore, the mass-transport coupled faradaic signal owing to the reduction of IO_3^- was examined also as a function of E_a by application of QHMV. These results will be discussed in the next section.

The reduction of IO_3^- was investigated further utilizing a RRDE with a Pt disk and Pt ring. The processes occurring at the disk and the ring electrodes are considered here in general terms for a reversible reaction before discussing results specific to IO_3^-. Solution flows axially to the disk of a RRDE then flows radially across the ring

Figure VII-3: I-E curves of 4 X 10^{-5} M IO_3^- in 0.5 M H_2SO_4 at a Pt RDE
Pt RDE as a function of E_a

Electrode rotation speed (W): 1000 rpm

Potential scan rate (ϕ): 6 V/min

———— 1.0 V

— · — 1.1 V

-------- 1.2 V

····· 1.3 V

— ·· — 1.4 V

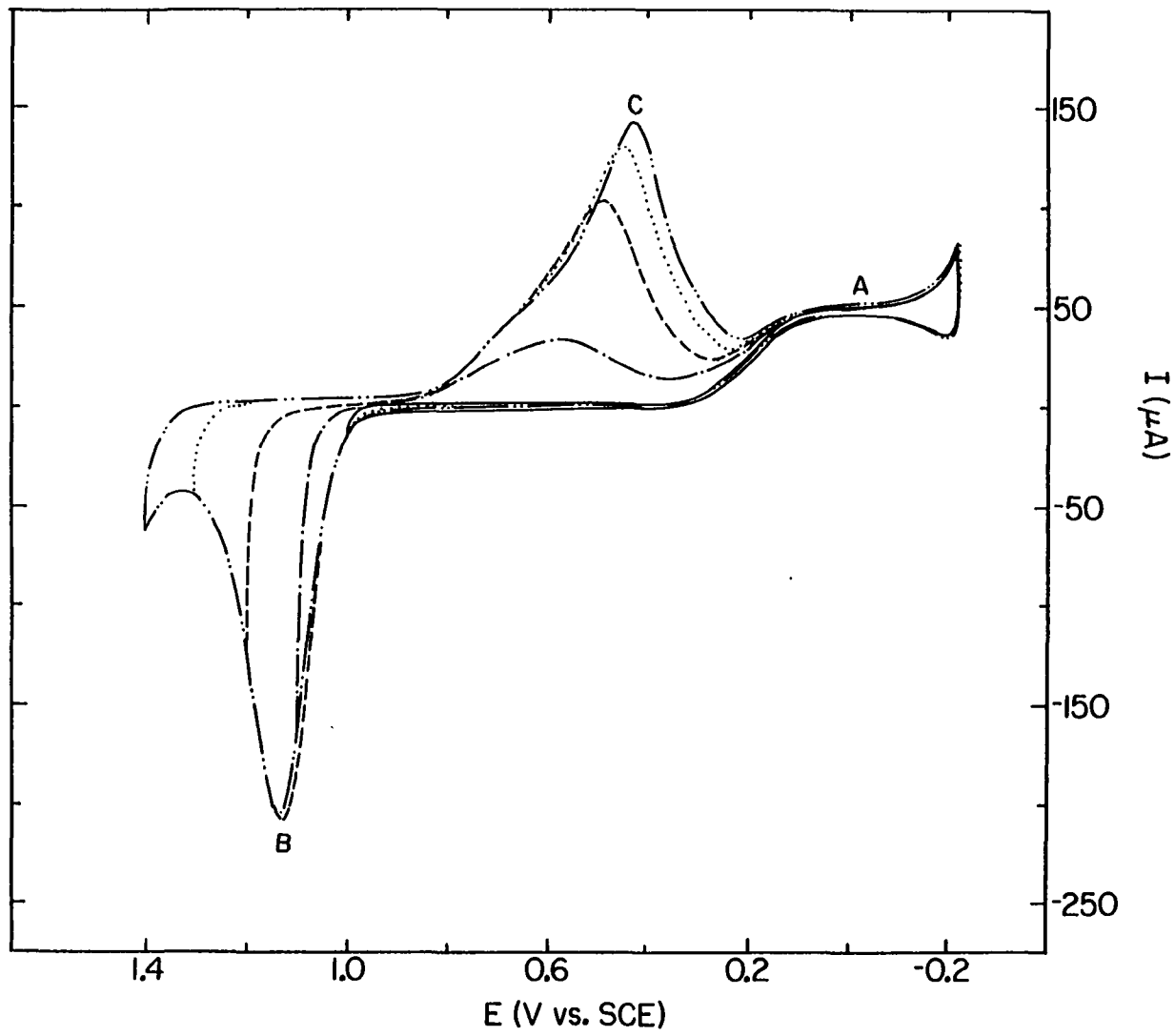
C
A
B
150
50
-50
-150
-250
I (μA)
1.4
1.0
0.6
0.2
-0.2
E (V vs. SCE)

electrode. Hence, the electrochemical production or consumption of an electroactive analyte at the disk can be monitored indirectly by observation of changes in the ring current. The ring electrode potential (E_r) usually is maintained at a constant value, while the potential of the disk electrode (E_d) is scanned between the anodic and cathodic limits. The current produced at the ring electrode (I_r) is recorded as a function of E_d.

The theoretical consideration of shielding and collection experiments has been described (1, 141, 142). The qualitative results will be discussed briefly. The so-called shielding experiment will be considered first. Suppose that the bulk solution contains an oxidized species (Ox), which can be reduced at $E < E^0_{Ox/Red}$, and the bulk concentration of the reduced species (Red) is zero. The potential of the ring electrode is maintained at $E_r = E_s$ where E_s is on the limiting current plateau for the reaction $Ox + ne^- \longrightarrow Red$, i.e., the concentration of Ox at the electrode surface is zero. At $E_d > E^0_{Ox/Red}$, no reaction occurs at the disk electrode and I_r remains at a constant value corresponding to the transport-limited value for reduction of Ox at the ring electrode (Figure VII-4, region A); the ring is said to be "deshielded". However, when $E_d < E^0_{Ox/Red}$, the Ox species transported to the disk electrode are reduced; thus, the flux of Ox to the ring electrode decreases and the observed I_r decreases (Figure VII-4, region B); the ring electrode is said to be "shielded" by the disk electrode.

For the so-called collection experiment, a value corresponding to the limiting current plateau for the reaction $Red \longrightarrow Ox + ne^-$, i.e., the

Figure VII-4: Theoretical I_d-E_d and I_r-E_d behavior

Shielding experiment

$E_r = E_s$ where the concentration of Ox at the electrode surface is zero

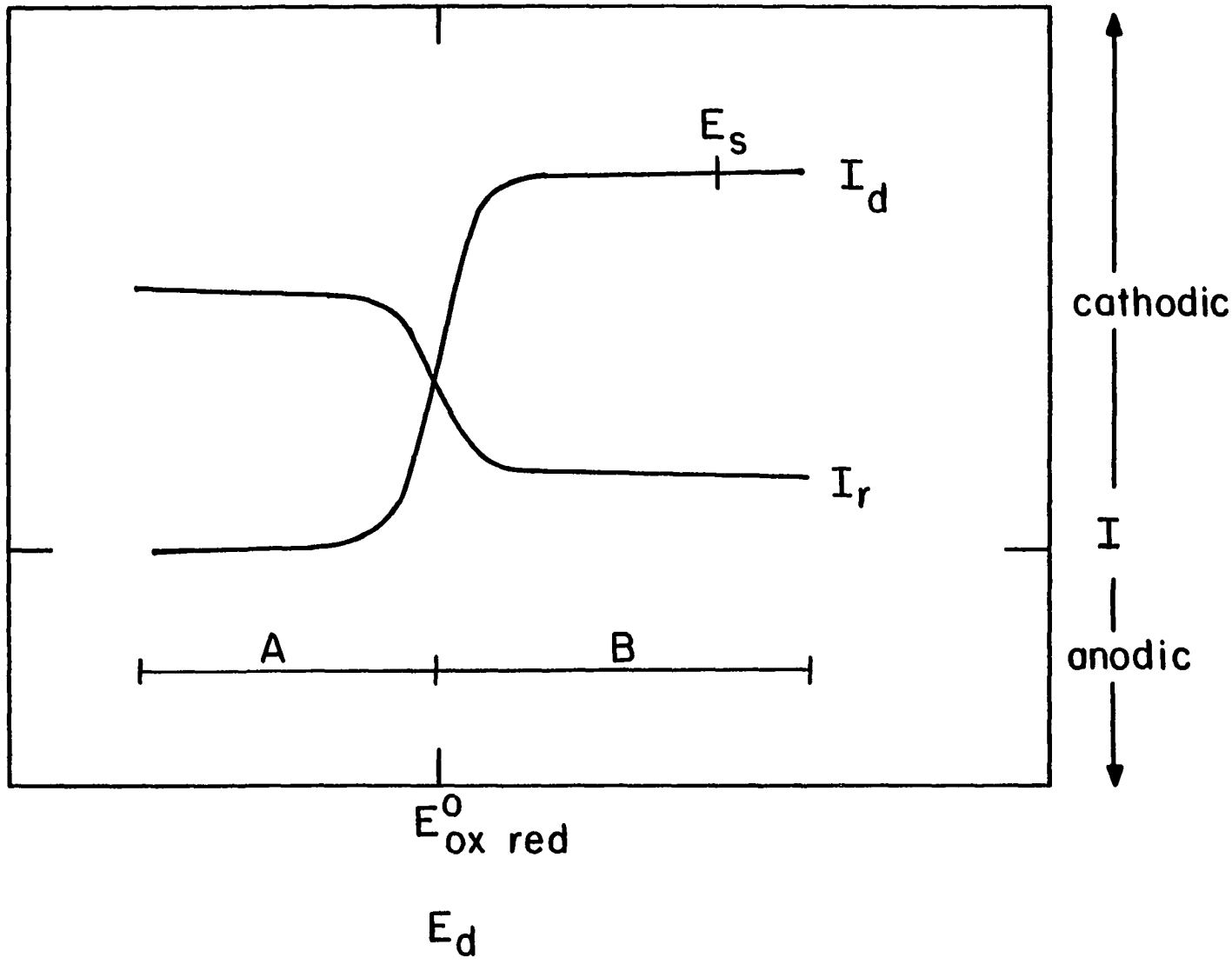
E_s
I_d
I_r
A
B
cathodic
I
anodic
$E^o_{ox\ red}$
E_d

surface concentration of Red is zero. At $E_d < E_{Ox/Red}$, no reaction occurs at the disk electrode and I_r is zero (Figure VII-5, region A). However, at $E_d > E_{Ox/Red}$, Red species are generated at the disk electrode and transported radially over the ring electrode. Oxidation of Red occurs at the ring producing an anodic I_r (Figure VII-5, region B).

The cathodic behavior of IO_3^- was characterized at a RRDE with a Pt disk and Pt ring by application of a shielding experiment. Therefore, the reduction of IO_3^- at the disk electrode was reflected by a decrease in the cathodic value of I_r. The ring electrode was potentiostated at E_r = -0.1 V, at which the mass-transport limited reduction of IO_3^- occurs (see Figure VII-2). The resultant I_r-E_d curve is shown in Figure VII-6. During the positive scan of E_d, I_r increased steadily over the region 0.0 V < E_d < 0.3 V as current produced by IO_3^- reduction at the reduced Pt surface decreased from the mass-transport limited value. The value of I_r was constant in the region 0.3 V < E_d < 1.03 V indicating that IO_3^- was not undergoing reaction at the disk electrode which was free of oxide at E_d < 1.03 V during the positive scan of potential. At E_d > 1.03 V, the cathodic value of I_r increased due to the oxidative desorption of I occurring at the disk electrode to produce additional IO_3^- which was transported radially to the ring electrode. At E_d > 1.25 V, IO_3^- was no longer produced at the disk electrode; therefore, I_r returned to the value observed in the region 0.3 V < E_d < 1.03 V. During the negative scan of E_d, I_r was constant over the region 1.3 V > E_d > 0.85 V. However, at E_d < 0.85 V, I_r

Figure VII-5: Theoretical I_d-E_d and I_r-E_d behavior

Collection experiment

$E_r = E_c$ where the concentration of Red at the electrode surface is zero

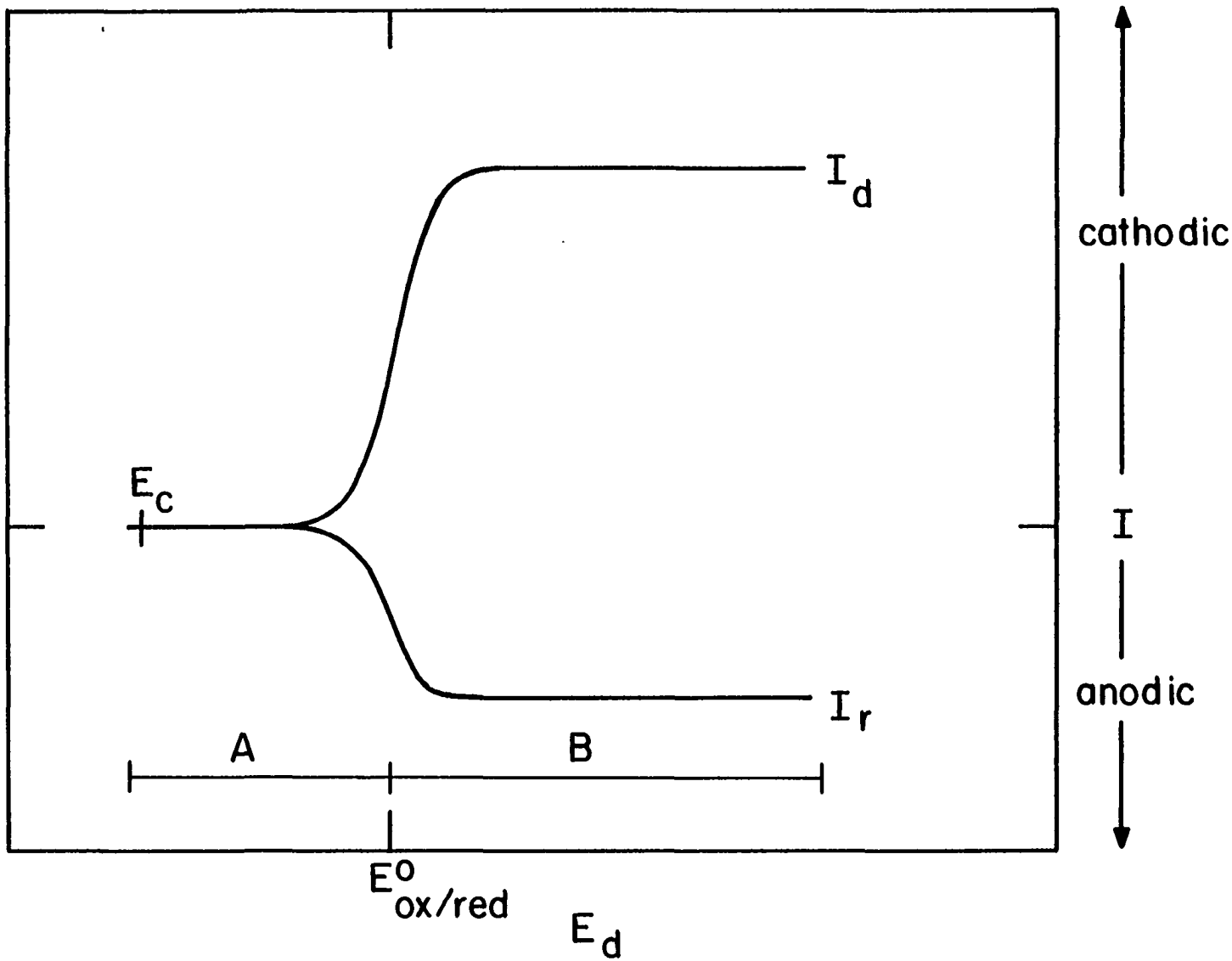
I_d
cathodic
E_c
I
I_r
anodic
A
B
$E^o_{ox/red}$
E_d

Figure VII-6: I_r-E_d curve of 4 X 10^{-5} M IO_3^- in 0.5 M H_2SO_4 at a Pt/Pt RRDE

Electrode rotation speed (W): 1000 rpm

Potential scan rate (ϕ): 6 V/min

E_r = -0.1 V

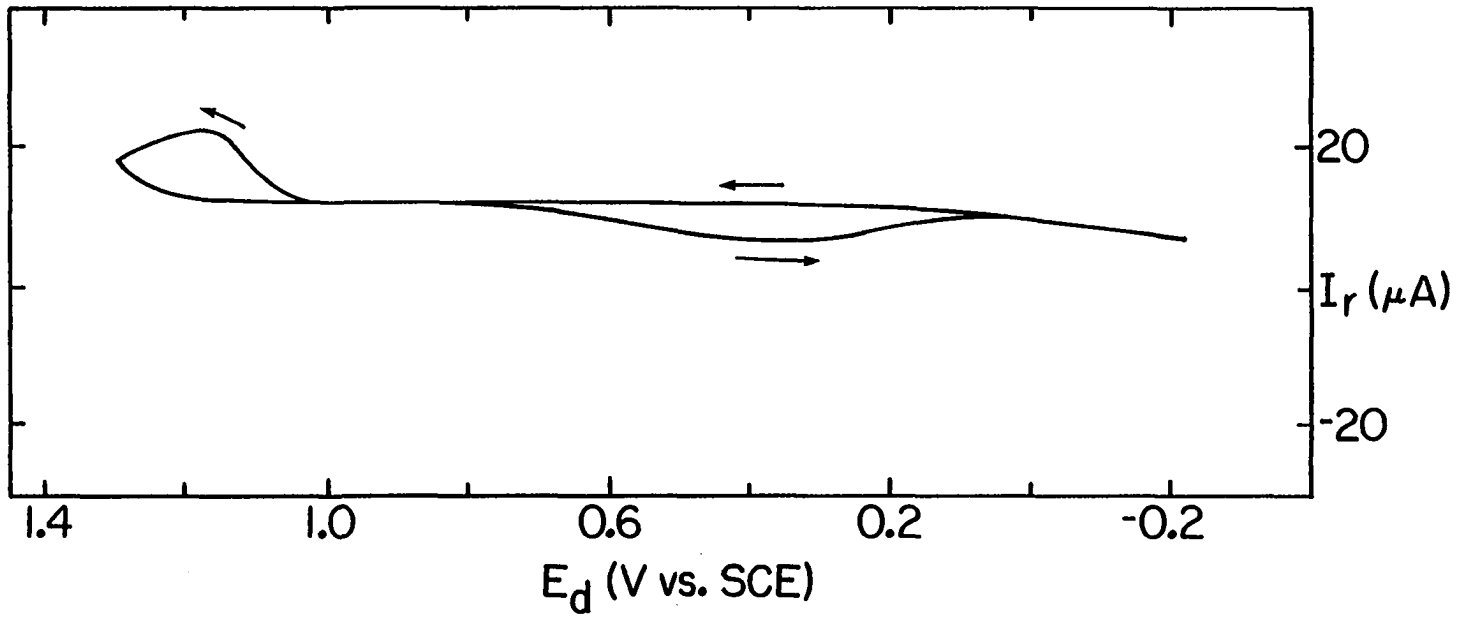
20
I_r (μA)
-20
1.4
1.0
0.6
0.2
-0.2
E_d (V vs. SCE)

decreased. This observed decrease in I_r is attributed to the reduction of IO_3^- at the disk electrode which causes a decrease in the amount of IO_3^- transported to the ring electrode, i.e., the ring electrode is "shielded" by the disk electrode. The value of I_r decreased to a minimum value at ca. E_d = 0.43 V, then increased as the reduction of IO_3^- at the disk electrode diminished. The decrease in IO_3^- consumption at the disk electrode was due to the depletion of the catalytically active oxide layer which was removed from the electrode surface by electro-reduction. The ring electrode was no longer shielded by the disk electrode. At E_d < 0.1 V, a decrease in I_r was observed as IO_3^- was reduced at the oxide free Pt surface.

The results obtained by potentiodynamic experiments just described are in support of the conclusion that catalysis of the reduction of IO_3^- occurs at an oxidized Pt surface, presumably by PtOH, generated during reduction of the oxide. In review: 1) no cathodic peak is observed for the reduction of IO_3^- at a reduced Pt electrode until η > 750 mV; and 2) the mass-transport coupled reduction of IO_3^- is observed simultaneously with Pt oxide reduction in the region 0.85 V > E_d > 0.15 V (peak C).

C. Square-Wave Hydrodynamically Modulated Voltammetry

QHMV, utilizing the staircase potential waveform, was applied to isolate the mass-transport coupled component of current due to the reduction of IO_3^- from the current produced simultaneously for reduction of Pt oxide. The ΔI-E curve is shown in Figure VII-7. During the

Figure VII-7: ΔI-E curve of 4×10^{-5} M IO_3^- in 0.5 M H_2SO_4 at a Pt RDE

Lower rotation speed (W_l): 1000 rpm

Upper rotation speed (W_u): 4000 rpm

Potential step increment (ΔE): 5 mV

Time delay (t_d): 150 ms

Number of data points (N): 10

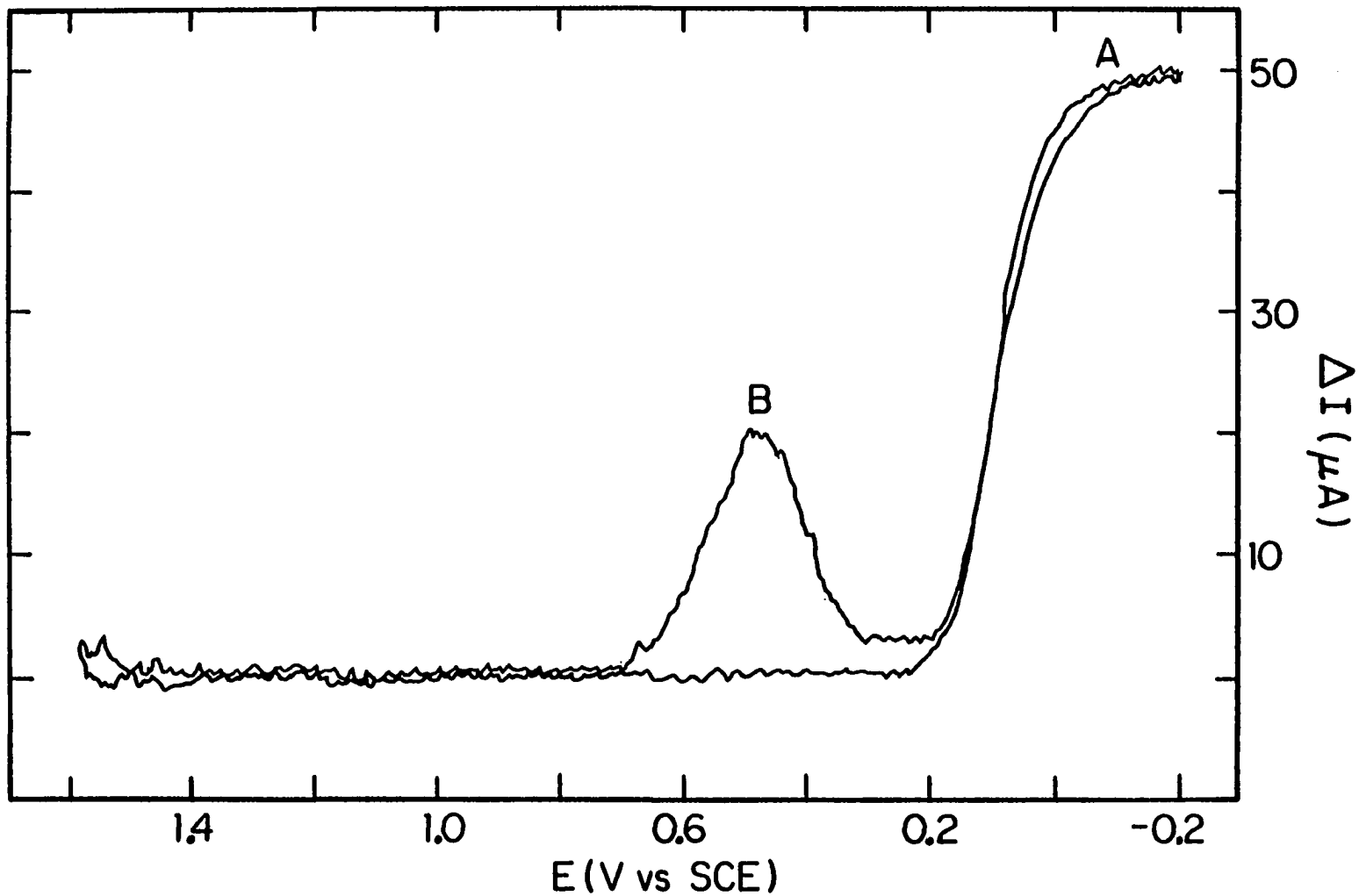
A
B
50
30
10
ΔI (μA)
1.4
1.0
0.6
0.2
-0.2
E (V vs SCE)

positive scan of potential, a cathodic wave (A) was observed at E < 0.2 V resulting from the mass-transport limited reduction of IO_3^- at a reduced Pt surface. No ΔI was observed throughout the remainder of the positive scan of potential. During the negative scan of potential, ΔI was zero until E < 0.7 V. Peak B is attributed to the mass-transport coupled reduction of IO_3^- occurring simultaneously with the surface-controlled cathodic reduction of Pt oxide. The reduction of IO_3^- ceased when Pt oxide reduction was complete (E = ca. 0.3 V). The mass-transport controlled reaction of IO_3^- at a reduced Pt electrode was observed at E < 0.2 V (wave A). A series of ΔI-E curves was recorded as a function of E_a (Figure VII-8) to determine if the quantity of oxide formed on the electrode surface exhibited any effect on the quantity of IO_3^- that can be reduced in the region of peak B. The height of peak B decreased as the potential scan was reversed at successively less positive values of potential; hence, the quantity of oxide present does effect the amount of IO_3^- that is reduced at an oxidized Pt electrode. The formation of Pt oxide is inhibited in the presence of adsorbed I therefore, no oxide formation occurs until E_a > 1.0 V. The ΔI-E curve recorded for E_a = 1.0 V contained no peak B which demonstrates that Pt oxide is essential for the reduction of IO_3^- at η < 750 mV in the region of peak B. The transport-controlled reduction of IO_3^- at a reduced Pt electrode (A) was not altered by changes in E_a.

Figure VII-8: ΔI-E curves of 4×10^{-5} M IO_3^- in 0.5 M H_2SO_4 at a Pt RDE as a function of E_a

Lower rotation speed (W_l): 1000 rpm

Upper rotation speed (W_u): 4000 rpm

Potential step increment (ΔE): 5 mV

Time delay (t_d): 150 ms

Number of data points (N): 10

——— 1.0 V

····· 1.2 V

------- 1.4 V

— · — 1.6 V

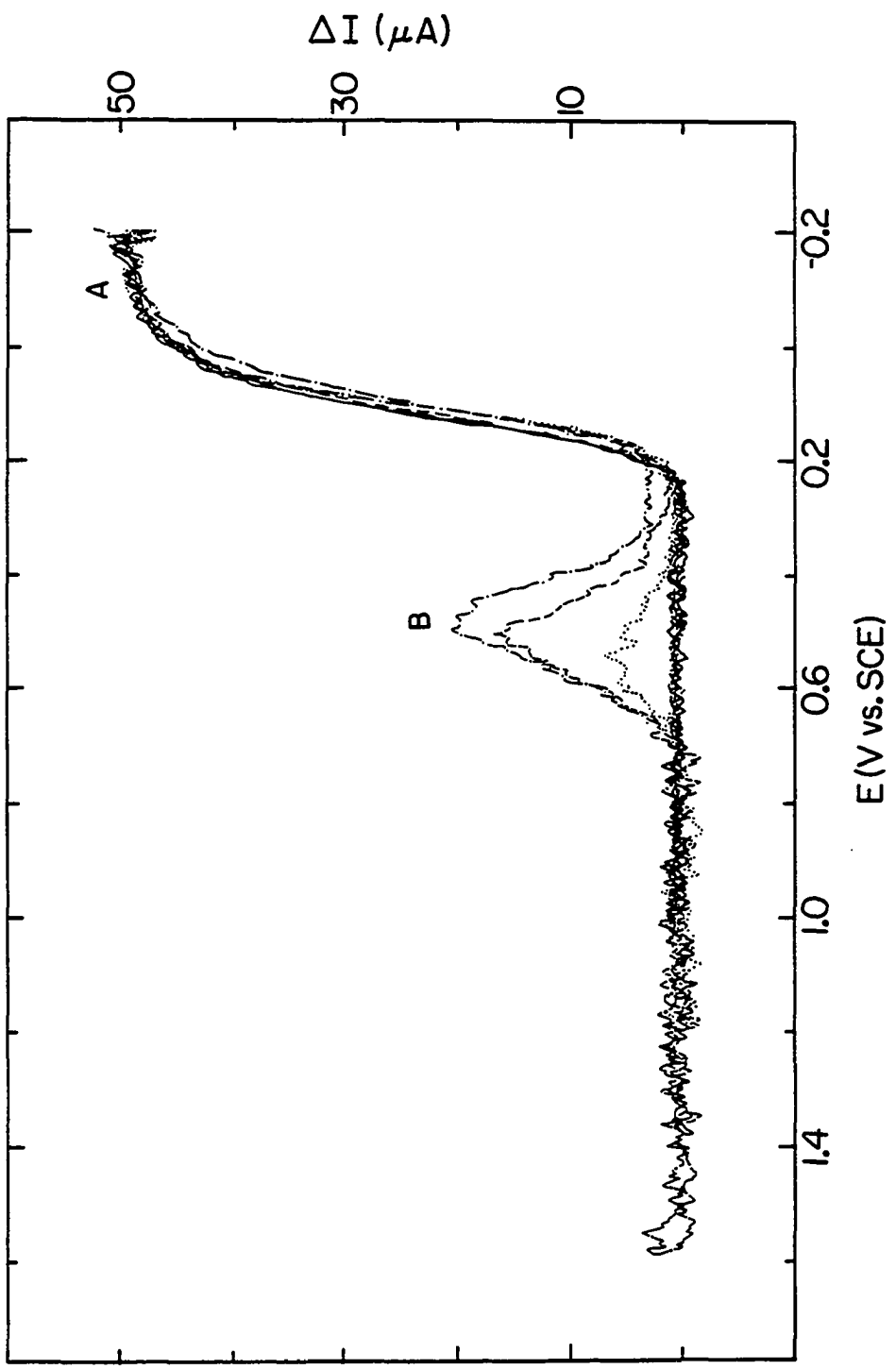
ΔI (μA)
50
30
10
A
B
-0.2
0.2
0.6
1.0
1.4
E (V vs. SCE)

VIII. CONCLUSIONS

The purpose of this research was to develop the software necessary for modulated hydrodynamic voltammetric techniques and to evaluate their application to the study of surface-catalyzed reactions. QHMV permits extraction of the convective-coupled faradaic current from the total electrode current. Application of QHMV allows one to investigate the effect that the potential-dependent surface state has on reactions which are coupled to the mass-transport of the analyte from the bulk solution. Of major significance is the ability to observe mass-transport coupled reactions occurring at an electrode, covered by an inhibiting oxide layer, which are catalyzed by the anodic evolution of O_2.

A survey of anodic reactions utilizing CV and QHMV demonstrated the complementary nature of the two techniques and illustrated that QHMV is an invaluable technique for the study of mass-transport coupled reactions that are occurring simultaneously with surface oxidation and O_2 evolution. It was a general observation that many of the reactions studied were kinetically inhibited, i.e., electrochemically irreversible, at metal surfaces without the oxide layer; however, in the process of forming the oxide, the overall rate of the reaction increased significantly, i.e., electrocatalysis of the reaction occurred. It was also observed that those reactions which involve the uptake of an O-atom derived the most electrocatalytic benefit from the oxide layer and the evolution of O_2.

The oxidative reactions of I^- in acidic media at a Pt electrode were examined in detail. The convective components of the total electrode current include: 1) the mass-transport limited formation of

I_2 at E > 0.45 V; 2) the mass-transport coupled oxidation of I^- to IO_3^-, which is catalyzed by the anodic formation of PtOH; and 3) the mass-transport limited production of IO_3^-, which is concluded to be electrocatalyzed by OH, an intermediate product of O_2 evolution. Observation of the latter two components was possible only upon application of QHMV. The catalytic reduction of IO_3^- at a Pt electrode was demonstrated also utilizing QHMV.

The anodic detection of I^- was investigated by constant and multistep potential amperometry. Iodide was detected by measuring the current resulting from: 1) the mass-transport limited production of I_2 from I^-, 2) the suppression of the anodic formation of Pt oxide, and 3) the electrocatalyzed oxidation of I^- to IO_3^-. Enhanced sensitivity of the measured signal was observed in the potential region where the electrocatalyzed oxidation of I^- to IO_3^- occurs.

IX. FUTURE RESEARCH

This research project has made possible the study of mass-transport coupled reactions occurring simultaneously with surface oxidation and O_2 evolution. Countless analyte/electrode combinations remain to be examined. Organic as well as inorganic reactants should be studied. Reactions occurring at metal electrodes with ad-atoms, e.g., Ru ad-atoms on Pt; metal-oxide electrodes, e.g., PbO_2 and RuO_2/TiO_2; and metal alloys should be investigated. By observing the behavior of the mass-transport coupled current, reactions and their mechanisms may be understood more completely. Also, properties of the electrode material and the oxide layers which form on the electrode surface may be elucidated further by the application of QHMV since the behavior of the mass-transport coupled current reflects changes occurring on the electrode surface, e.g., changes in the catalytic properties or changes in the conductance properties.

The development of computer-controlled QHMV should continue by investigating the possibility that the positive potential limit may be extended even further and could be limited, ultimately, only by dissolution of the electrode material. This can be accomplished by increasing the potential range of the A/D converter and reducing the noise, both of which are limiting factors in the present system.

X. BIBLIOGRAPHY

1. Bard, A. J.; Faulkner, L. R. "Electrochemical Methods"; John Wiley: New York, 1980.

2. Appleby, A. J. In "Comprehensive Treatise of Electrochemistry"; Conway, B. E.; Bockris, J. O'M.; Yeager, E.; Khan, S. U. M.; White, R. E., Eds.; Plenum: New York, 1983; Vol. 7, Chapter 4.

3. Bowden, F. P.; Rideal, E. K. Proc. R. Soc. London, Ser. A 1928, 120, 59.

4. Veselovskii, V. I. Geterogennyi Kataliz v Khim. Prom. Sbornik 1955, 194; Chem. Abstr. 1958, 52, 18012c.

5. Rozental, K. I.; Veselovskii, V. I. Zh. Fiz. Khim. 1953, 27, 1163; Chem. Abstr. 1954, 48, 1174e.

6. Veselovskii, V. I. Tr. Soveshch. Elektrokhim., 4th 1956, 241; Chem. Abstr. 1960, 54, 10590e.

7. Damjanovic, A.; Bockris, J. O'M. Electrochim. Acta 1966, 11, 376.

8. Damjanovic, A.; Dey, A.; Bockris, J. O'M. J. Electrochem. Soc. 1966, 113, 739.

9. Bockris, J. O'M.; Wroblowa,H. J. Electroanal. Chem. 1964, 7, 428.

10. Wroblowa, H.; Piersma, B. J.; Bockris, J. O'M. J. Electroanal. Chem. 1963, 6, 401.

11. Osteryoung, R. A.; Anson, F. C. Anal. Chem. 1964, 36, 975.

12. Osteryoung, R. A.; Anson, F. C. Anal. Chem. 1966, 38, 692.

13. Osteryoung, R. A. Anal. Chem. 1963, 35, 1100.

14. Lane, R. F.; Hubbard, A. T. Anal. Chem. 1976, 48, 1287.

15. Breiter, M. W. Electrochim. Acta 1963, 8, 925.

16. Lane, R. F.; Hubbard, A. T. J. Phys. Chem. 1975, 79, 808.

17. Johnson, D. C. J. Electrochem. Soc. 1972, 119, 331.

18. Austin, D. S.; Johnson, D. C.; Hines, T. G.; Berti, E. T. Anal. Chem. 1983, 55, 2222.

19. Osteryoung, R. A.; Lauer, G.; Anson, F. C. J. Electrochem. Soc. 1963, 110, 926.

20. Johnson, D. C.; Bruckenstein, S. J. Electrochem. Soc. 1970, 117, 460.

21. Kuhn, A. T.; Randle, T. H. J. Chem. Soc., Faraday Trans. I 1983, 79, 417.

22. Slaidens, G.; Actina, A. Latv. PSR Zinat. Akad. Vestis, Kim. Ser. 1980, 4, 497; Chem. Abstr. 1980, 93, 157778.

23. Zakharov, V. A.; Songina, O. A. Russ. J. Phys. Chem. 1964, 38, 412.

24. Lown, J. A.; Johnson, D. C. Anal. Chim. Acta 1980, 116, 41.

25. Cabelka, T. D.; Austin, D. S.; Johnson, D. C. J. Electrochem. Soc. 1984, 131, 1595.

26. Seo, E. T.; Sawyer, D. T. J. Electroanal. Chem. 1964, 1, 184.

27. Comtat, M.; Mahenc, J. Bull. Soc. Chem. Fr. 1969, 11, 3862.

28. Appleby, A. J.; Pichon, B. J. Electroanal. Chem. 1979, 95, 59.

29. Audry, C.; Vornov, M. Electrochim. Acta 1980, 25, 299.

30. Rozental, K. I.; Veselovskii, V. I. Zh. Fiz. Khim. 1957, 31, 1732; Chem. Abstr. 1958, 52, 6022d.

31. McCallum, C.; Pletcher, D. J. Electroanal. Chem. 1976, 70, 277.

32. Gilman, S. J. Phys. Chem. 1964, 68, 70.

33. Gibbs, T. K.; McCallum, C.; Pletcher, D. Electrochim. Acta 1977, 22, 525.

34. Watanabe, M.; Motoo, S. J. Electroanal. Chem. 1975, 60, 275.

35. Motoo, S.; Shibata, M.; Watanabe, M. J. Electroanal. Chem. 1980, 110, 103.

36. Motoo, S.; Watanabe, M. J. Electroanal. Chem. 1980, 111, 261.

37. Bilmes, S. A.; de Tacconi, N. R.; Arvia, A. J. J. Electrochem. Soc. 1980, 127, 2184.

38. Najdeker, E.; Bishop, E. J. Electroanal. Chem. 1973, 41, 79.

39. Loucka, T. J. Electroanal. Chem. 1971, 31, 319.

40. Loucka, T. J. Electroanal. Chem. 1973, 44, 221.

41. Zakharov, V. A.; Songina, O. A.; Kal'nitskaya, L. P. Electrokhimiya 1971, 7, 1702.

42. Erlikh, Yu. I.; Anni, K. L.; Palm, U. V. Electrokhimiya 1978, 14, 1066.

43. Erlikh, Yu. I.; Anni, K. Electrokhimiya 1979, 15, 1573.

44. Lu, P. W. T.; Ammon, R. L. J. Electrochem. Soc. 1980, 127, 2610.

45. Bilmes, S. A.; de Tacconi, N. R.; Arvia, A. J. J. Electroanal. Chem. 1983, 143, 179.

46. Gilman, S. In "Electroanalytical Chemistry-A Series of Advances"; Bard, A. J., Ed.; Marcel Dekker: New York, 1967; Vol. 2, Chapter 2.

47. Belanger, G.; Vijh, A. K. In "Oxides and Oxide Films"; Vijh, A. K., Ed.; Marcel Dekker: New York, 1977; Vol. 5.

48. Cabelka, T. D. Ph.D. Dissertation, Iowa State University, Ames, Iowa, 1983.

49. Hoare, J. P. "The Electrochemistry of Oxygen"; Interscience: New York, 1968.

50. Angerstein-Kozlowska, H.; Conway, B. E.; Sharp, W. B. A. J. Electroanal. Chem. 1973, 43, 9.

51. Conway, B. E.; Gottesfeld, S. J. Chem. Soc., Faraday Trans. I 1973, 69, 1090.

52. Tilak, B. V.; Conway, B. E.; Angerstein-Kozlowska, H. J. Electroanal. Chem. 1973, 48, 1.

53. Angerstein-Kozlowska, H.; Conway, B. E.; Barnett, B.; Mozota, J. J. Electroanal. Chem. 1979, 100, 417.

54. Damjanovic, A.; Jovanovic, B. J. Electrochem. Soc. 1976, 123, 374.

55. Rozental, K. I.; Veselovskii, V. I. Dokl. Akad. Nauk SSSR 1956, 111, 637; Chem. Abstr. 1957, 51, 12699b.

56. Churchill, C. R.; Hibbert, D. B. J. Chem. Soc., Faraday Trans. I 1982, 78, 2937.

57. Gottesfeld, S.; Yaniv, M.; Lasir, D. Passivity Met., Proc. Int. Symp. 4th 1977, 134; Chem. Abstr. 1980, 93, 175938j.

58. Hoare, J. P. Electrochim. Acta 1964, 9, 1289.

59. Gottesfeld, S.; Babai, M.; Reichman, B. Surf. Sci. 1976, 56, 373.

60. Schultze, J. W.; Vetter, K. J. Ber. Bunsenges. Phys. Chem. 1971, 75, 470.

61. Dickertmann, D.; Schultze, J. W.; Vetter, K. J. J. Electroanal. Chem. 1974, 55, 429.

62. Dickinson, T.; Povey, A. F.; Sherwood, P. M. J. Chem. Soc., Faraday Trans. I 1975, 71, 298.

63. Vinnikov, Y. Y.; Shepelin, V. A.; Veselovskii, V. I. Electrokhimiya 1972, 8, 1229.

64. Gottesfeld, S.; Babai, M.; Reichman, B. Surf. Sci. 1976, 57, 251.

65. Nguyen Van Huong, G.; Hinnen, C.; Lecoeur, J. J. Electroanal. Chem. 1980, 106, 185.

66. Watanabe, T.; Gerischer, H. J. Electroanal. Chem. 1981, 117, 185.

67. Watanabe, T.; Gerischer, H. J. Electroanal. Chem. 1981, 122, 73.

68. Kim, K. S.; Sell, C. D.; Winograd, D. In "Electrocatalysis"; Breiter, M. W., Ed.; Electrochemical Society: Princeton, 1974.

69. Makrides, A. C.; J. Electrochem. Soc. 1966, 113, 1158.

70. Hoare, J. P. Electrochim. Acta 1966, 11, 311.

71. Barnartt, S. J. Electrochem. Soc. 1959, 106, 722.

72. Frankenthal, R. P.; Thompson, D. E. J. Electrochem. Soc. 1976, 123, 799.

73. Bolzan, A. E.; Martins, M. E.; Arvia, A. J. J. Electroanal. Chem. 1983, 157, 339.

74. Chierchie, T.; Mayer, C.; Lorenz, W. J. J. Electroanal. Chem. 1982, 135, 211.

75. Gossner, K.; Mizera, E. J. Electroanal. Chem. 1981, 125, 347.

76. Capon, A.; Parsons,R. J. Electroanal. Chem. 1972, 39, 275.

77. Hoare, J. P. J. Electrochem. Soc. 1965, 112, 1129.

78. Rand, D. A. J.; Woods, R. J. Electroanal. Chem. 1974, 55, 375.

79. Frazer, E. J.; Woods, R. J. Electroanal. Chem. 1979, 102, 127.

80. Gottesfeld, S.; Srinivasen, S. J. Electroanal. Chem. 1978, 86, 89.

81. Miller, B.; Bellavance, M. I.; Bruckenstein, S. Anal. Chem. 1972, 44, 1983.

82. Bruckenstein, S.; Bellavance, M. I.; Miller, B. J. Electrochem. Soc. 1973, 120, 1351.

83. Miller, B.; Bruckenstein, S. J. Electrochem. Soc. 1974, 121, 1558.

84. Miller, B.; Bruckenstein, S. Anal. Chem. 1974, 46, 2026.

85. Tokuda, K.; Bruckenstein, S.; Miller, B. J. Electrochem. Soc. 1975, 122, 1316.

86. Tokuda, K.; Bruckenstein, S. J. Electrochem. Soc. 1979, 126, 431.

87. Kanzaki, Y.; Bruckenstein, S. J. Electrochem. Soc. 1979, 126, 437.

88. Rosamilia, J. M.; Miller, B. Anal. Chem. 1983, 55, 1142.

89. Miller, B.; Rosamilia, J. M. Anal. Chem. 1983, 55, 1281.

90. Blaedel, W. J.; Engstrom, R. C. Anal. Chem. 1978, 50, 476.

91. Blaedel, W. J.; Hahn, Y. Arch. Pharmacal Res. 1979, 2, 111; Chem. Abstr. 1980, 93, 138048y.

92. Blaedel, W. J.; Engstrom, R. C. Adv. Autom. Anal., Technicon Int. Congr., 7th 1976, 1, 63; Chem. Abstr. 1978, 89, 102900y.

93. Engstrom, R. C.; Blaedel, W. J. Chem. Biomed. Environ. Instrum. 1979, 9, 61.

94. Wang, J. Talanta 1981, 28, 369.

95. Blaedel, W. J.; Yim, Z. Anal. Chem. 1980, 52, 564.

96. Hsi, T. Ph.D. Dissertation, Iowa State University, Ames, Iowa, 1983.

97. Albery, W. J.; Hillman, A. R.; Bruckenstein, S. J. Electroanal. Chem. 1979, 100, 687.

98. Cabelka, T. D.; Austin, D. S.; Johnson, D. C. J. Electrochem. Soc., in press.

99. Loucka, T. J. Electroanal. Chem. 1973, 47, 103.

100. Guidelli, R.; Pergola, F; Raspi, G. Anal. Chem. 1972, 44, 745.

101. Zakharov, V. A.; Songina, O. A. Russ. J. Phys. Chem. 1962, 36, 649.

102. Conway, B. E.; Novak, D. M. J. Electroanal. Chem. 1979, 99, 133.

103. Conway, B. E.; Novak, D. M. J. Chem. Soc., Faraday Trans. I 1979, 75, 2454.

104. Novak, D. M.; Conway, B. E. J. Chem. Soc., Faraday Trans. I 1981, 77, 2341.

105. Galizzioli, D.; Tantardini, F.; Trasatti, S. J. Appl. Electrochem. 1974, 4, 57.

106. Faita, G.; Fiori, G. J. Appl. Electrochem. 1972, 2, 31.

107. Kuhn, A. T.; Mortimer, C. J. J. Appl. Electrochem. 1972, 2, 283.

108. Vukovic, M.; Angerstein-Kozlowska, H.; Conway, B. E. J. Appl. Electrochem. 1982, 12, 193.

109. Burke, L. D.; O'Sullivan, E. J. M. J. Electroanal. Chem. 1979, 97, 123.

110. Janssen, L. J. J.; Visser, G. J.; Barendrecht, E. Electrochim. Acta 1983, 28, 155.

111. Burrows, I. R.; Entwisle, J. H.; Harrison, J. A. J. Electrochem. Soc. 1977, 77, 21.

112. Burrows, I. R.; Denton, D. A.; Harrison, J. A. Electrochim. Acta 1978, 23, 493.

113. Denton, D. A.; Harrison, J. A.; Knowles, R. I. Electrochim. Acta 1979, 24, 521.

114. Denton, D. A.; Harrison, J. A.; Knowles, R. I. Electrochim. Acta 1980, 25, 1147.

115. Denton, D. A.; Harrison, J. A.; Knowles, R. I. Electrochim. Acta 1981, 26, 1197.

116. Harrison, J. A.; Caldwell, D. L.; White, R. E. Electrochim. Acta 1983, 28, 1561.

117. Harrison, J. A.; Caldwell, D. L.; White, R. E. Electrochim. Acta 1984, 29, 203.

118. Novak, D. M.; Tilak, B. V.; Conway, B. E. In "Modern Aspects of Electrochemistry" Bockris, J. O'M.; Conway, B. E.; White, B. E., Eds.; Plenum: New York, 1982; Vol. 14, Chapter 4.

119. Caldwell, D. L. In "Comprehensive Treatise of Electrochemistry" Bockris, J. O'M.; Conway, B. E.; Yeager, E.; White, R. E., Eds.; Plenum: New York, 1981; Vol. 2, Chapter 2.

120. Venkatesh, S.; Tilak, B. V. J. Chem. Educ. 1983, 60, 276.

121. Bagotzky, V. S.; Vassilyev, Y. B.; Weber, J.; Pirtskhalava, J. N. J. Electroanal. Chem. 1970, 27, 31.

122. Conway, B. E.; Novak, D. M. Croat. Chem. Acta 1980, 53, 183.

123. Conway, B. E.; Mozota, J. J. Chem. Soc., Faraday Trans. I 1982, 78, 1717.

124. Novak, D. M. J. Electrochem. Soc. 1979, 126, 209c.

125. Beer, H. B. Neth. Pat. Appl. 216 199, 1957.

126. Janssen, L. J. J. Mod. Chlor-Alkali Technology, Pap. Int. Chlorine Symp., 3rd 1982, 271; Chem. Abstr. 1984, 100, 128697h.

127. Ardizzone, S.; Carugati, A.; Lodi, G.; Trasatti, S. J. Electrochem. Soc. 1982, 129, 1689.

128. Burke, L. D.; O'Neill, J. F. J. Electroanal. Chem. 1979, 101, 341.

129. Nicol, M. J. Gold Bull. 1980, 13, 46.

130. Podesta, J. J.; Piatti, R. C. V.; Arvia, A. J. Electrochim. Acta 1979, 24, 633.

131. Cadle, S. H.; Bruckenstein, S. J. Electroanal. Chem. 1973, 48, 325.

132. Herrera Gallego, J.; Castellano, C. E.; Calandra, A. J.; Arvia, A. J. J. Electroanal. Chem. 1975, 66, 207.

133. Gaur, J. N.; Schmid, G. M. J. Electroanal. Chem. 1970, 24, 279.

134. Takamura, T.; Takamura, K.; Yeager, E. J. Electroanal. Chem. 1971, 29, 279.

135. Besenhard, J. O.; Parsons, R.; Reeves, R. M. J. Electroanal. Chem. 1979, 96, 57.

136. Nicol, M. J. Report 1981, NIM-1844; Chem. Abstr. 1983, 98, 24500n.

137. Horikoshi, T.; Yoshimura, S.; Kubota, N.; Sato, E. Nippon Kagaku Kaishi 1983, 8, 1118; Chem. Abstr. 1983, 99, 95755f.

138. Gottesfeld, S.; Reichman, B. J. Electroanal. Chem. 1976, 67, 169.

139. Rubenstein, I. J. Phys. Chem. 1981, 85, 1899.

140. Zittel, H. E.; Miller, F. J. Anal. Chim. Acta 1962, 34, 939.

141. Albery, W. J.; Hitchman, M. L. "Ring-disc Electrodes"; Clarendon: Oxford, 1971.

142. Prater, K. B.; Bard, A. J. J. Electrochem. Soc. 1970, 117, 335.

143. Cadle, S. H.; Bruckenstein, S. Anal. Chem. 1974, 46, 16.

144. Soriaga, M. P.; Wilson, P. H.; Hubbard, A. T.; Benton, C. S. J. Electroanal. Chem. 1982, 142, 317.

145. Soriaga, M. P.; Hubbard, A. T. J. Amer. Chem. Soc. 1982, 104, 2735.

146. Soriaga, M. P.; Hubbard, A. T. J. Amer. Chem. Soc. 1982, 104, 2742.

147. Soriaga, M. P.; Hubbard, A. T. J. Amer. Chem. Soc. 1982, 104, 3937.

148. Soriaga, M. P.; Stickney, J. L.; Hubbard, A. T. J. Electroanal. Chem. 1983, 144, 207.

149. Soriaga, M. P.; Chia, V. K. F.; White, J. H.; Song, D.; Hubbard, A. T. J. Electroanal. Chem. 1984, 162, 143.

150. Chia, V. K. F.; Soriaga, M. P.; Hubbard, A. T. J. Electroanal. Chem. 1984, 167, 97.

151. Soriaga, M. P.; Hubbard, A. T. J. Phys. Chem. 1984, 88, 1758.

152. Soriaga, M. P.; Hubbard, A. T. J. Electroanal. Chem. 1984, 167, 79.

153. Soriaga, M. P.; White, J. H.; Song, D.; Hubbard, A. T. J. Phys. Chem. 1984, 88, 2284.

154. Felter, T. E.; Hubbard, A. T. J. Electroanal. Chem. 1979, 100, 473.

155. Garwood, G. A., Jr.; Hubbard, A. T. Surf. Sci. 1980, 92, 617.

156. Lau, A. L. Y.; Hubbard, A. T. J. Electroanal. Chem. 1971, 33, 77.

157. Davenport, R. J.; Johnson, D. C. Anal. Chem. 1973, 45, 1758.

158. Larochelle, J. H.; Johnson, D. C. Anal. Chem. 1978, 50, 240.

159. Newson, J. D.; Riddiford, A. C. J. Electrochem. Soc. 1961, 108, 699.

160. Jordan, J.; Javick, R. A. J. Amer. Chem. Soc. 1950, 80, 1264.

161. Jordan, J.; Javick, R. A. Electrochim. Acta 1962, 6, 23.

162. Dane, L. M.; Janssen, L. J. J.; Hoogland, J. G. Electrochim. Acta 1968, 13, 507.

163. Anson, F. C.; Lingane, J. J. J. Amer. Chem. Soc. 1957, 79, 1015.

164. Brown, O. R. In "Physical Chemistry of Organic Solvent Systems"; Covington, A.; Dickinson, T., Eds.; Plenum: New York, 1973; p. 761.

165. Clark, D.; Fleischmann, M.; Pletcher, D. J. Electroanal. Chem. 1972, 36, 137.

166. MacDonald, A.; Duke, P. D. J. Chromatogr. 1973, 83, 331.

167. Stulik, K.; Hora, V. J. Electroanal. Chem. 1976, 70, 253.

168. Hughes, S.; Meschi, P. L.; Johnson, D. C. Anal. Chim. Acta 1981, 132, 1.

169. Hughes, S.; Johnson, D. C. Anal. Chim. Acta 1981, 132, 11.

170. Hughes, S.; Johnson, D. C. Anal. Chim. Acta 1983, 149, 1.

171. Polta, J. A.; Johnson, D. C. J. Liq. Chromatogr. 1983, 6, 1727.

172. Edwards, P.; Haak, K. K. Am. Lab.(Fairfield, Conn.) 1983, 15, 78.

173. Austin, D. S.; Polta, J. A.; Polta, T. Z.; Tang, A. P.-C.; Cabelka, T. D.; Johnson, D. C. J. Electroanal. Chem. 1984, 168, 227.

174. Gilroy, D. J. Electroanal. Chem. 1976, 71, 257.

175. Gilroy, D. J. Electroanal. Chem. 1977, 83, 329.

176. Greef, R.; Aulich, H. J. Electroanal. Chem. 1968, 18, 295.

177. Herberlin, J. M.; Andersen, T. N.; Eyring, H. Electrochim. Acta 1970, 15, 1455.

178. Feldberg, S. W.; Enke, C. G.; Bricker, C. E. J. Electrochem. Soc. 1963, 110, 825.

179. Anson, F. C. J. Amer. Chem. Soc. 1959, 81, 1554.

180. Davis, D. G. Talanta 1960, 3, 335.

XI. ACKNOWLEDGEMENTS

I would like to express my gratitude to Professor Dennis Johnson for his guidance and support throughout my graduate studies. His enthusiasm towards research is highly contagious.

I wish to acknowledge the past and present members of the electrochemistry group for the exchange of ideas. A special thanks to Jodi Johnson for her time and patience in collecting the data for flow injection detection.

I would like to thank Pine Instrument Company for the computer system and the financial support they provided for the summer of 1982. Special thanks to Ted Hines and family for inviting me into their home while I was in Grove City learning to use the computer. I appreciate the expertise of Ed Berti in constructing the computer interface. I especially enjoyed working in conjunction with Guenter Eickmann.

I owe a great deal to my family, especially my parents, who provided the opportunity and encouragement for me to further my education. More importantly, my Mom and Dad were always there to listen- to share in the happy moments and to help me through the hard times; they are very special people.

To Wayne, thanks for waiting patiently while I finished my graduate work so many miles away.

XII. APPENDIX

This appendix contains printouts of the computer programs for: 1) QHMV utilizing a staircase potential waveform, 2) QHMV utilizing a triple-step potential waveform, and 3) the collection of data for ΔI vs. t_2 plots to examine the time dependence for conversion of active PtOH to the inactive OHPt and PtO.

```
10 REM SQUARE-WAVE MODULATION VOLTAMMETRY
15 REM ********SWHMVA.BAS*********     9/17/82
20 REM SET D/A CONVERTERS TO ZERO
30 HP=128:LP=0
40 POKE(HEX("C008")),LP:POKE(HEX("C009")),HP
50 POKE(HEX("C00A")),LP:POKE(HEX("C00B")),HP
60 POKE(HEX("C00C")),LP:POKE(HEX("C00D")),HP
70 POKE(HEX("C00E")),LP:POKE(HEX("C00F")),HP
75 REM DATA STORAGE MATRICES
80 DIM E(1150):DIM DI(1150)
90 REM PRINT CHANNEL ASSIGNMENTS
100 PRINT "D/A CHANNEL ASSIGNMENTS"
110 PRINT "     A-----POTENTIAL OUTPUT TO ROTATOR"
120 PRINT "     B-----POTENTIAL TO ESTAT OR ANALOG SCALING DEVICE"
130 PRINT "     C-----CURRENT OUTPUT TO RECORDER"
140 PRINT "     D-----POTENTIAL OUTPUT TO RECORDER"
150 PRINT:PRINT "A/D CHANNEL ASSIGNMENTS"
160 PRINT "     0-----CURRENT INPUT FROM POTENTIOSTAT"
170 PRINT "     1-----POTENTIAL FROM ESTAT OR ANALOG DEVICE"
180 PRINT:PRINT
200 REM EXPERIMENTAL CONDITIONS
210 INPUT "VOLTAGE FOR LOW AND HIGH ROTATION SPEEDS (1000 RPM/V)",WL,WH
220 INPUT "CATHODIC AND ANODIC LIMITS (V)",EC,EA
230 INPUT "POTENTIAL INCREMENT",EI
240 INPUT "TIME DELAY (MSEC); NOT LESS THAN 100 MSEC",TD
250 INPUT "NUMBER OF DATA POINTS COLLECTED",N
255 REM COMPENSATION FOR ANALOG SCALING DEVICE
260 INPUT "ENTER 'Y' IF ANOLOG SCALING DEVICE IS BEING USED",SD$
270 IF SD$="Y" THEN 275 ELSE 300
275 INPUT "ENTER DEAMP VALUE",DV
280 EA=EA/DV:EC=EC/DV:EI=EI/DV
282 TD=TD-100
290 REM SET INITIAL CONDITIONS
300 Q=EC:U=1:Y=0
310 REM SET LOW ROTATION SPEED
320 W=(WL+10)*12.8:H=INT(W):L=(W-H)*256
330 POKE(HEX("C008")),L:POKE(HEX("C009")),H
340 IF U=1 THEN 470
400 REM AVERAGE HIGH CURRENT VALUES
410 IH=I/N:IH=IH*1000:IH=INT(IH):IH=IH/1000
420 DI=IH-IL:DI=DI*1000:DI=INT(DI):DI(U-1)=DI/1000
425 PRINT U-1;E(U-1),IL,IH,DI(U-1)
430 REM CALCULATE AND TEST NEW POTENTIAL VALUE
440 Q=Q+EI
450 IF Q>EA THEN 770
460 IF Q<EC THEN 800
470 REM SET POTENTIAL
480 E=(Q+10)*12.8:H=INT(E):L=(E-H)*256
```

```
485 PRINT Q,
490 POKE(HEX("C00A")),L:POKE(HEX("C00B")),H
500 REM CHECK AND STORE POTENTIAL VALUE
510 Z=9:POKE(HEX("C003")),Z
520 H=PEEK(HEX("C005")):L=PEEK(HEX("C004"))
530 H=H-128:L=(INT(L/16))/16:E=(H+L)*320/4096
532 IF DV=0 THEN 538 ELSE 534
534 E=E*DV
538 E(U)=E
540 REM TIME DELAY BEFORE MEASURING CURRENT
550 FOR T=1 TO TD:NEXT T
600 REM SAMPLE CURRENT
610 I=0
620 FOR C=1 TO N
630 Z=8:POKE(HEX("C003")),Z
640 H=PEEK(HEX("C005")):L=PEEK(HEX("C004"))
650 H=H-128:L=(INT(L/16))/16:II=(H+L)*320/4096
660 I=I+II
670 NEXT C
690 REM CHECK VALUE OF ROTATION SPEED
700 IF Y=1 THEN U=U+1:Y=0:GOTO 310
710 REM SET HIGH ROTATION SPEED
720 W=(WH+10)*12.8:H=INT(W):L=(W-H)*256
730 POKE(HEX("C008")),L:POKE(HEX("C009")),H
740 IL=I/N:IL=IL*1000:IL=INT(IL):IL=IL/1000
750 Y=1:GOTO 540
770 REM REVERSE SCAN DIRECTION
780 EI=0-EI:Q=Q+(2*EI):GOTO 470
800 REM SET ROTATION SPEED TO ZERO
810 H=128:L=0:POKE(HEX("C008")),L:POKE(HEX("C009")),H
820 X=U-1
825 REM PLOT DATA
830 INPUT "DATA COLLECTED, ENTER 'Y' TO PLOT DATA",DC$
840 IF DC$="Y" THEN 860 ELSE INPUT "ARE YOU SURE",DC$
850 IF DC$="Y" THEN 2000 ELSE 830
860 FOR U=1 TO X
870 E=E(U):E=(E+10)*12.8:H=INT(E):L=(E-H)*256
880 POKE(HEX("C00E")),L:POKE(HEX("C00F")),H
890 I=DI(U):I=(I+10)*12.8:H=INT(I):L=(I-H)*256
900 POKE(HEX("C00C")),L:POKE(HEX("C00D")),H
910 NEXT U
920 INPUT "RECHECK DATA (Y OR N)",P$:IF P$="Y" THEN 860
930 INPUT "REPEAT EXPERIMENT WITH SAME CONDITIONS",P$
940 IF P$="Y" THEN 950 ELSE 970
950 EI=0-EI:GOTO 300
970 INPUT "REPEAT EXPERIMENT WITH DIFFERENT CONDITIONS",P$
980 IF P$="Y" THEN 990 ELSE 2000
990 DV=0:GOTO 200
2000 END
```

```
10 REM SQUARE WAVE TRIPLE PULSE
15 REM ************TPULSQ.BAS*********************1/20/83
20 REM SET D/A CONVERTERS TO ZERO
30 H=128:L=0
40 POKE (HEX("C008")),L:POKE(HEX("C009")),H
50 POKE(HEX("C00A")),L:POKE(HEX("C00B")),H
60 POKE(HEX("C00C")),L:POKE(HEX("C00D")),H
70 POKE(HEX("C00E")),L:POKE(HEX("C00F")),H
75 REM LIST CHANNEL ASSIGNMENTS
80 PRINT "D/A CHANNEL ASSIGNMENTS"
90 PRINT "A------POTENTIAL OUTPUT TO ROTATOR"
100 PRINT "B------POTENTIAL TO ESTAT"
110 PRINT "C------CURRENT OUTPUT TO RECORDER"
120 PRINT "D------POTENTIAL OUTPUT TO RECORDER"
130 PRINT:PRINT "A/D CHANNEL ASSIGNMENTS"
140 PRINT "0------CURRENT INPUT FROM ESTAT"
150 PRINT "1------POTENTIAL FROM ESTAT"
160 PRINT:PRINT
200 REM DEFINE DATA STORAGE MATRICES
210 DIM E(200):DIM I(200):DIM II(2)
300 REM DEFINE VARIABLE EXPERIMENTAL CONDITIONS
310 INPUT "LOW AND HIGH ROTATION SPEEDS (1000 RPM/V)",LW,HW
315 PRINT "ENTER POTENTIAL VALUES IN VOLTS, TIME DELAYS IN MSEC"
320 INPUT "E(RED),E(OX)",E1,E2
330 INPUT "E(SAMPLE,INITIAL),E(SAMPLE,FINAL),E(SAMPLE,STEP)",E3,E4,E5
340 INPUT "TIME DELAYS AT EACH POTENTIAL RESPECTIVELY",TA,TB,TC
350 INPUT "NUMBER OF DATA POINTS COLLECTED AT EACH POTENTIAL",NN
360 X=0:Y=1:EA=E3
400 REM SET LOW ROTATION SPEED
410 W=(LW+10)*12.8:H=INT(W):L=(W-H)*256
420 POKE(HEX("C008")),L:POKE(HEX("C009")),H
425 X=X+1
430 REM SET REDUCING POTENTIAL
440 E=(E1+10)*12.8:H=INT(E):L=(E-H)*256
450 POKE(HEX("C00A")),L:POKE(HEX("C00B")),H
460 FOR T=1 TO TA:NEXT T
470 REM SET OXIDIZING POTENTIAL
480 E=(E2+10)*12.8:H=INT(E):L=(E-H)*256
490 POKE(HEX("C00A")),L:POKE(HEX("C00B")),H
500 FOR T=1 TO TB:NEXT T
510 REM SET SAMPLING POTENTIAL
520 E=(EA+10)*12.8:H=INT(E):L=(E-H)*256
530 POKE(HEX("C00A")),L:POKE(HEX("C00B")),H
540 FOR T=1 TO TC:NEXT T
630 REM SAMPLE CURRENT
640 I=0
650 FOR XX=1 TO NN
660 Z=8:POKE(HEX("C003")),Z
```

```
670 H=PEEK(HEX("0005")):L=PEEK(HEX("0004"))
680 H=H-128:L=(INT(L/16))/16:II=(H+L)*320/4096
690 I=I+II
700 NEXT XX
710 I=I/NN:I=I*1000:I=INT(I):I=I/1000
720 II(Y)=I
730 PRINT II(Y),
732 REM CHECK POTENTIAL VALUE AND STORE
733 EE=0
734 FOR HH=1 TO 10
735 Z=9:POKE(HEX("0003")),Z
736 H=PEEK(HEX("0005")):L=PEEK(HEX("0004"))
737 H=H-128:L=(INT(L/16))/16:E=(H+L)*320/4096
738 EE=E+EE:NEXT HH
739 E(X)=EE/10
740 PRINT E(X)
750 REM TEST ROTATION SPEED
760 IF Y=1 THEN 770
762 IF Y=2 THEN 790
770 Y=2:W=(HW+10)*12.8:H=INT(W):L=(W-H)*256
772 POKE(HEX("0008")),L:POKE(HEX("0009")),H
774 GOTO 430
790 REM CALCULATE DIFFERENCE CURRENT AND STORE IN MATRIX
792 I(X)=II(2)-II(1)
794 Y=1
800 REM CALCULATE NEW POTENTIAL VALUE
810 EA=EA+E5
820 IF EA>E4 THEN 900 ELSE 400
900 REM SET ROTATION SPEED AND POTENTIAL TO ZERO
910 H=128:L=0
920 POKE(HEX("0008")),L:POKE(HEX("0009")),H
930 POKE(HEX("000A")),L:POKE(HEX("000B")),H
1000 INPUT "PLOT DATA",PD$
1010 IF PD$="Y" THEN 1020 ELSE 1980
1011 PRINT "DATA IS PLOTTED POINT BY POINT"
1012 PRINT "ELECTRIC PENLIFT IS NOT CONTROLLED IN THIS PLOTTING ROUTINE"
1015 REM SET RECORDER TO INITIAL POTENTIAL, ZERO CURRENT
1020 PRINT "SET RECORDER TO INITIAL POTENTIAL, ZERO CURRENT"
1030 HH=E3:ZX=(HH+10)*12.8:H=INT(ZX):L=(ZX-H)*256
1040 POKE(HEX("000E")),L:POKE(HEX("000F")),H
1045 H=128:L=0
1050 POKE(HEX("000C")),L:POKE(HEX("000D")),H
1060 INPUT "DATA TO RECORDER",DR$
1070 IF DR$="Y" THEN 1100 ELSE 1980
1100 FOR M=1 TO X
1110 E=E(M):E=(E+10)*12.8:H=INT(E):L=(E-H)*256
1120 POKE(HEX("000E")),L:POKE(HEX("000F")),H
1130 I=I(M):I=(I+10)*12.8:H=INT(I):L=(I-H)*256
1140 POKE(HEX("000C")),L:POKE(HEX("000D")),H
```

```
1150 FOR SS=1 TO 500:NEXT SS
1200 FOR CC=1 TO 400:NEXT CC
1210 NEXT M
1300 INPUT "RECHECK DATA",RD$
1310 IF RD$="Y" THEN 1020 ELSE 1800
1800 INPUT "REPEAT EXPERIMENT WITH SAME CONDITIONS",SC$
1810 IF SC$="Y" THEN 360 ELSE 1820
1820 INPUT "REPEAT EXPERIMENT WITH DIFFERENT CONDITIONS",DC$
1830 IF DC$="Y" THEN 310 ELSE 2000
1980 INPUT"ARE YOU SURE",R$
1985 IF R$="N" THEN 1000 ELSE 1800
2000 END
```

```
10 REM ************IPULST.BAS*******************1/20/83
20 REM SET D/A CONVERTERS TO ZERO
30 H=128:L=0
40 POKE (HEX("C008")),L:POKE(HEX("C009")),H
50 POKE(HEX("C00A")),L:POKE(HEX("C00B")),H
60 POKE(HEX("C00C")),L:POKE(HEX("C00D")),H
70 POKE(HEX("C00E")),L:POKE(HEX("C00F")),H
80 PRINT "D/A CHANNEL ASSIGNMENTS"
90 PRINT "A-----POTENTIAL OUTPUT TO ROTATOR"
100 PRINT "B-----POTENTIAL TO ESTAT"
110 PRINT "C-----CURRENT OUTPUT TO RECORDER"
120 PRINT "D-----POTENTIAL OUTPUT TO RECORDER"
130 PRINT:PRINT "A/D CHANNEL ASSIGNMENTS"
140 PRINT "0-----CURRENT INPUT FROM ESTAT"
150 PRINT "1-----POTENTIAL FROM ESTAT"
160 PRINT:PRINT
200 REM DEFINE MATRIX
210 DIM E(200):DIM I(200):DIM II(2)
300 REM DEFINE VARIABLE EXPERIMENTAL CONDITIONS
310 INPUT "LOW AND HIGH ROTATION SPEEDS (1000 RPM/V)",LW,HW
315 PRINT "ENTER POTENTIAL VALUES AS VOLTS, TIME DELAYS AS MSEC"
320 INPUT "E(RED),E(OX),E(SAMPLE)",E1,E3,E2
330 INPUT "TIME DELAY AT REDUCING POTENTIAL",TA
340 INPUT "INITIAL AND FINAL TIME DELAYS AND STEP",T1,T2,TS
345 INPUT "TIME DELAY BEFORE SAMPLING CURRENT",TT
350 INPUT "NUMBER OF DATA POINTS COLLECTED AT EACH POTENTIAL",NN
360 X=0:Y=1:TC=T1
400 REM SET LOW ROTATION SPEED
410 W=(LW+10)*12.8:H=INT(W):L=(W-H)*256
420 POKE(HEX("C008")),L:POKE(HEX("C009")),H
425 X=X+1
430 REM SET REDUCING POTENTIAL
440 E=(E1+10)*12.8:H=INT(E):L=(E-H)*256
450 POKE(HEX("C00A")),L:POKE(HEX("C00B")),H
460 FOR T=1 TO TA:NEXT T
470 REM SET OXIDIZING POTENTIAL
480 E=(E3+10)*12.8:H=INT(E):L=(E-H)*256
490 POKE(HEX("C00A")),L:POKE(HEX("C00B")),H
500 FOR T=1 TO TC:NEXT T
510 REM SET SAMPLING POTENTIAL
520 E=(E2+10)*12.8:H=INT(E):L=(E-H)*256
530 POKE(HEX("C00A")),L:POKE(HEX("C00B")),H
540 FOR T=1 TO TT:NEXT T
630 REM SAMPLE CURRENT
640 I=0
650 FOR XX=1 TO NN
660 Z=8:POKE(HEX("C003")),Z
670 H=PEEK(HEX("C005")):L=PEEK(HEX("C004"))
```

```
680 H=H-128:L=(INT(L/16))/16:II=(H+L)*320/4096
690 I=I+II
700 NEXT XX
710 I=I/NN:I=I*1000:I=INT(I):I=I/1000
720 II(Y)=I
730 PRINT II(Y),
732 REM CHECK POTENTIAL VALUE AND STORE
733 EE=0
734 FOR HH=1 TO 10
735 Z=9:POKE(HEX("0003")),Z
736 H=PEEK(HEX("0005")):L=PEEK(HEX("0004"))
737 H=H-128:L=(INT(L/16))/16:E=(H+L)*320/4096
738 EE=E+EE:NEXT HH
739 E(X)=EE/10
740 PRINT E(X)
750 REM TEST ROTATION SPEED
760 IF Y=1 THEN 770
762 IF Y=2 THEN 790
770 Y=2:W=(HW+10)*12.8:H=INT(W):L=(W-H)*256
772 POKE(HEX("0008")),L:POKE(HEX("0009")),H
774 GOTO 430
790 REM CALCULATE DIFFERENCE CURRENT AND STORE IN MATRIX
792 I(X)=II(2)-II(1)
794 Y=1
800 REM CALCULATE NEW TIME DELAY
810 TC=TC+TS
820 IF TC>T2 THEN 900 ELSE 400
900 REM SET ROTATION SPEED AND POTENTIAL TO ZERO
910 H=128:L=0
920 POKE(HEX("0008")),L:POKE(HEX("0009")),H
930 POKE(HEX("000A")),L:POKE(HEX("000B")),H
1000 INPUT "PLOT DATA",PD$
1010 IF PD$="Y" THEN 1020 ELSE 1980
1020 PRINT "SET RECORDER TO ZERO"
1030 H=128:L=0
1040 POKE(HEX("000E")),L:POKE(HEX("000F")),H
1045 H=128:L=0
1050 POKE(HEX("000C")),L:POKE(HEX("000D")),H
1060 INPUT "DATA TO RECORDER",DR$
1070 IF DR$="Y" THEN 1100 ELSE 1980
1100 FOR M=1 TO X
1110 E=TS*Y*0.004:E=(E+10)*12.8:H=INT(E):L=(E-H)*256
1120 POKE(HEX("000E")),L:POKE(HEX("000F")),H
1130 I=I(M):I=(I+10)*12.8:H=INT(I):L=(I-H)*256
1140 POKE(HEX("000C")),L:POKE(HEX("000D")),H
1150 FOR SS=1 TO 500:NEXT SS
1160 REM LOWER PEN
1180 REM LIFT PEN
```

```
1200 FOR CC=1 TO 400:NEXT CC
1210 NEXT M
1300 INPUT "RECHECK DATA",RD$
1310 IF RD$="Y" THEN 1020 ELSE 1800
1800 INPUT "REPEAT EXPERIMENT WITH SAME CONDITIONS",SC$
1810 IF SC$="Y" THEN 360 ELSE 1820
1820 INPUT "REPEAT EXPERIMENT WITH DIFFERENT CONDITIONS",DC$
1830 IF DC$="Y" THEN 310 ELSE 2000
1980 INPUT"ARE YOU SURE",R$
1985 IF R$="N" THEN 1000 ELSE 1800
2000 END
```